# Measuring Adhesion Forces Between Hydrophilic Surfaces with Atomic Force Microscopy Using Flat Tips

ARZU ÇOLAK

# Measuring Adhesion Forces Between Hydrophilic Surfaces with Atomic Force Microscopy Using Flat Tips

**ARZU ÇOLAK**

**Composition of the Graduation Committee:**

| | | |
|---|---|---|
| *Chairman and secretary :* | Prof. Dr. G. van der Steenhoven | University of Twente |
| *Promotors:* | Prof. Dr. Ir. B. Poelsema | University of Twente |
| | Prof. Dr. Ir. H.J.W. Zandvliet | University of Twente |
| *Assistant-promotor:* | Dr.Ir. H. Wormeester | University of Twente |
| *Members:* | Prof. Dr. S. Speller | University of Rostock |
| | Dr. G. Palasantzas | University of Groningen |
| | Prof. Dr. J.C.T. Eijkel | University of Twente |
| | Dr. M.H.G. Duits | University of Twente |

The work described in this thesis was carried out at the Physics of Interfaces and Nanomaterials group, MESA+ Institute for Nanotechnology, University of Twente, The Netherlands.

The research was financially supported by Marie Curie Early-Stage Researcher (ESR) Fellowship of European Community's Seventh Framework Programme [FP7/2007-2013] under grant agreement number [215723].

Arzu Çolak
Measuring adhesion forces between hydrophilic surfaces with Atomic Force Microscopy using flat tips.
ISBN: 978-90-365-1612-9
DOI: 10.3990/1.9789036516129
URL: http://dx.doi.org/10.3990/1.9789036516129

Published by Physics of Interfaces and Nanomaterials group, University of Twente.
Printed by Ipskamp Drukkers, Rotterdam, The Netherlands.

Cover : Ebru (marbling) © Dr. Mehmet Refii Kileci, 2013
Cover Design: Arzu Çolak

# MEASURING ADHESION FORCES BETWEEN HYDROPHILIC SURFACES WITH ATOMIC FORCE MICROSCOPY USING FLAT TIPS

## DISSERTATION

to obtain
the degree of doctor at the University of Twente,
on the authority of the rector magnificus,
Prof. Dr. H. Brinksma,
on account of the decision of the graduation committee,
to be publicly defended
on Friday 28 June 2013 at 16:45

by

**ARZU ÇOLAK**

born on 27 September 1979
in Kocaeli, Turkey

This dissertation is approved by:

Promotors: Prof. Dr. Ir. Bene Poelsema
Prof. Dr. Ir. Harold J.W. Zandvliet
Assistant promotor: Dr. Ir. Herbert Wormeester

*…to my mother, father, and brother*

# Table of Contents

# Chapter 1

## Introduction

*In the last decades micro technology has opened new possibilities for mobile communication, safety, and health science products. Today, markets demand ever smaller, cheaper, energy friendly and more different consumer products. To meet these demands, science and technology continue to move forward in fabrication of micro/nanodevices and application of physical, chemical, and biological systems that scale from individual atoms to submicron dimensions with integrating the resulting nanostructures into larger systems.*

*With further down scaling the size of features on wafers the magnitude of adhesive forces becomes a prohibitive factor in further increasing handling speeds and throughput of wafers in expensive and complicated equipment. This has inspired us to investigate the adhesion forces in greater detail.*

*This thesis aims at providing a better understanding of the factors that are of prime importance for the magnitude of the adhesion forces, for instance surface roughness and environmental humidity. Contact mode atomic force microscopy is the key source of information on the adhesion forces and the influence of experimental parameters as load, approach and retraction speeds, contact time and tip size are investigated. In this introductory chapter, a basic overview of the adhesion phenomena and the important surface forces which lie behind the adhesion property of surfaces are discussed.*

## 1.1 Definition of adhesion

The word "adhesion" comes from the Latin verb "haerere", and in general simply signifies the tendency of two different bodies to be held together [1]. The mechanical force that is needed to separate both bodies from one another is often named as adhesion force or pull-off force. Theoretically, the work of adhesion upon separation of surfaces is defined by the surface energy and interfacial surface tensions of the interacting materials, and can be predicted by the Dupré equation [1]:

$$W_A = \gamma_1 + \gamma_2 - \gamma_{12} \tag{1.1}$$

where $\gamma_1$ and $\gamma_2$ stand for the specific surface energy per unit area of the newly formed surfaces while $\gamma_{12}$ is the specific interfacial energy between the involved materials. It is important to note a few things. The definition is an equilibrium description and assumes the presence of only two well defined substances making a full contact via an atomically flat interface. This has important consequences since the adhesion forces are normally measured by disrupture of the contact, for instance, as is the case here, by pulling – off a tip in an atomic force microscope in contact with a surface. This process is in essence a dynamic process and for instance the speed of retraction may cause deviations from equilibrium. What is actually measured in the experiment is the pull – off force rather than the adhesion force. In spite of the principle difference we do refer to the force needed to separate the tip and the sample as adhesion force, in order to avoid inconsistencies with the overwhelming majority in literature. In real life, however, the situation is even much more complicated, since the contact area is usually not flat and the contact area may be much smaller than macroscopically assumed due to interfacial roughness. Moreover, in real systems a thin water film is almost always present under atmospheric conditions. This can give rise to an important increase or decrease of the adhesion force, depending on the hydrophilicity / hydrophobicity of the contact surfaces. Other factors that may influence the measured adhesion force include plastic deformation of the contact area. In the past decades, a great deal of attention has been paid to understand the (non-) equilibrium effects on the adhesion of materials and devices at micro and nano scales, but still adhesion is far from being completely understood.

## 1.2 High or low adhesion?

Surface interactions play an important role in many engineering applications as well as in everyday life. When considering applications at macro and/or micro scales, adhesion cannot be ignored. For instance, a lack in adhesion of toner particles on a support paper during the photocopying process can result in low quality images [2]. Adhesion is also useful in technological applications, e.g. in sticky tapes. Adhesion is beneficial for various biological processes of creatures. Many animals, e.g. beetles, flies, spiders, and especially the Tokay gecko (Gekko gecko) possess an extraordinary ability to move on vertical surfaces and ceilings with a special adhesion property. On the other hand, in microcontact printing technology, adhesion leads to stamp deformation and limits the application of the technology [3]. For wafer tray technology in semiconductor industry, the existence of adhesion between the wafer and the wafer table could cause problems with overlaying of images that the wafer stepper machine print, or breaking of wafers due to the stress on them. That is why, depending on the purpose, adhesion needs to be controlled in one way or the other [4].

## 1.3 Surface forces

The force acting between two surfaces through an intervening medium are named as surface forces. Contrary to the macro – world ruled by gravity, when the objects are scaled down to micro or nano size, surface effects induced strong surface forces become more important [5]. Depending on the physics and chemistry of the interacting surfaces, the adhesion property of surfaces is a consequence of interatomic and intermolecular surface forces such as Van der Waals forces, electrostatic forces, chemical forces, capillary forces, and others. A better understanding of their individual contributions is of crucial importance to control adhesion.

### 1.3.1 Van der Waals forces

Van der Waals forces play a critical role in all phenomena involving intermolecular forces, and these forces are always present for virtually all media. This interaction force may have varying importance depending on the system but it is usually dominant in particle adhesion with meniscus forces. The Van der Waals force, depending on the situation, can be effective from long – range distance of ≥10 nm down to interatomic spacing (about 0.2 nm) [1]. The Van der Waals force between molecules originates from three different interactions:

- **(i)** The *Keesom* interaction (or orientation interaction), is the interaction of a permanent dipole with another permanent dipole which are allowed to rotate freely.
- **(ii)** The *Debye* interaction (or induction interaction), is the interaction between a permanent dipole and an induced dipole.
- **(iii)** The *London* interaction (or dispersion interaction), occurs when an induced dipole, which are created by a temporarily charge fluctuation, interacts with another induced dipole.

The attractive Van der Waals force between atoms and/or molecules is equal to the sum of the above interaction forces. Since all of these interaction forces are proportional to $r^{-6}$, the attractive Van der Waals interaction potential, at a distance $r$, can be written as [1]:

$$U_{vdW}(r) = -\frac{C_K + C_D + C_L}{r^6} \tag{1.2}$$

where $C_K$, $C_D$, and $C_L$ are the coefficients due to the Keesom, Debye and London interactions. The negative sign shows the attracting potential action.

The Van der Waals force between two macroscopic bodies is larger than between single atoms and molecules, and can be calculated by summing up the forces between single atoms or molecules within the bodies. In general, there are two approaches to do this calculation. In the first one, Hamaker [6] used the integration of the interaction potential to calculate the total interaction between two macroscopic bodies. For two arbitrarily shaped bodies the Van der Waals force is given by:

$$F_{vdW} = \rho_1 \rho_2 \int_{\Omega_1} \int_{\Omega_2} F(r)\, d\Omega_1 d\Omega_2 \tag{1.3}$$

where $\Omega_1$ and $\Omega_2$ are the volumes of bodies 1 and 2 respectively, while $\rho_1$ and $\rho_2$ are the number densities of molecules in the solids. The second approach, based on the Lifshitz theory [7], is more rigorous and gives the Van der Waals interaction energy as a function of macroscopic electrodynamic properties of the interaction media, such as their dieletric permittivities and refractive indices. The summation method of Hamaker neglects the fact that the state of each atom inside the body is changed by the presence of the other neighbouring atoms. The problem of additivity is completely avoided in the Lifshitz theory. The Lifshitz theory is a continuum theory which neglects the atomic structure. This theory is in qualitative agreement with the results deduced by Hamaker's summation method.

For the effect of the Van der Waals forces on adhesion, where very small distances between the bodies are considered, it is needed only to look at the dispersion forces as a power function of the distance, according to Hamaker's summation method. On the basis of Hamaker's summation method the Van der Waals forces between bodies with different geometries, can be calculated with the negative derivation of the interaction energy ($w_{vdW}$) versus distance between the bodies. The Table 1.1 below shows non-retarded Van der Waals forces between bodies of different geometries that were calculated with Hamaker's summation method. [1]. In the Table 1, $A_H$ is called as Hamaker constant and is given by:

$$A_H = \pi^2 C \rho_1 \rho_2 \tag{1.4}$$

with the parameters of the Lennard-Jones potential ($C = 4\varepsilon\sigma$) and the number densities of the species 1 and 2, i.e., $\rho_1$ and $\rho_1$.

One notices the significantly impacted distance dependences. While, Van der Waals atom – atom interactions are very short ranged ($\sim 1/r^6$), macroscopic Van der Waals interactions are long ranged (e.g., sphere – flat surface: $\sim 1/d^2$).

***Table 1.1*** *Van der Waals interaction energy and force between macroscopic bodies of different geometries*

| Geometry of bodies with surface “d” apart (d<<r) | Van der Waals Interactions | |
|---|---|---|
| | Energy | Force |
| Two flat surfaces (per unit area) | $w_{vdW}(d) = \frac{A_H}{12\pi d^2}$ | $F_{vdW}(d) = \frac{A_H}{6\pi d^3}$ |
| Sphere of radius “r” near a flat surface | $w_{vdW}(d) = \frac{A_H r}{6d}$ | $F_{vdW}(d) = \frac{A_H r}{6d^2}$ |
| Two identical spheres of radius “r” | $w_{vdW}(d) = \frac{A_H r}{12d}$ | $F_{vdW}(d) = \frac{A_H r}{12d^2}$ |
| Cylinder of radius “r” near flat surface (per unit length) | $w_{vdW}(d) = \frac{A_H \sqrt{r}}{12\sqrt{2}d^{3/2}}$ | $F_{vdW}(d) = \frac{A_H \sqrt{r}}{8\sqrt{2}d^{5/2}}$ |
| Two identical parallel cylinders of radius “r” (per unit length) | $w_{vdW}(d) = \frac{A_H \sqrt{r}}{24d^{3/2}}$ | $F_{vdW}(d) = \frac{A_H \sqrt{r}}{16d^{5/2}}$ |
| Two identical perpendicular cylinders of radius “r” | $w_{vdW}(d) = \frac{A_H r}{6d}$ | $F_{vdW}(d) = \frac{A_H r}{6d^2}$ |

Van der Waals forces are strong forces, and there are animals which take advantage of Van der Waals interactions between their legs and grounding to stand upside down or walk on a ceiling. For instance, geckos have specialized toe pads that enable them to climb on smooth vertical surfaces and cross indoor ceilings easily even though they have a relatively huge body. The complex hierarchical structure of their toes (Figure 1.1) allow the animal to adhere to wide variety of surfaces with an adhesive force in the mN to N range. If a gecko had every one of his spatulae in contact with a surface, it would be capable of holding a 120 kg man [8,9].

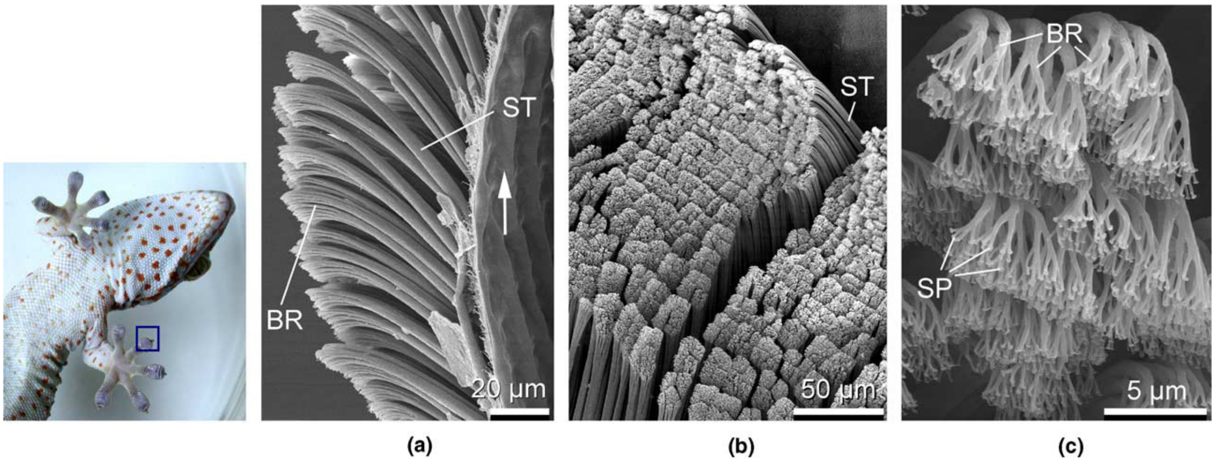

***Figure 1.1*** *The hierarchical adhesive structures of Gekko gecko. A toe of gecko contains hundreds of thousands of keratinous hairs or setae, and each seta contains hundreds of protruding submicron structures called spatulae.* ***(a)*** *and* ***(b):*** *scanning electron micrographs of rows of setae at different magnifications and* ***(c):*** *spatulae (SP), the finest terminal branches (BR) of seta (ST). [10]*

### 1.3.2 Capillary forces

Water plays a key role in the interactions between surfaces in nature. For instance, it is only possible to build a sand castle from slightly wet sand but not from dry sand. Wet sand can be shaped because neighboring particles make clusters by the liquid menisci which form around the contact areas of particles. The force holding particles together by such liquid menisci is called "capillary force". The capillary force is important in micro- and nano material applications due to a large contribution to the adhesion force. Therefore, understanding the properties of capillary forces is very important.

The water vapor present in air forms a thin layer of water on surfaces exposed to the air, if the surfaces are lyophilic with respect to the surrounding vapor [11]. This water layer causes a capillary bridge formation at the contact area between surfaces when two surfaces are brought in close proximity to each other. Even under low relative humidity conditions, it is not possible to completely eliminate such capillary condensation near the contact spots.

At equilibrium, the surface curvature of the meniscus is described by the Kelvin radius, $r_K$ :

$$\frac{1}{r_K} = \left( \frac{1}{r_1} + \frac{1}{r_2} \right) \tag{1.5}$$

where $r_1$ and $r_2$ are the radii of curvature of the meniscus perpendicular and parallel to the solid surfaces, respectively.

The Kelvin radius is connected with the relative vapor pressure of the liquid by the following the Kelvin equation [12]:

$$r_K = \frac{\gamma V_m}{RT} \frac{1}{\log P / P_S} \tag{1.6}$$

where $R$ is the gas constant, $T$ is the temperature, $V_m$ is the molar volume of the liquid, $P / P_s$ is the relative vapor pressure (relative humidity for water), $\gamma$ is the surface tension of the liquid. For typical situations, the actual vapor pressure, $P$, is smaller than the saturation vapor pressure, $P_s$, over a liquid surface.

The pressure inside the menisci is lower than the pressure outside in accordance with the Laplace equation which is given by [13]:

$$\Delta P = \gamma \left( \frac{1}{r_1} + \frac{1}{r_2} \right) \tag{1.7}$$

This pressure difference acts over the cross – sectional area of the meniscus and attracts the surfaces towards to each other with the capillary force, $F_C$, in general form given as;

$$F_C = \int_S \Delta P dS \tag{1.8}$$

where $S$ is the cross-sectional area of the meniscus.

### 1.3.3 Electrostatic forces

Numerous everyday phenomena are governed by electrostatic interactions that occur between charged particles or bodies in both air and water. Electrostatic forces are produced by one or more valence electrons transferring completely from one atom to another. When the separation between two surfaces is approximately equal to the atomic spacing, the generated bond is quite strong and resembles that within the bulk material. However, in the discussion of the interactions between a micro or nano particle and a surface, the electrostatic force when compared to the Van der Waals and capillary forces could be neglected.

### 1.3.4 Covalent or Chemical forces

When two or more atoms come together to form a molecule, as when two hydrogen atoms and one oxygen atom combine to form a water molecule, the forces that bind the atoms together within the molecule are called covalent forces [1]. Covalent forces operate over very short distances of the order of interatomic separations (0.1 – 0.2 nm). They are mainly in the range 200 – 800 kJmol$^{-1}$, and tend to decrease in strength with increasing bond length. Due to that, covalent forces are neglegible when compared to the Van der Waals and capillary forces.

## 1.4 Concept and organization of the thesis

The experimental work in this thesis aimed at the quantification of nanoscale adhesion of Si(001) with an AFM Si-tip. We elucidate the effects of roughness, environmental conditions, and instrumental parameters of the AFM on the adhesion force.

Chapter 2 provides information about experimental methods to measure the adhesion forces. In this chapter, the fabrication of surfaces with high roughness for adhesion measurements is also explained.

In Chapter 3, the influence of surface roughness and relative humidity on the adhesion force is studied.

It is also a necessity to know the impact of instrumental parameters of an AFM on adhesion force measurements, for correct and reproducible analysis of the adhesion force. In Chapter 4, the effect of the residence time of the tip at the substrate, the maximum applied load on the cantilever, the retracting velocity of the cantilever on the adhesion force are analyzed for the flat-on-flat contact geometry.

In Chapter 5, the influence of the singular instrumental parameters, introduced in Chapter 4, on the adhesion force was studied for the flat-on-rough contact.

## 1.5 References

1. Israelachvili, J. N. *Intermolecular and Surface Forces*, Academic Press, London, 2nd edition (1992).
2. Mastrangelo, C. J., *Photogr. Sci. Eng.* **1982**, *26*, 194 – 197.
3. Tang, T.; Hui, C. Y.; Glassmaker N. J., *J. R. Soc. Interface* **2005**, *2*, 505 – 516.
4. Ferreira, O. D. S.; Gelinck E.; de Graat D.; Fischer H., *Appl. Surf. Sci.* **2010**, *257*, 48 – 55.
5. Zhao, Y. -P.; Wang, L. S.; Yu, T. X., *J. Adh. Sci. Technol.* **2003**, *17*, 519 – 546.
6. Hamaker, H. C., *Physica* **1937**, *4*, 1058 – 1072.
7. Lifshitz, E. M., *Soviet Phys. JETP* **1956**, *2*, 73 – 83.
8. Autumn, K.; Liang, Y. A.; Hsieh, S. T.; Zesch, W.; Chan W. P.; Kenny, T. W.; Fearing, R.; Full, R. J., *Nature* **2000**, *405*, 681 – 684.
9. Irschick, D. J.; Austin, C. C.; Petren, K.; Fisher, R. N.; Losos, J. B.; Ellers, O., *Biol. J. Linn. Soc.* **1996**, *59*, 21 – 35.
10. Gao, H.; Wang, X.; Yao, H.; Gorb, S.; E. Arzt, *Mech. Mater.* **2005**, *37*, 275 – 285.
11. Melrose J. C., *Amer Inst. Chem. Engrs. J.* **1966**, *12*, 986 – 994.
12. Thomson, W., *Philos. Mag.* **1871**, *42*, 448 – 452.
13. Rowlinson, J. S.; Widom, B., *Molecular Theory of Capillarity*, Clarendon Press, Oxford, (1982).

# *Chapter 2*

## Experimental methods and materials

*In this chapter, the principals of experimental techniques used for carrying out adhesion force measurements in a controllable way are discussed. Furthermore, the sample preparation methods for adhesion measurements are explained.*

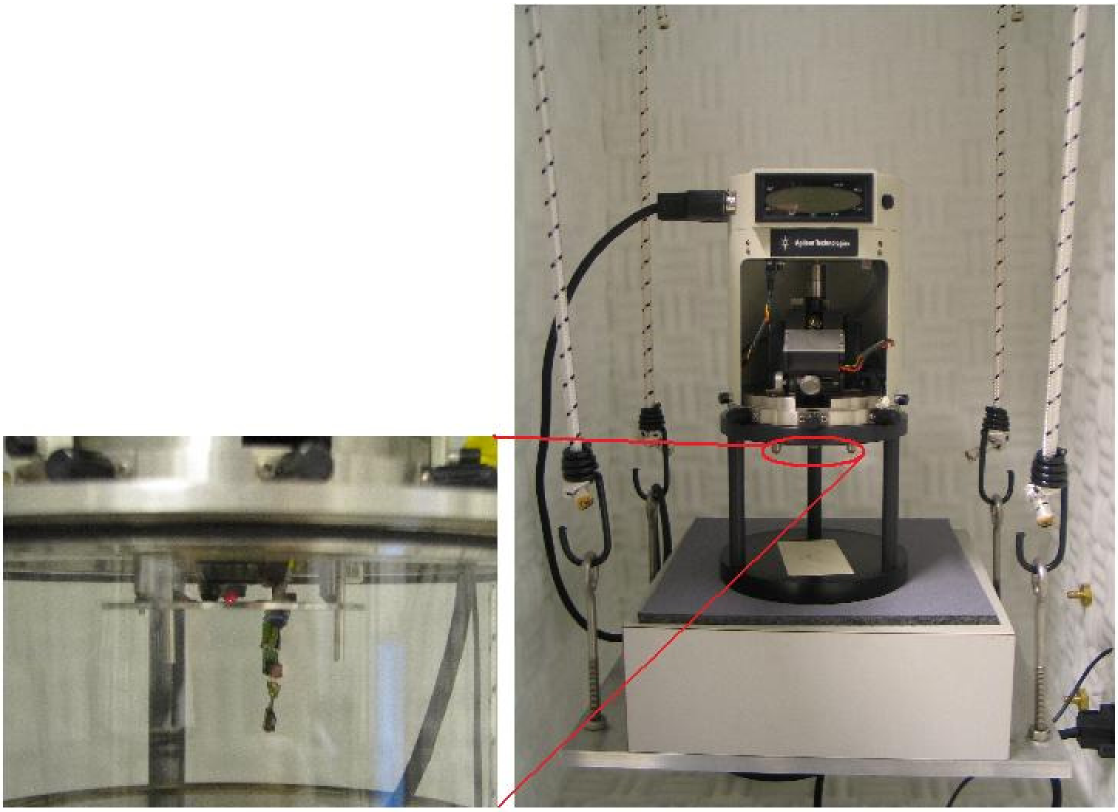

## 2.1 Measuring adhesion

Observing what is going on at the nanoscale level is of crucial importance to understand what occurs at the macroscopic level. Over the past decade, the necessity of controlling the adhesion properties of surfaces at the macroscopic scale accelerated the interest of researchers to study adhesion forces on the nanoscale. In general, direct force measurement tools are used to study the adhesion force between surfaces. In the following section I will introduce the most common and powerful tools used for studying the adhesion force at the nanoscale.

### 2.1.1 Surface Force Apparatus (SFA)

The Surface Force Apparatus (SFA) was invented by Tabor, and Winterton [1] for measuring Van der Waals forces in air or vacuum. Later, the SFA was further developed by Israelachvili and Tabor [2] for measuring Van der Waals forces in the range of 1.5 to 130 nN. In SFA, two atomically flat sheets of mica affixed on glass surfaces are approached towards each other with a piezoelectric crystal transducer. The distance between the two mica surfaces is controlled by using optical interferometry. Unfortunately, there are severe limitations of the instrument. For instance, the mica is the only surface that can be directly studied. It is possible to overcome this limitation and allow the use of different surfaces with coating or adsorbing some layers such as polymers, surfactants, or lipid layers on mica. However, the lateral resolution of the SFA is in the range of several micrometers, and UHV measurements are extremely difficult. There can be considerable loss of information resulting from instabilities in the attractive forces, or rapidly changing interactions. Also, the calculations of the distance using interferometry could be time consuming.

### 2.1.2 Atomic Force Microscopy (AFM)

Atomic Force Microscopy (AFM) is a scanning probe technique that allows the measurement of three dimensional representations of a surface topography with a high resolution (lateral ~1 nm, vertical ~ 0.1 nm). It monitors the deflection of a probe (tip) or dynamic changes of vibration parameters due to interaction forces between the sample and the probe as it scans the surface.

AFM was introduced in 1986 by Binnig et al. [3], and since then has become an important instrument in widespread applications in physics, chemistry, biology and material science by the acquision of images both in air or in a liquid environment without needing any surface treatments or coatings. In addition to imaging surfaces, AFM is a powerful technique to probe friction, adhesion and viscoelasticity of surfaces.

The basic configuration of an AFM is represented in Figure 2.1. In this technique the surface topography is obtained from the movement of a tip, that is attached to the free end of a flexible cantilever. The tip is brought in close proximity to, or into contact with the surface. A laser beam is focused on the back of the cantilever, and is reflected from the cantilever to a split photodiode detector. The photodiode measures the difference in light intensities between the top and bottom photo detector and thus the angular deflection of the cantilever, and then produces a signal depending on the deflection of the cantilever. In general, the cantilever is mounted on a piezoelectric tube scanner that is usually in the form of a hollow cylinder and consists of seperate electrodes that permit movement in the x-y place in a raster pattern over the sample (depending on the configuration of the AFM, the sample can be mounted on the piezoelectric tube scanner while the cantilever is fixed in its place). During scanning of the surface due to features on the sample and the interaction forces, the cantilever deflects in the vertical and lateral directions. These deflections of the cantilever move the position of the laser spot on the photo detector and lead to a change in the detector output signal. The feedback loop control circuit is used to adjust the interaction between the tip and the sample to a fixed pre-set value by using the detector output signal. To arrive at this goal the cantilever is moved in the vertical (z) direction by piezoelectric scanner to compensate for changes with help of the feedback loop controller. At the end, a topographic image of the surface is obtained by plotting the z-position of the piezo as a function of the x-y position for a fixed cantilever deflection.

In this study a Molecular Imaging AFM was used for both surface scans and the adhesion force measurements of flat and rough silicon wafers. To measure surface roughness, non-contact mode AFM probes (PPP-NCLR-20 and Tap190DLC) were used, while for the adhesion force measurements a flat silicon tip (Nanosensors, PL2-NCLR-10) was used at different humidity conditions.

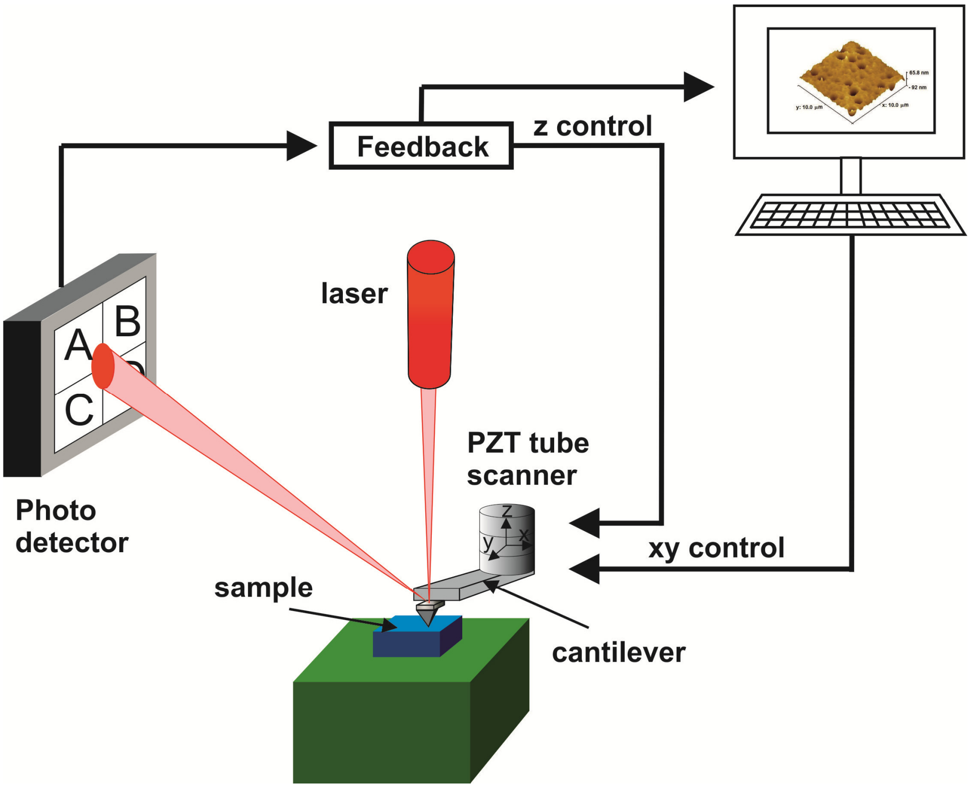

***Figure 2.1.*** *Basic configuration of an AFM*

### 2.1.2.1 AFM imaging

There are three main imaging modes of the AFM that are distinguished depending on the interaction between the tip and the sample surface.

#### (i) Contact mode

The contact mode is the most common mode used in AFM. In this mode, the tip scans the sample in contact with the surface, and due to that the probe is sensitive to the normal and the lateral forces to the sample surface. However, because of the applied lateral force load, the sample and the tip can be damaged. That is why, this AFM mode is generally used for flat samples that can withstand high lateral forces during scanning. For this mode, the probes with low spring constants ($k < 1$ N/m) are used for scanning samples in order to minimize the amount of applied force on the sample and the tip.

In contact mode the deflection of the cantilever is sensed and compared in a DC feedback amplifier with a desired setpoint deflection value. If the measured cantilever deflection is different from setpoint deflection, the feedback amplifier applies a voltage to the scanner to regulate the position between the probe and the sample surface. This applied voltage is a measure of the height of features on the samples surface. A 3-dimensional AFM image is generated from z piezo movements as a function of x-y position.

#### (ii) Tapping (or intermittent contact) mode

This operation mode of an AFM is called dynamic mode and can yield a higher resolution of topographic images of surfaces than those made in contact mode. This type of working mode decreases the impact of lateral forces and can access the topography of softer samples without damaging them. However, it allows a lower scan speed than in contact mode.

In tapping mode, the cantilever is vibrated sinusoidally by a piezo mounted above it, and the oscillating tip taps the surface at or near resonance frequency of cantilever (70-400 kHz) with a constant amplitude ranging typically from 20 to 100 nm. During imaging, a constant oscillation amplitude is maintained with a feedback loop. When the space between the probe and the sample surface is decreased during the scan due to a protrusion, the cantilever oscillation amplitude decreases. However, when the space is increased because of passing over a deep feature on surface, the oscillation amplitude increases. By varying z-position of the cantilever the decreases or the increases in the oscillation amplitude are regulated to keep it constant. At the end, the change of the z-piezo, needed to keep the amplitude constant, is recorded as a function of x-y positions to measure a surface image.

### (iii) Non-contact mode

As in tapping mode, this mode of an AFM is also known as dynamic mode. In the non-contact mode, the tip does not come into contact with the sample surface, but stays a distance several nm away it. The cantilever is oscillated at a frequency slightly above its resonance frequency with an amplitude that is < 10 nm. During the scan, the tip feels attractive long-range forces, such as Van der Waals and electrostatic forces, that increases or decreases the amplitude of the oscillation by changing the spring constant of the tip, and its resonant frequency. A feedback loop is used to keep the tip-sample distance at a value that leads to a stable oscillation amplitude.

This mode of AFM has the advantage of dealing with low lateral and normal forces between the probe and the sample that prevent the sample to be damaged. However, this a very difficult mode to operate in ambient conditions due to formation of a liquid layer on surface, which causes the formation of capillary bridge between the tip and the sample and hence may cause the tip to snap – in to the surface.

## 2.1.2.2 AFM force – distance spectroscopy

AFM has the ability of measuring the interaction forces between the cantilever and the substrate with force – distance spectroscopy. A schematic representation of the force – distance spectroscopy is shown in Figure 2.2. In order to get such a curve, a sawtooth voltage is applied to the $z$ electrode of the piezo tube, while the voltages of $x$ and $y$ electrodes are kept constant at zero. When the applied voltage of the piezo tube is changed, the cantilever is moved in the vertical direction towards the stationary sample and than withdrawn. During the up and down movement of the cantilever, the cantilever deflects due to the forces between tip and sample. These deflections of the cantilever change the position of reflected laser point of photodiode. At the end, the changes on the detector signal due to cantilever deflections are recorded as a function of the piezo position to get a graph as in Figure 2.2.(A).

In the graphs, the arrow heads indicate the direction of piezo travel. Between the positions (1) and (2), the tip approaches the surface without experiencing a noticeable interaction, since the tip is still far away from the surface. The cantilever is at its equilibrium position and the net force experienced by the AFM tip is zero. As the tip approaches the surface to within a few nanometers, the AFM probe will eventually experience a net attractive force gradient that is larger than force constant of the cantilever. As a result, the AFM probe jumps into contact with the surface (2). From this point, the piezo extends further, and the cantilever deflection increases. This continues until a predetermined force limit is reached (3). After that, the retraction of the AFM probe starts (4–5). However the adhesion forces hinder the withdrawal of the tip, and the tip moves beyond the initial zero deflection point (flat line between 1–2). At (5), the net force is zero and the tip immediately snaps off. Subsequently, the cantilever goes back to its original starting position (6–7). The horizontal distance between the maximum deflection point of the cantilever during retraction (5) and the zero deflection point

(6) gives the distance moved by the tip in the adhesion regime. After recording the deflection of cantilever as a function of the piezo position, by applying the spring constant value to Hooke's Law ($F = kx$, where $k$ is the cantilever's spring constant), a force-distance curve is obtained from the deflection – piezo position curve (Figure 2.2.(B)).

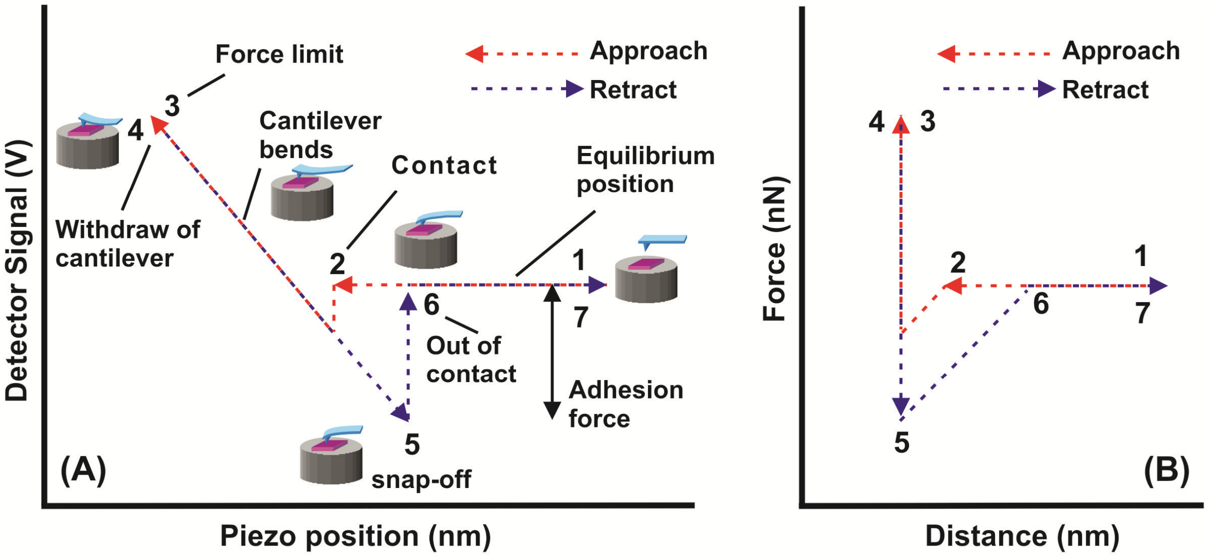

***Figure 2.2.*** *Schematic representation of* ***(A)*** *detector signal versus piezo position,* ***(B)*** *a force-distance curve converted from detector signal versus piezo position curve.*

## 2.2 Calibration of cantilever spring constant

The value of the cantilever spring constant is required for proper interpretation of a force-distance curve in order to extract the mechanical properties of samples correctly. In literature, several methods have been described for calibrating AFM cantileves, each with advantages and limitations [4]. Among all methods we prefered the theoretical calculation method of Poggi et al. [5] due to its simplicity and limitations of our AFM. According to the theory, if the density and elastic modulus of the cantilever material are known, accurately determined dimensions of the cantilever are enough to calculate the spring constant.

For calculating the spring constant of the flat silicon probe (Nanosensors, PL2-NCLR-10), the geometry of the tip was determined by He Ion Microscopy (HIM). Figure 2.3 presents a set of HIM images. As clearly visible in these images, the tip is not rectangular but has a trapezoidal cross section. This is the result of the dynamic etching process that AFM probe manufacturers now use.

The spring constant of the cantilever in the normal direction is calculated with

$$k = \frac{3EI}{L^3} \tag{2.1}$$

where $E$ is the Young's modulus, $L$ is the length of the cantilever, $I$ is the second moment of the cantilever. For the trapezoidal cross sectional area, the second moment is given by [6],

$$I_{trapezoid} = \left( \frac{t^3(a^2 + 4ab + b^2)}{36(a+b)} \right) \tag{2.2}$$

where $t$ is the cantilever thickness, $a$ and $b$ are the width of top and bottom surfaces of the cantilever, respectively (see Figure 2.3).

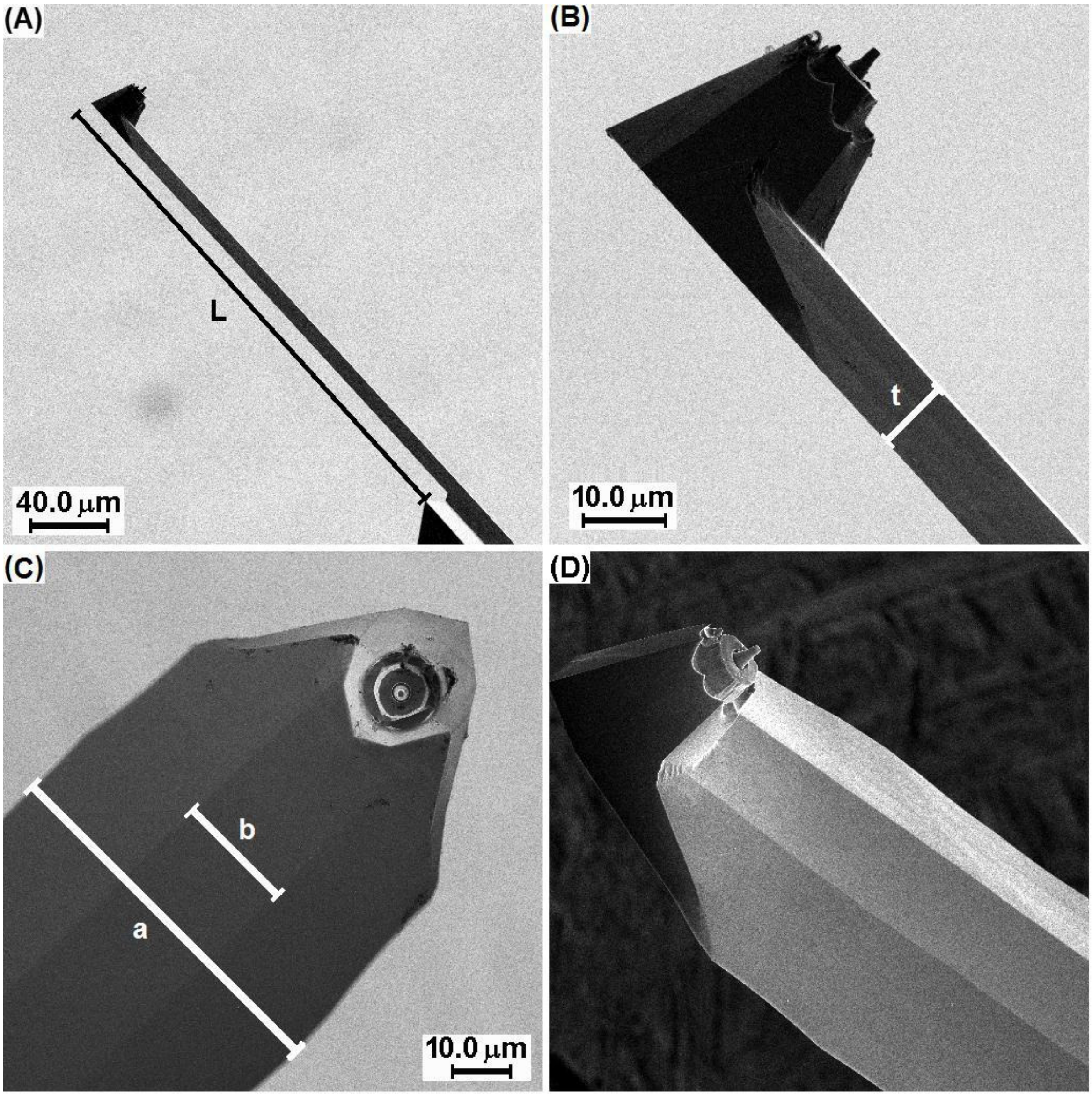

***Figure 2.3.*** *He Ion Microscopy (HIM) images of flat silicon probe (Nanosensors, PL2-NCLR-10).* ***(A)*** *Side view of the entire cantilever for length (L) measurement;* ***(B)*** *an increased magnification of the side view of the cantilever for thinckness (t) measurement;* ***(C)*** *the bottom view of the cantilever for the width measurement, (a) is top surface width, (b) is bottom surfaces width of the cantilever;* ***(D)*** *view of the slightly tilted cantilever showing the trapezoidal cross-sectional shape.*

## 2.3 Surface preparation (wet chemical etching)

In our experiments two different samples were used to study the influence of surface roughness on the adhesion force. The first sample is a smooth, p-type, Si(001) wafer with a 2 nm native oxide layer. The second sample is a rough Si(001) wafer that was roughened with an anisotropic wet chemical etchant. Anisotropic wet chemical etching was prefered as the method for surface roughening due to its ease of use and low cost. It also provides rather rough surfaces without physical damage to the bulk structure of the material [7,8].

The anisotropy of the etching process refers to the orientation dependence of the etch rate. This simply means that different surface sites show different reaction rates, i.e. it is slower along certain orientations than along others [9]. For silicon oxides in nonfluoride aqueous solutions, the anisotropic wet chemical etching process is determined by the reaction with water:

$$SiO_2 + 2H_2O = Si(OH)_4 \tag{2.3}$$

in three steps – adsorption, activated complex formation, and hydrolysis [10] as shown in Figure 2.4. The formation of bonds between the adsorbed hydrogen and bridging oxygen weakens the Si – O bond. This reaction causes removal of the silicon atom from surface as a $Si(OH)_4$.

Among the anisotropic etchants, we used ammonium hydroxide ($NH_4OH$) due to its mild toxicity and compatibility for working in our laboratory conditions. Before etching, the Si wafer pieces were cleaned in an ultrosonic bath of methanol for 15 min. Subsequently the wafers were placed in a piranha solution with a 3:1 volume ratio mixture of $H_2SO_4$ and $H_2O_2$ for 30 min. After these two cleaning steps, the Si wafers were rinsed in deionised water (DI), and dried with a flow of dry nitrogen. Finally, the Si wafers were chemically roughened in a solution of $NH_4OH : H_2O$ (1:5) at 80 °C for varying amounts of time from 1 min to 9 min, and again rinsed in DI water, and dried with $N_2$.

The etched samples were scanned with Scanning Electron Microscope (SEM) as shown in Figure 2.5. No pattern formation was observed between 1 min to 4 min of etching. However, from 5 min to 9 min of etching the formation of near-pyramidal hillocks, and shallow round pits with different size were observed. In literature, pyramidal hillocks are reported as the most characteristic surface features of Si(001) after anisotropic etching [11-16]. Even though the formation of this surface feature is still under debate, in general it is associated with four conditions [7,16]: (1) the existence of a micromasking agent which stabilizes the apex atom/s; (2) a fast downward motion of the floor surface; (3) stable pyramidal edges; (4) very stable pyramidal facets. If any one of these conditions fails, the hillocks will not be formed. For instance, if there is no pinning, the hillocks could not be generated, even if the other three conditions are fully satisfied. Like the pyramidal hillocks, the reasons of shallow round pits formation are also debated. The formation of round pits is thought to be associated with hydrogen bubbles, due to the geometrical match of the two objects. The round pits have also been related to bulk microdefects [17], although no conclusive evidence is provided. In contrast to the appearance of pyramidal hillocks, the round pits on Si(001) are claimed to appear when the stabilization mechanism is not present [7]. That means pyramidal hillocks and shallow round pits can not appear together on the same surface.

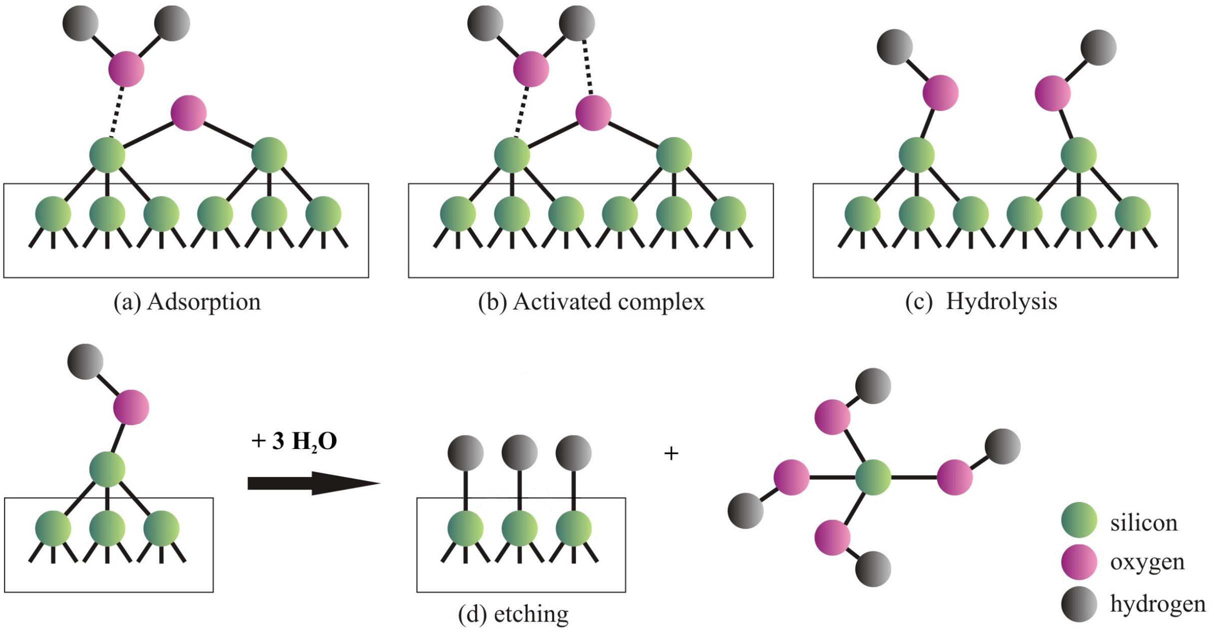

***Figure 2.4.*** *Three steps of etching process for silicon oxide in nonfluoride aqueous solutions. The etching leads to the removal of the silicon atoms as* $Si(OH)_4$ *products. Only the nearest underlying bulk atoms in the neighborhood of the surface are depicted in the figure.*

The hydrophilicity of all etched surfaces was characterized by a contact angle measurement using the sessile drop method. The contact angle experiments were performed with a Dataphysics OCA15+ goniometer at ambient conditions. The results of each sample are shown in the insets of Figure 2.5. A contact angle of 50±3° is found which shows that the average surface energy is not affected significantly by the etching process.

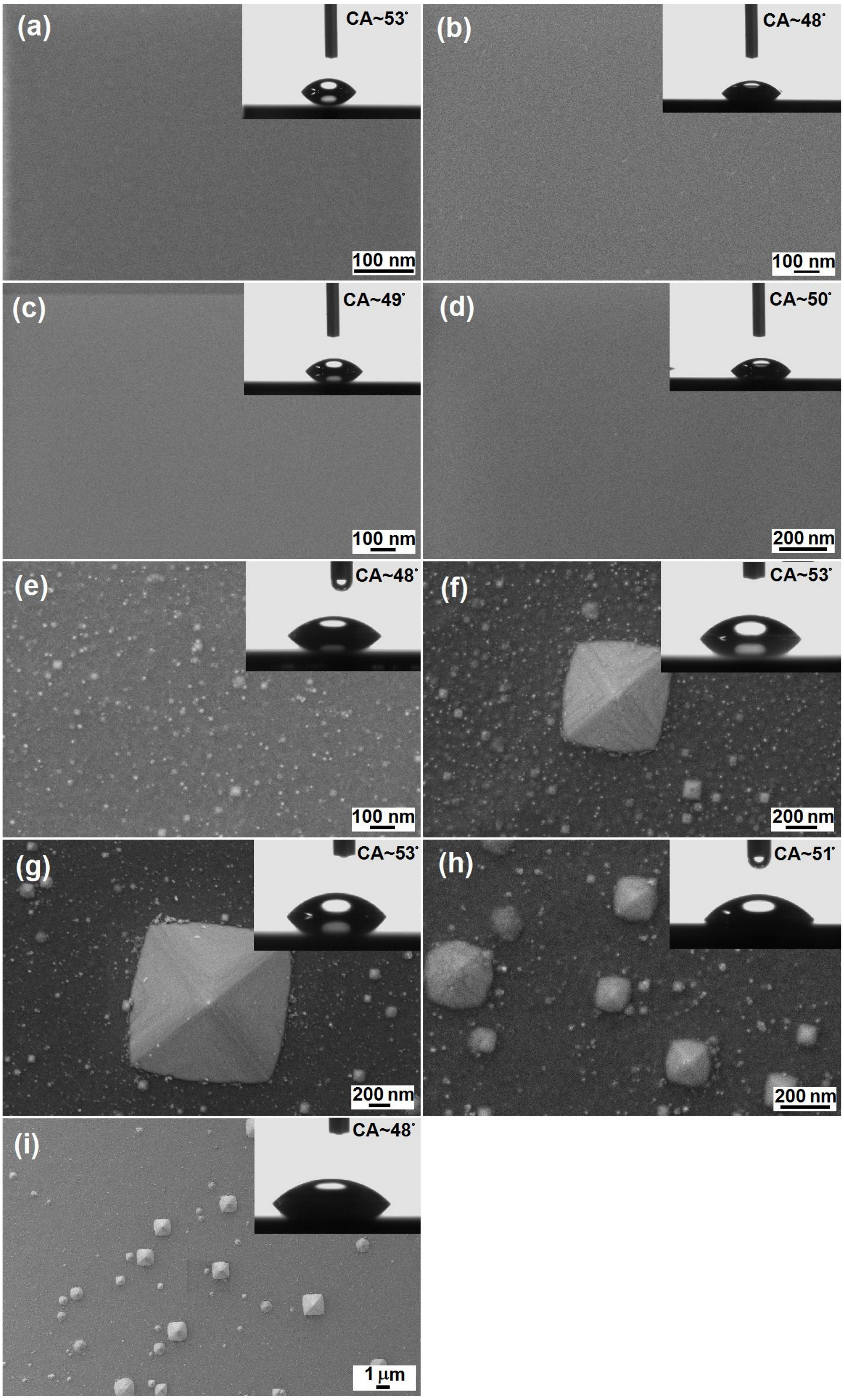

***Figure 2.5.*** *Scanning Electron Microscopy (SEM) image of chemically etched Si(001) surfaces for various etching time from 1 min* ***(a)*** *to 9 min* ***(i)*** *with 1 min increment. The insets depict a water droplet on surfaces with varying contact angles.*

## 2.4 Morphology characterization, the derivation of statistical quantities from AFM images

In order to resolve the morphology of the surfaces better, the AFM images of etched Si(001) were also recorded for etching times from 5 min to 9 min. A widely available software package Gwyddion, version 2.30, was used to analyse the AFM scans. Before analyses of the images, a suitable background subtraction has to be done. In this work the removal of the background in the AFM images was done in two steps. In the first step, the influence of misalignment of the sample and the bow of the scanner was removed by fitting a third order polynomial (in both directions) to the raw data. After the global surface curvature has been subtracted, many of the details in the images become clear. However, still some long range waviness and sometimes jumps in height in the slow scan direction were observed. This was directly related to the way the actual imaging takes place. Therefore a line by line median line correction was used as the second step. As a result, the AFM images of etched Si(001) surfaces were obtained as in Figure 2.6 for etching times from 5 min to 9 min with 1 min increments.

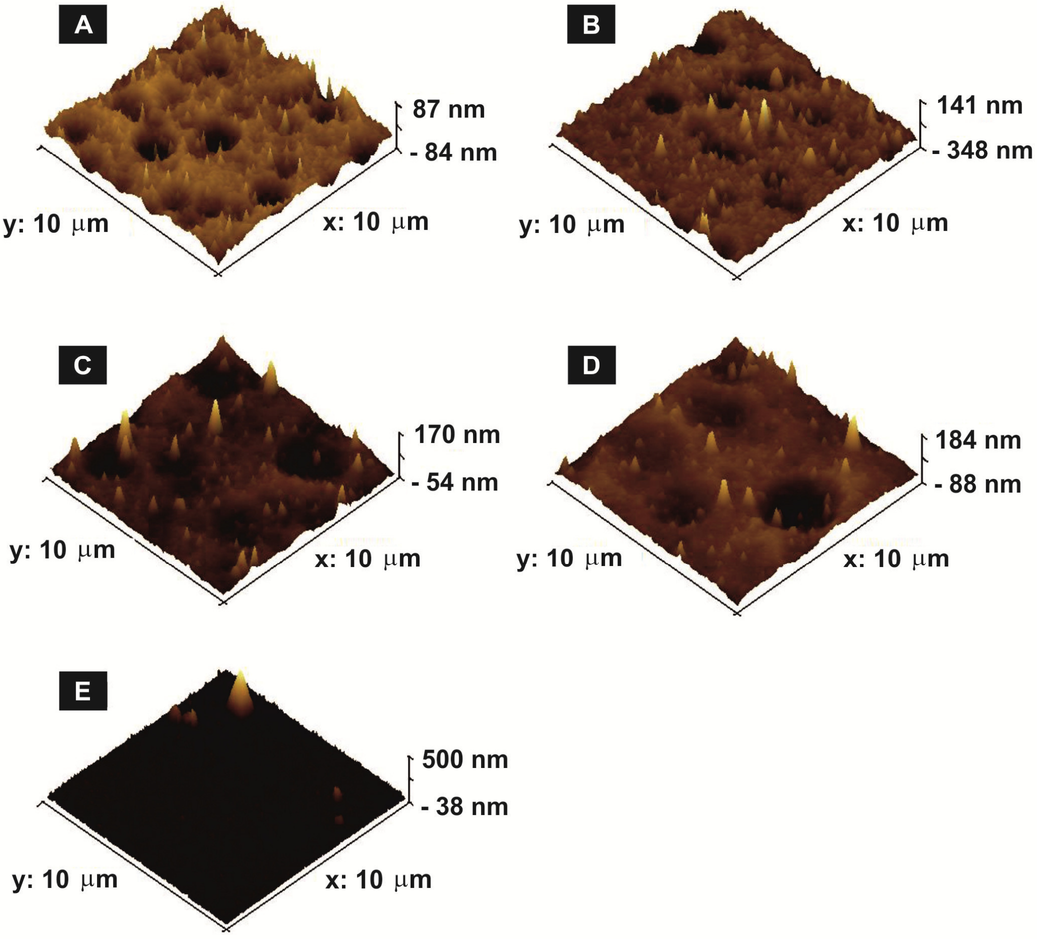

***Figure 2.6.*** *3-D Atomic Force Microscopy (AFM) image of etched Si(001) surfaces for etching time from 5 min* ***(A)*** *to 9 min* ***(E)*** *with 1 min increment. Here, the rms of the surfaces were measured as 13.7, 16.5, 17.5, 22.8, 28.1, respectively, with a silicon tip (Nanosensors, PPP-NCL-20) in tapping mode.*

As can been seen in both Figure 2.5 and Figure 2.6, only on 5 min etched sample, the pyramidal hillocks with large size are not observed. Most probably 5 min etching time is not enough for this surface pattern to grow up in large sizes on surface. The pyramidal hillock formation on etched surfaces would be a trouble for the adhesion force measurements. Therefore, we prefered to use only 5 min etched Si(001) for the adhesion force analysis, which will be the subject of future chapters of this Thesis. We need to make sure that the rough surface is homogeneous for the adhesion measurements. A simple way to test the homogeneity is to scan the sample in different places and compares the statistical properties obtained from different places. For that reason, extensive studies on morphology characterization and derivation of statistical quantities from AFM images were done for the 5 min etched Si(001) surface. Figure 2.7 shows the 3 different AFM images of chemically etched Si(001) for 5 min. These scans were taken with a size of 10x10, 20x20, and 80x80 µm and contain 512x512, 1024x1024, and 2048x2048 data points, respectively.

The characterization of the morphology of a surface describes the reduction of the height variation on the surface observed with an AFM into a few relevant statistical quantities, either as a set of numbers or in a graphical representation. Two different sets of morphology characterization tools are relevant, the first – order and second – order statistics.

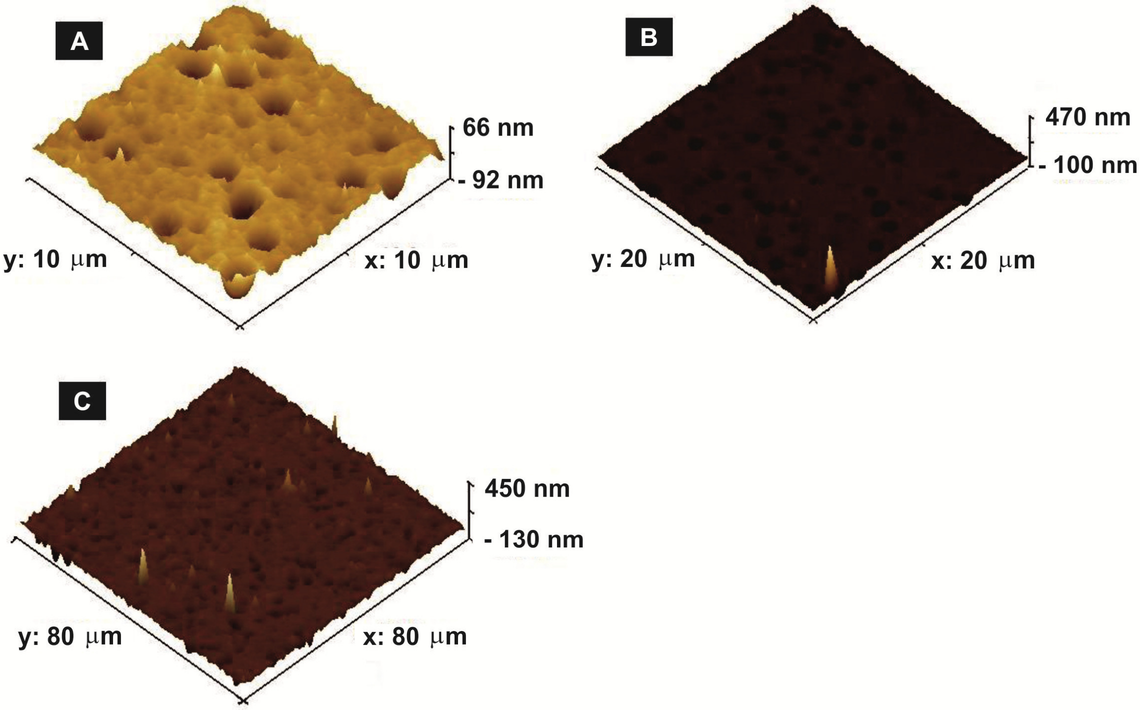

***Figure 2.7.*** *3-D Atomic Force Microscopy (AFM) image of etched Si(001) surfaces for an etching time of 5 min.* ***(A)*** *scan size is 10 x 10 µm with 512x512 data points* ***(B)*** *scan size is 20 x 20 µm with 1024x1024 data points* ***(C)*** *scan size is 80 x 80 µm with 2048x2048 data points. The scans were done with a diamond-like-carbon coated tip (Budget sensors, Tap190DLC) in tapping mode.*

## 2.4.1 First – order statistics

With first – order statistics the variation of the height with respect to a zero level is described. In this work the mean of the height variation is used as the zero level. The height variations of a surface can be depicted with a histogram of the distribution $p(h)$ of occurring heights $h$ [18]. Figure 2.8 shows the height histograms for 3 different AFM scans of chemically etched Si(001) for 5 min which shown in Figure 2.7. These histograms are normalized in such a way that :

$$\int_{-\infty}^{\infty} p(h)dh = 1 \tag{2.4}$$

The height variation can be expressed with a series of values, the so called moments $m_n$ defined as:

$$m_n = \int_{-\infty}^{\infty} p(h)h^n dh \tag{2.5}$$

Because usually at most only the first four moments are calculated, they have their own specific names:

- $m_1$ is the mean value, which has to be zero as a result of the background subtraction procedure used.
- $m_2$ is the variance of the surface height. The root mean square (rms) roughness, $w$, of a surface is defined as, $w = \sqrt{m_2}$ .
- $m_3$ is used to calculate the skewness $= m_3 / m_2^{3/2}$. The division makes that the skewness is a normalized dimensionless value. A non-zero value of the skewness implies an asymmetric distribution with the sign and magnitude a description of this asymmetry. For a symmetric distribution like a Gaussian distribution, the skewness is zero.
- $m_4$ is used to calculate the kurtosis $= m_4 / m_2^2 - 3$. The division makes that the kurtosis is a normalized dimensionless value. The kurtosis describes the deviation from a Gaussian distribution that has a kurtosis of 3.0.

The use of especially higher order moments has to be done with a great care. Just a few (dust) particles on the surface that are easily recognized as extreme heights in the image will alter the determined value of $w$ and especially the skewness and kurtosis.

The height histograms depicted in Figure 2.8 are very close to each other. This means that for the same sample, statistically the height distribution does not change with scan size. The height distribution is uniform over the entire sample. This ensures the homogeneity of the surface. Unfortunately, these distributions deviate from a Gaussian distribution, since all have an asymmetric tail extending out toward more negative height with respect to mean surface. This tells that the farther points on the surface are relatively below the mean surface level. In other words, the hole shapes are dominant on the surface which can be also seen clearly on AFM scans in Figure 2.7.

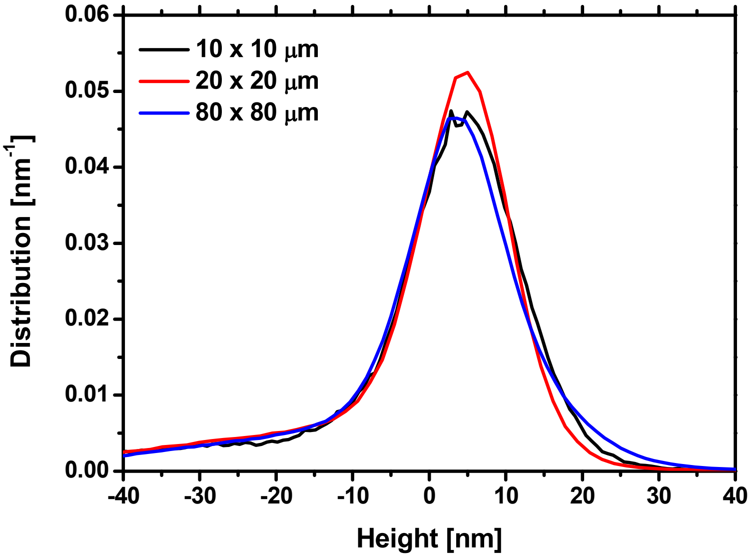

***Figure 2.8.*** *Histogram of a chemically etched Si(001) for 5 min for 3 different AFM images.*

### 2.4.2 Second – order statistics

In second – order statistics the relation between various heights on the surface is investigated. The basic idea behind this is that although points on the opposite side of an image can strongly vary in height, points that are within each others vicinity can differ in height only by a limited amount. The maximum difference at a large distance is directly related to the rms roughness of a surface. The lateral distance on which the heights can differ by an amount smaller than this maximum difference is called as the correlation length, $\xi$. There are three basic statistical depictions of this lateral relation between height: *the Autocorrelation*, *the Height-Height correlation* and *the Power Spectral Density function*. Because an AFM image is in essence a sequential probing of linescans, the analysis is limited to the fast scan directions. The results are an average of these fast scan spectra in the slow scan direction.

The 2D autocorrelation (AC) on a surface with a height profile $h(x, y)$ is defined as:

$$AC(\tau_1, \tau_2) = \int \int_{-\infty}^{\infty} h(x, y) h(x + \tau_1, y + \tau_2) dx dy \tag{2.6}$$

In a numerical implementation over the fast scan $(x)$ direction of a NxN image for the AC for a distance $r_m$:

$$AC(r_m) = \frac{1}{N(N-m)} \sum_{l=1}^{N} \sum_{k=1}^{M-m} h_{k+m,l} h_{k,l} \tag{2.7}$$

The value of AC(0) is the variance or rms value found from first order statistics.

The height-height correlation (HH) in the fast scan direction is defined as:

$$HH(r_m) = \frac{1}{N(N-m)} \sum_{l=1}^{N} \sum_{k=1}^{M-m} (h_{k+m,l} - h_{k,l})^2 \tag{2.8}$$

The relation between the AC and HH is clear when writing out the above formula. It gives $HH(r_m) = 2w^2 - 2AC(r_m)$. The reason for using the height-height correlation is that on a log-log scale a few of the basic parameters like rms roughness ($w$), the lateral correlation length ($\xi$), and the roughness exponent ($\alpha$) can be determined in a graphical manner as in Figure 2.9 :

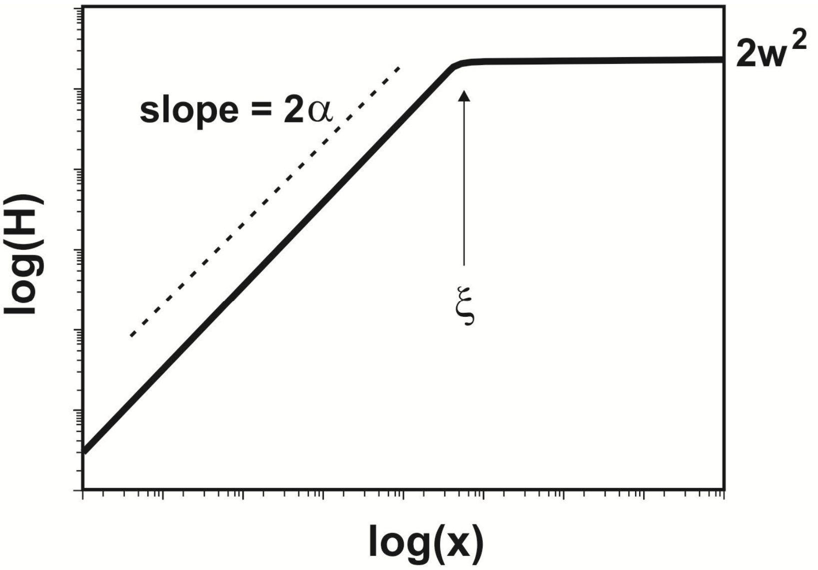

***Figure 2.9.*** *Log – log plot of the height – height correlation function of a surface. The rms roughness $w$ can be determined from the plateau at large x. The roughness exponent $\alpha$ can be extracted from the slope in the short range regime, and the lateral correlation length $\xi$ can be determined at the crossover region.*

The 1D Power Spectral Density (PSD) of a surface is essentially the Fourier transform of the Autocorrelation Function. Usually depicted on a log-log scale, it shows which lateral frequencies contribute to the image. For an ideally self-affine fractal surface, the PSD is a straight line with respect to $k$, and the slope tells the fractal dimension. In reality, there is a low-frequency cutoff due to component size, surface inhomogeniety or grain size. The high-frequency cutoff is usually due to the measurement resolution.

In Figure 2.10, the AC, HH and PSD graphs are shown that obtained with Gwyddion software for the AFM scans of etched Si(001) shown in Figure 2.7. From the HH correlation graph (Figure 2.10.b) the three parameters, $w, \xi$, and $\alpha$ have been derived graphically as 17.7 nm, 850 nm, and 0.503 nm, respectively. For $\alpha$, all AFM scans give different number, but we showed an average value here. The variation in the value of $\alpha$ would be related with the impact of the scan size and number of data points in each scan on determination of the value of $\alpha$. The PSD spectrum (Figure 2.10.c) shows a very similar behavior for 10 x 10 μm and 20 x 20 μm scan sizes, but for 80 x 80 μm scan beyond 0.01 nm$^{-1}$ a deviation occurs. In the beginning, the PSD of all scans is proportional to $k^{2+2\alpha}$, but for high frequency region (i.e. beyond 0.01 nm$^{-1}$) a deviation occurs. Part of this is associated with finite size effects. Also noise contributions, which also can explain the sharp peaks, play an important role. In order to make a reasonable approximation for the spatial wave vector dependence a green dashed line fitted to the high frequency region of the PSD with a slope of -2.

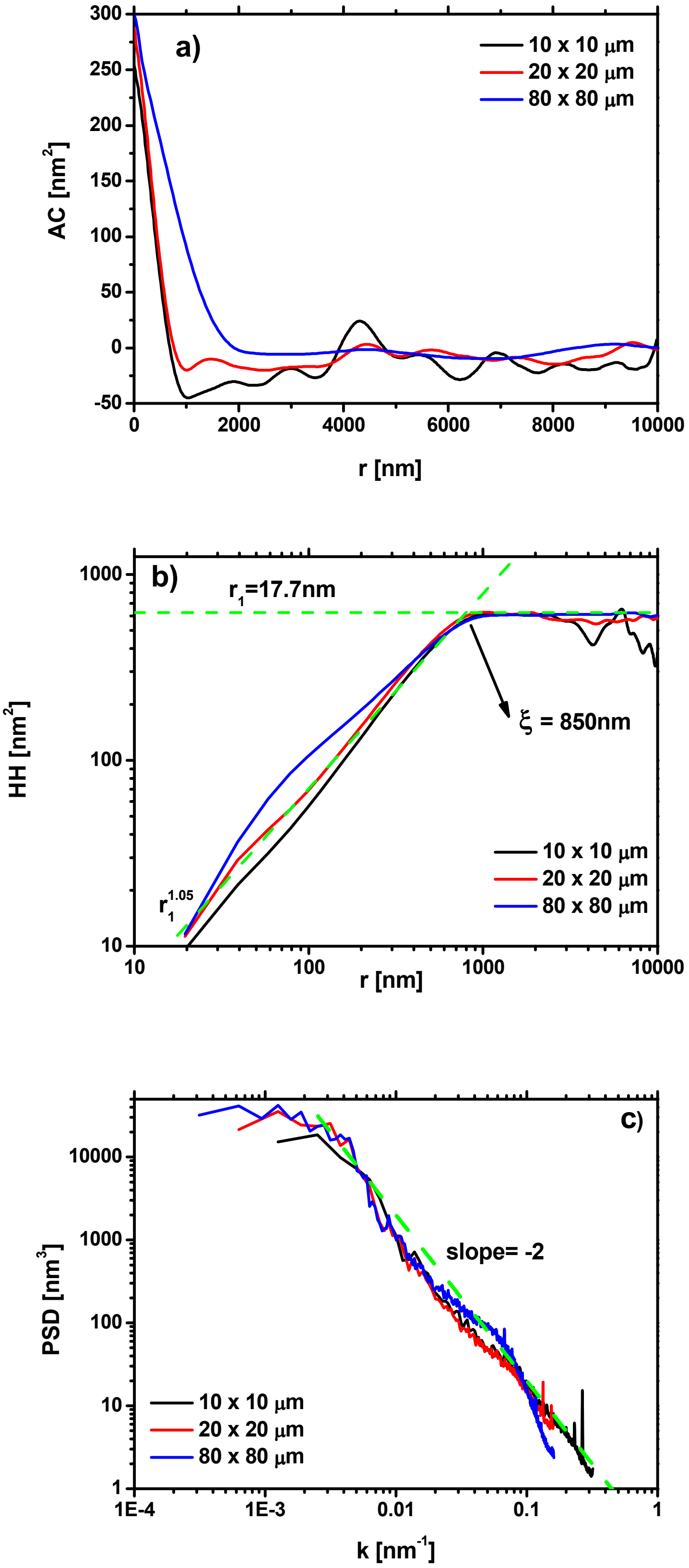

***Figure 2.10.*** *Second order statictics of 5 min etched Si(001).* ***a)*** *autocorrelation function* ***b)*** *height-height correlation,* ***c)*** *power spectrum density function of three different scan size.*

## 2.5 Humidity control system

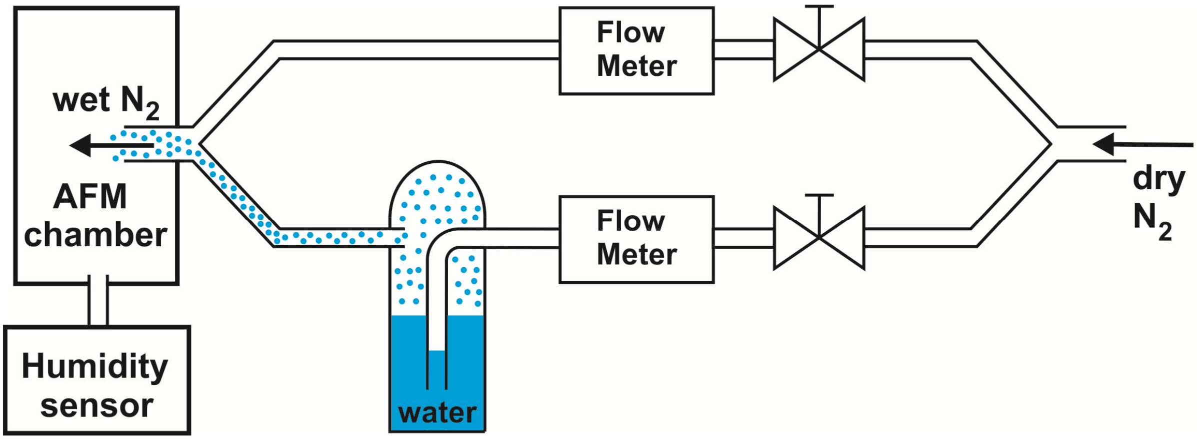

***Figure 2.11.*** *Schematic of the humidity control in the environmental chamber enclosing the AFM. The humidity was changed in a controllable way. The stream of dry* $N_2$ *was either fed into the chamber directly or mixed with the stream of wet* $N_2$ *that bubbled through pure water in a parallel channel. Humidity sensors were used for monitoring the change in humidity.*

The adhesion measurements with AFM were performed at controlled humidity conditions. This was realized by placing the AFM in an environmental chamber having a controlled and adjustable air flow. The air flow was a mixture of dry nitrogen and a stream of wet nitrogen. The latter flow was realized by bubbling the nitrogen gas through distilled water. Both flow lines were combined before entering the AFM chamber, which has a volume of around 1 liter. By adjusting the flow ratio the RH in the AFM chamber can be controlled. The actual RH was measured by two humidity sensors (SHT 75 Sensirion, Switzerland) located at different positions within the chamber to ensure a uniform humidity. The sensors have an absolute accuracy of 1.8% within the range 10% - 90%. The adhesion measurements were performed in this range of RH. A RH value of 0% was realized by using only dry nitrogen flow for 24 h prior to the adhesion force measurement. For each humidity value, the RH was allowed to reach its equilibrium value by waiting for at least 1h.

## 2.6 References

1. Tabor, D.; Winterton, R. H. S., *Proc. R. Soc. Lond.* **1969**, *A312*, 435 – 450.
2. Israelachvili, J. N.; Tabor, D., *Proc. R. Soc. Lond.* **1972**, *A331*, 19 – 38.
3. Binnig, G.; Quate, C. F.; Gerber, C., *Phys. Rev. Lett.* **1986**, *56*, 930 – 933.
4. Burnham, N. A.; Chen, X.; Hodges, C. S.; Matei, G. A.; Thoreson, E. J.; Roberts, C. J.; Davies, M. C.; Tendler, S. J. B., *Nanotechnol.* **2003**, *14*, 1 – 6.
5. Poggi, M. A.; McFarland, A. W.; Colton, J. S.; Bottomley, L. A., *Anal. Chem.* **2005**, *77*, 1192 – 1195.
6. Oberg, E.; Jones, F. D.; Horton, H. L.; Ryffel, H. H.; Grenn, R. E., *Machinery's Handbook*; Industrial Press, New York, **1996**.
7. Gosálves, M. A.; Nieminen, R. M., *New J. Phys.* **2003**, *5*, 100.
8. Knoch, J.; Appenzeller, J.; Lengeler, B.; Martel, R.; Solomon, P.; Avouris, P.; Dieker, C.; Lu, Y.; Wang, K. L.; Scholving, J.; del Alamo, J.A., *J. Vac. Sci. Technol. A.* **2000**, *19*, 1737 – 1741.
9. Gosálves, M. A.; Sato, K.; Foster, A. S.; Nieminen, R. M.; Tanaka, H., *J. Micromech. Microeng.* **2006**, *17*, S1 – S26.
10. Dove, P. M.; Rimstidt, J. D., *Reviews in Mineralogy and Geochemistry*, **1994**, *29*, 258 – 308.
11. Baum, T.; Schiffrin, D. J., *J. Micromech. Microeng.* **1997**, *7*, 338 – 342.
12. Baum, T.; Satherley, J.; Schiffrin, D. J., *Langmuir* **1998**, *14*, 2925 – 2928.
13. Tan, S. S.; Reed, M. L.; Han, H.; Boudreau, R., *J. Micromech. Microeng.* **1994**, *4*, 147 – 155.
14. Tan, S. S.; Reed, M. L.; Boudreau, R., *J. Microelectromech. Syst.* **1996**, *5*, 66 – 73.
15. Nijdam, A. J.; Van Veenendaal, E.; Cuppen, H. M.; Van Suchtelen, J.; Reed, M. L.; Gardeniers, J. G. E.; Van Enckevort, W. J. P.; Vlieg, E.; Elwenspoek, M., *J. Appl. Phys.* **2001**, *89*, 4113 – 4123.
16. Landsberger, L. M.; Naseh, S.; Kahrizi, M.; Paranjape, M., *J. Microelectromech. Syst.* **1996**, *5*, 106 – 116.
17. Haimi, E.; Lindroos, V. K., *Proc. 3rd Workshop on Physical Chemistry of Wet Etching of Silicon,* Nara, Japan, June **2002**, pp 74 – 77.
18. Zhao, Y.; Wang, G.-C.; Lu, T.-M., *Characterization of amorphous and crystalline rough surface: principles and applications*, Academic Press, London, **2001**.

# Chapter 3

# Surface adhesion and its dependence on surface roughness and humidity measured with a flat tip

*The adhesion force between a surface and the tip of an atomic force microscope cantilever has been determined by recording force-distance curves with an atomic force microscope. Flat tips with a diameter of 2 μm were used to mimic the adhesion between two parallel surfaces. In such a configuration, the location for the formation and breaking of the capillary water neck is a stochastic by nature, significantly different from that of a spherical tip. The adhesion force is measured as a function of relative humidity for smooth and chemically etched Si(001) surfaces. The roughness of the etched substrate reduces the adhesion by more than an order of magnitude, depending on the exact value of the relative humidity. The adhesion force increases with increasing humidity until a relative humidity of about 70%. Beyond a relative humidity of 70% a decrease of the adhesion force is observed. We anticipate that the latter is due to a decrease of the cross section of the water neck at the snap-off point with increasing relative humidity.*

## 3.1 Introduction

Adhesion refers to the attractive interaction between dissimilar surfaces. Adhesion plays a critical role in many technologically relevant areas, ranging from the processing of fine powders to the design and use of actuators in micro-electromechanical systems (MEMS) [1]. In all cases, the adhesion needs to be controlled [2]. For instance in the case of photocopying, a lack of adhesion of toner particles results in low quality images [3]. On the other hand, lithography in integrated circuit technology requires a low adhesion between the silicon (Si) wafer and the wafer tray. The throughput in such a system is severely affected by a strong adhesion between the wafer and the wafer tray. The strong adhesion can easily lead to breaking of precious processed Si wafers.

Surface adhesion can be tuned by structuring surfaces on the nanoscale. The influence of a nanoscale height variation on the actual adhesion force has been analyzed in several theoretical studies. A principal parameter used in most of these studies is the so-called root mean square (rms) roughness of the surface, i.e. the standard deviation of the height. In an analysis of Persson and Tosatti [4], the length scale of the height variation has also been considered. However, not only the morphology of a surface influences the adhesion, but also the surface energy, electrostatic contributions, Van der Waals forces, and capillary forces have to be taken into account. At ambient conditions, a water film is present on hydrophilic surfaces. This thin water film results in a curved meniscus between the substrate and the atomic force microscope (AFM) tip. The pressure drop across the meniscus gives rise to a capillary effect that produces a significant contribution to adhesion. Several experimental and theoretical studies [5-21] have been devoted to study capillary effects under controlled humidity by using AFM. They have demonstrated how sensitive the capillary force is to both the relative humidity as well as the tip/particle shape. The majority of adhesion studies are performed with a spherical shaped AFM tip, i.e. by sticking a small spherical particle at the apex of the AFM tip. In this study, however, we used a large flat AFM tip with a radius of 2 $\mu m$. This tip mimics the effect of the adhesion between two parallel surfaces. For such a geometry, the formation and breaking of the capillary water neck between a smooth substrate and a flat tip significantly differ from that between a smooth surface and a spherical tip. In the latter case, the position of the neck directly results from the geometry, while for two parallel surfaces the location(s) of neck formation(s) is a stochastic process. Despite this uncertainty in neck formation it is for many technological relevant applications much more appropriate to consider the interaction of a flat AFM tip with a substrate, rather than that of a spherical tip with a substrate.

In this study, we have measured the relationship between the adhesion force and relative humidity (RH) for both smooth and rough Si (001) surfaces by using an AFM tip with a large and flat cylindrical end (diameter of 2 $\mu m$). Large size flat AFM tips have only been used in a few experiments [22,23] to study adhesion behavior. Ando [22] measured the effect of condensed water on the friction and adhesion forces of hemispherical asperity arrays on Si produced by focused ion beam (FIB). He used a large tip in order to realize the multi-asperity contact, and measured the adhesion forces on separate asperities with radii of 129 and 427 nm respectively, as a function of humidity (up to 67%). Subsequently, he compared these results with arrays having radii of 168 and 452 nm, respectively. Ando found that the adhesion force of single asperities is independent of the RH, whilst on asperity arrays it increased with increasing value of RH.

In a subsequent publication [23], **he** studied the effect of condensed water on pull-off forces between a Ni tip with a 0.1 $\mu m^2$ flat area and a flat Si substrate by varying the contact time at a substrate temperature of 27 °C at a RH of 14%, 62% and 83%. **He** found that the adhesion force exhibited a local maximum at a RH of 14% RH. This local maximum decreased for a RH of 62% and 83% with increasing contact time.

In contrast to the previous studies we have used very large flat silicon tips with contact area of ~ 4 $\mu m^2$. The influence of roughness was studied by using smooth (rms roughness smaller than 1 nm) and etched surfaces (rms roughness of ~15 nm). The influence of the relative humidity was studied in the range of 0% to 80%.

## 3.2 Experimental details

### 3.2.1 Sample preparation and roughness measurement

Two different samples were used in our experiments. The first sample is a smooth, p-type, (001) oriented Si wafer with a 2 nm native oxide layer. Before the measurements, the surface was thoroughly cleaned in order to remove impurities, such as particulates, organic residues, metals and ionic species [24]. In order to clean the Si wafer it was placed in an ultrasonic bath of methanol for 15 min, followed by two cycles of rinsing in deionised water (DI) and drying using a dry $N_2$ flow. This resulted in a surface with very reproducible adhesion properties.

The second sample is a rough Si surface that was obtained using an anisotropic wet chemical etch. This method results in a slightly rough surfaces without physical damage to the materials bulk structure [25]. Before etching, the Si wafer was cleaned in an ultrasonic bath of methanol for 15 min Subsequently, the Si wafer was placed in a piranha solution with a 3:1 volume ratio mixture of $H_2SO_4$ and $H_2O_2$ for 30 min. After these two cleaning steps, the Si wafers were rinsed in DI water, and dried using a flow of dry nitrogen. Finally, the Si samples were chemically roughened in a solution of $NH_4OH / H_2O$ (1/5) at 80 °C for 5 min, again rinsed in DI water and dried using a flow of $N_2$.

In Figure 3.1.(a) a scanning electron microscope (SEM) image of a chemically etched Si(001) substrate is shown. After etching several large pyramidal hillocks and many small and shallow round pits were observed. These pits are better resolved in the AFM image shown in Figure 3.1.(b). These surface structures are characteristic for anisotropically etched Si(001) substrates [26-32]. For our adhesion measurements, we deliberately select areas which do not contain any large pyramidal hillocks, since this would lead to scatter in the adhesion force data.

The hydrophilicity of the smooth and etched surfaces was characterized by a contact angle measurement using the sessile drop method. The contact angle experiments were performed with a Dataphysics OCA15+ goniometer at ambient conditions. For both surfaces a contact angle 48 ± 2° was found, showing that the average surface energy is not affected significantly by the etching process.

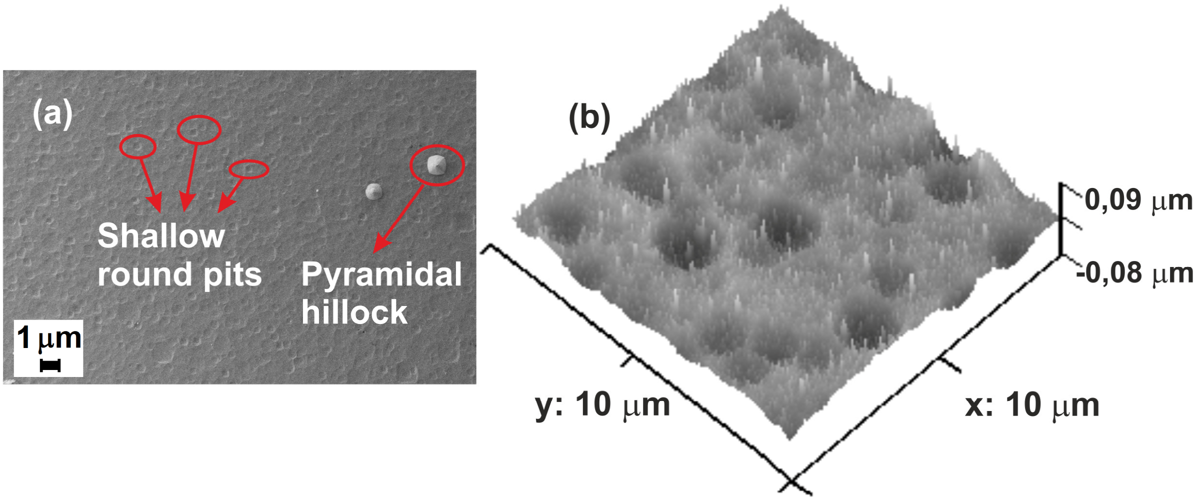

***Figure 3.1.*** ***(a)*** *SEM image of Si(001) after chemical etching for 5 min, and* ***(b)*** *AFM image of a selected area where the adhesion measurements are performed.*

The roughness of the samples was determined by analyzing many topographical AFM images (Figure 3.1.(b)). The AFM images were recorded with a silicon tip (Nanosensors, PPP-NCL-20) in tapping mode AFM. For the smooth silicon surface, an rms roughness of 0.67 nm was found, whilst for the 5 min etched sample an rms roughness value of 13.7 nm was measured.

### 3.2.2 Force – distance spectroscopy

The essence of force – distance spectroscopy is represented by the schematic cartoon of a force – distance curve in Figure 3.2. It shows the observed cantilever deflection (i.e. force) versus the displacement of the cantilever. Between positions (1) and (2), the tip approaches the surface without experiencing a noticeable interaction, since the tip is still far away from the surface. The cantilever is at its equilibrium position and the net force experienced by the AFM tip is zero. Upon approaching the surface, the AFM probe will eventually experience a net attractive force and the tip probe jumps into contact (2). This continues until a predetermined force limit is reached (3). Retraction of the AFM probe leads to the reverse process (4 – 5), however adhesion forces hinder the withdrawal of the tip. At 5, the net force is zero and the tip immediately snaps off. Subsequently, the cantilever goes back to its original starting position (6 – 7). From such a force-distance curve the adhesion force can be extracted by taking the distance between the maximum deflection point of the cantilever (5) during retraction and the zero deflection point (2).

The force – distance curves were collected with a Molecular Imaging AFM using a flat silicon tip (Nanosensors, PL2-NCLR-10). These tips were produced with a FIB and have a 2 $\mu m$ diameter contact area (see the inset of Figure 3.2). The force experienced by the tip was evaluated from the recorded deflection by multiplication with the spring constant of the cantilever. The spring constant (the normal component), $k$, of the cantilever was calculated according to

$$k = \frac{3E}{L^3}\left(\frac{t^3(a^2+4ab+b^2}{36(a+b)}\right) \qquad (3.1)$$

where $E$ is Young's modulus of silicon, $L$ is the length of the cantilever, $t$ is the cantilever thickness, and $a$ and $b$ are the width of top and bottom surfaces of the cantilever, respectively. A sweep time for recording the force – distance curve of 5 s was used.

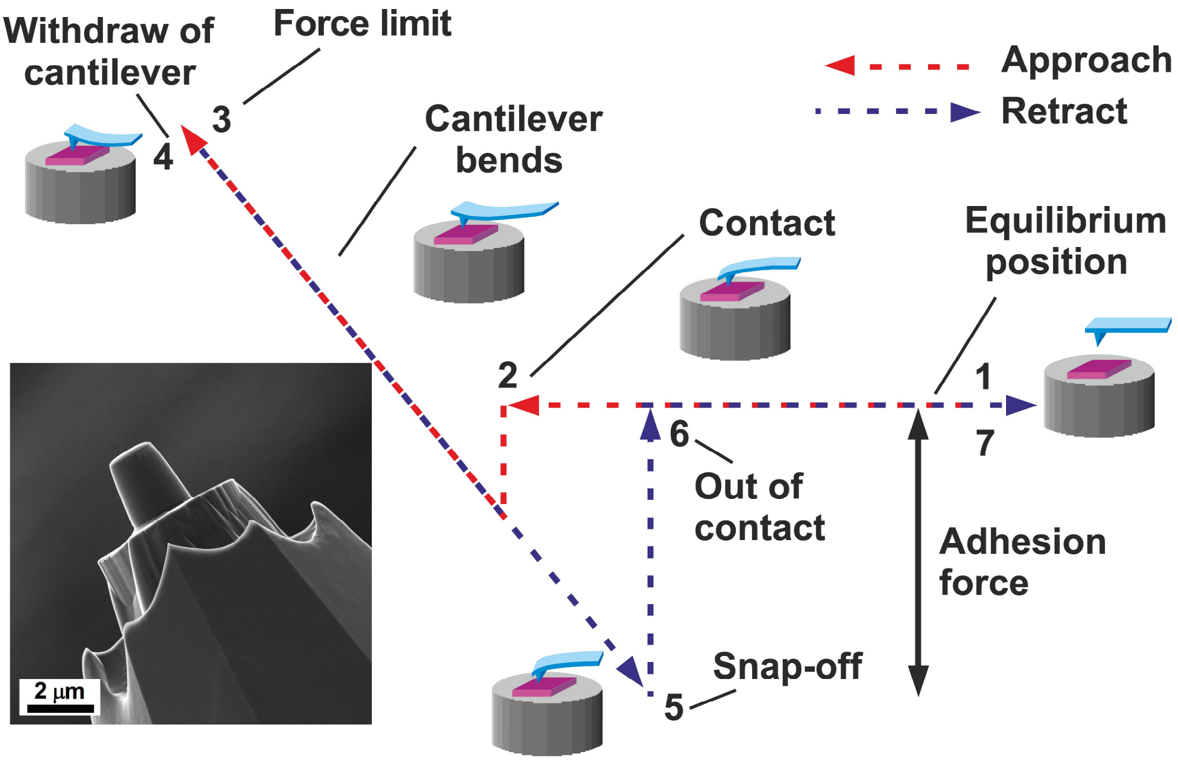

*Figure 3.2. Schematic representation of a force – distance curve. The inset shows a He ion microscope image of our flat AFM tip.*

### 3.2.3 Humidity control

The adhesion measurements with AFM were performed at controlled humidity conditions. This was realized by placing the AFM in an environmental chamber having a controlled and adjustable air flow. The air flow is a mixture of dry nitrogen and a stream of wet nitrogen. The latter flow was realized by bubbling the nitrogen gas through distilled water. Both flow lines were combined before entering the AFM chamber, which has a volume of around 1 liter. By adjusting the flow ratio the RH in the AFM chamber can be controlled. The actual RH was measured by two humidity sensors (SHT 75 Sensirion, Switzerland) located at different positions within the chamber to ensure a uniform humidity. The sensors have an absolute accuracy of 1.8% within the range 10% - 90%. The adhesion measurements were performed in this range of RH with 10% RH increments. A RH value of 0% was realized by using a dry nitrogen flow only. To minimize the amount of adsorbed water, the samples were placed in the chamber in a dry nitrogen ambient for at least 24 h prior to the adhesion force measurement. For each humidity value, the RH was allowed to reach its equilibrium value by waiting for at least 1 h.

## 3.3 Results and discussion

In the first series of experiments the adhesion force was measured at ambient conditions (RH around 40%). On the etched and smooth Si surfaces 25 force distance curves were measured at 10 different locations. No significant deviation between the different locations was observed. A histogram of the adhesion force evaluated from these 250 measurements is depicted in Figure 3.3. The distributions on both surfaces exhibit a log normal distribution as indicated by the dashed lines. These measurements showed that under ambient conditions, the adhesion force of an etched Si substrate is about 12 times smaller than the adhesion force of a smooth, unprocessed Si substrate.

In a second series of experiments the AFM was placed in the humidity controlled environment. Furthermore, great care was taken to properly align the flat tip with respect to the substrate. For a spherical tip this alignment is not crucial. However, for a flat tip a misalignment of one degree with respect to the parallel alignment between the surface of the flat tip and a smooth substrate leads to a dramatic decrease of the adhesion force as shown in the inset of Figure 3.4. For that reason, a best possible paralel orientation of tip and smooth substrate was adjusted by finding the maximum of the adhesion force as a function of the angle between flat tip and substrate. Note that, the shape of the f-d curve is not changed with this alignment procedure, as depicted in Figure 3.4. For etched surfaces the adhesion force is only weakly dependent on the alignment angle. The results depicted with this alignment procedure at a RH of 0% are also depicted in Figure 3.3. These experiments reveal that a proper control of alignment and humidity results in very narrow adhesion force distributions. We attribute the smaller distribution to the more standardized procedures observed for alignment and humidity. The average value of the adhesion force for the etched surface is slightly smaller with the more well defined conditions. This lower value can be attributed to the lower humidity. However, a much higher adhesion force for the smooth surface is found by optimizing the alignment procedure. A reduction by factor 64 due to surface roughness is now found. These measurements were repeated several times extending over a period of several months, revealing a very repeatable and precise value for the adhesion force of smooth Si(001). Therefore, the smooth Si(001) substrate is an excellent reference substrate for adhesion measurements.

In Figure 3.5.(a) the average values of the adhesion forces obtained with a flat tip for as received and chemically etched Si(001) surfaces are plotted as a function of relative humidity. As can be extracted from the graphs, the adhesion forces for both the smooth and the etched Si(001) surfaces depend strongly on the RH. This strong dependence is caused by the hydrophilicity of substrate and tip. The increase in adhesion force with increasing RH becomes notably steeper in the range of 30% to 70%. This observation is consistent with previous studies [33-35] and has been attributed to the influence of capillary forces.

Around 70% RH, the adhesion force shows a maximum value for the smooth as well as the etched surfaces. This significantly deviates from the results reported by Ando [23], who also used a flat tip to measure the adhesion force. In **his** measurement, the largest value of adhesion was observed at 14% RH. A lower value was found at RHs of 62% and 83%. The reason for the observed discrepancy is yet unclear. It is noted, however, that Ando's measurements were performed with a considerably smaller tip and also the material (Ni) of the tip is different.

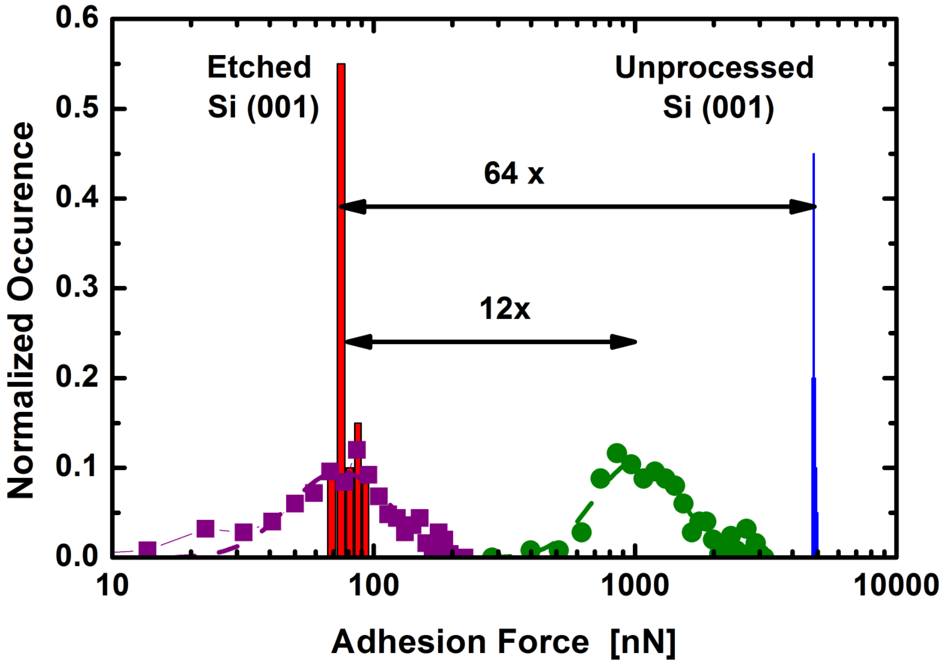

*Figure 3.3. Histograms of the adhesion forces between a flat tip and etched Si(001) (squares), and smooth Si(001) (circles). The bars indicate the adhesion force measurements for an accurately aligned tip at RH of 0% for both the etched (red) and smooth Si(001) (blue) surface.*

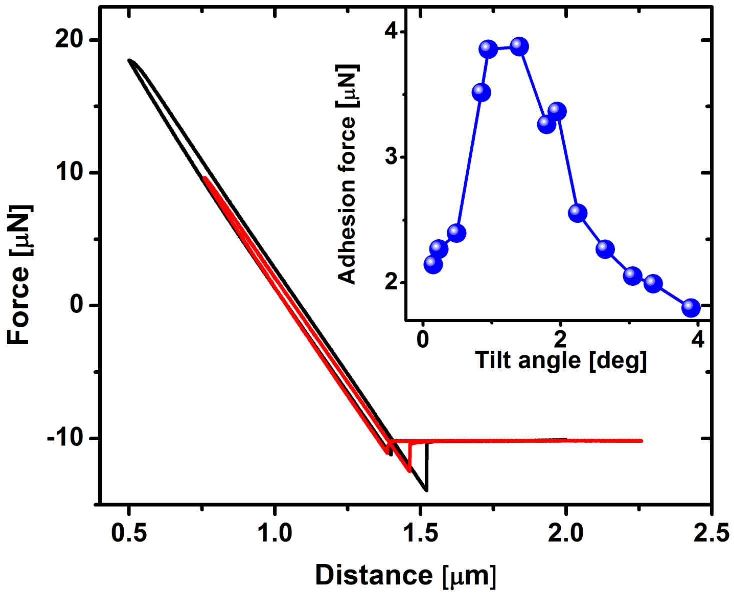

***Figure 3.4.*** *Force – distance curves between a flat tip and a smooth Si(001) surface. The best possible parallel alignment between the tip and sample surface is defined as the position with the highest adhesion force (black line). A random alignment of flat tip and substrate leads to a significant lower value of the adhesion force (red line). The inset shows the adhesion force as a function of the angle between flat tip and smooth Si(001) surface.*

At a RH larger than 70% a pronounced decrease in the adhesion force is observed for the smooth as well as the etched surfaces. Binggeli and Mate [36] explained this decrease in adhesion force at high RH by a delicate interplay between capillary forces and forces related to the chemical bonding of the water molecules [24]. It should be noted that our experimental results are in good agreement with several theoretical studies [18,37], which predicted a decrease of the adhesion force with increasing RH.

The influence of roughness as a function of humidity is quantified by the adhesion decrease graphed in Figure 3.5.(b). This shows that humidity strongly influences the effect of roughness. For the smooth surface, humidity results in a 40% increase in adhesion force, while for the rough surface a 4 fold increase is found. This results in a decrease in adhesion, of the rough substrate compared to the smooth one, of 64 at zero humidity to barely a factor 15 for RH of 70%. This can be explained by the rupture of the water film on the roughened surface. This results in a much smaller contact area of the water film. The much smaller remaining water contact area(s) on the rough surface will show a much smaller neck radius. The capillary effect of these smaller necks leads to a larger increase of the adhesion with the humidity.

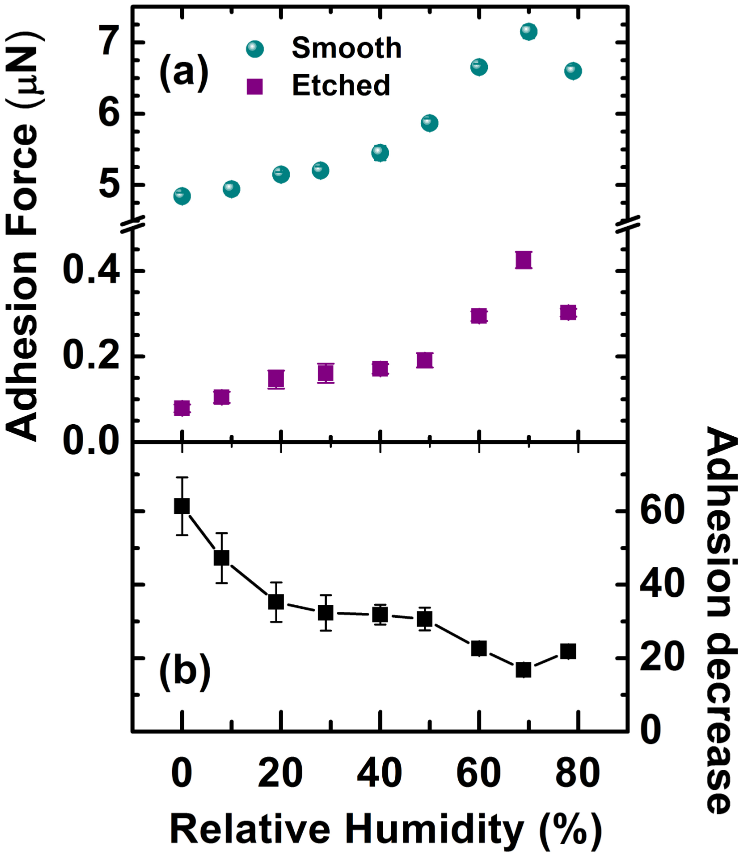

***Figure 3.5.*** ***(a)*** *Adhesion force as a function of RH for smooth and chemically etched Si(001) surfaces* ***(b)*** *The ratio of the adhesion forces (smooth divided by etched) versus RH.*

In an attempt to relate the adhesion force to the surface morphology, the power spectral density (PSD) of the smooth and etched surfaces was measured and evaluated. The PSD of each individual line scan was calculated and the averaged PSD of all scan lines is displayed in Figure 3.6. The PSD of the smooth surface is properly described by an algebraic relation, i.e. PSD = $wK^{\alpha}$ where $K$ is the spatial wave vector, $\alpha$ is a critical exponent and $w$ is a proportionality constant. For the exponent $\alpha$, a value of 1.9 was found. The rough surface can, however, not be fitted as properly by an algebraic relation. However, the red dashed line is a reasonable approximation for the spatial wave vector dependence. With this approximation, the PSD of the rough surface is about a factor of 100 larger than that of the smooth surface. This implies a factor of 100 increase in roughness, which is significantly more than the factor of 20 found from the rms roughness. The factor of 100 increase in roughness can be directly related to the factor of 64 decrease in surface adhesion for zero humidity as shown in Figure 3.5. Note that even for zero humidity a water layer remains on the surface. This results in an underestimation of the influence of roughness. Theoretical descriptions of the adhesion force based on surface contact area predict a linear relation between adhesion force and surface roughness, provided at least that the surface energy remains unaltered [38,39]. Contact angle measurements of both surfaces showed a similar contact angle indicating that the surface energy of smooth an etched is the same. It should however be pointed out that the aforementioned theories did not take capillary forces into account.

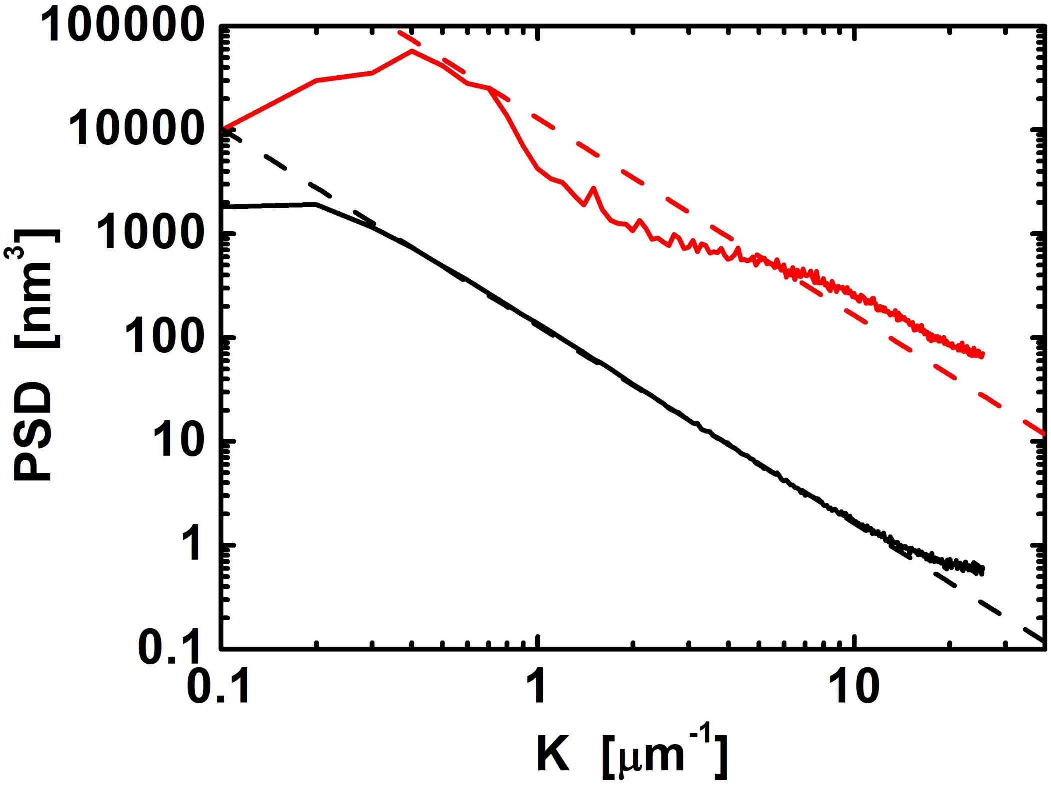

***Figure 3.6.*** *Power spectral densicty of the morphology of smooth Si(001) (black) and etched Si(001) (red). The dashed lines are algebraic fits of the PSD's.*

### 3.4 Conclusions

We have measured the adhesion force between a surface and a flat tip with a diameter of 2 $\mu m$ by recording force – distance curves with an atomic force microscope. The adhesion force is measured as a function of humidity for smooth and chemically etched Si(001) surfaces. The adhesion force of a smooth as received Si(001) substrate is more than an order of magnitude larger than that of a chemically etched Si(001) substrate. The roughened surface shows a much larger relative increase in adhesion with humidity than the smooth surface. As a result, the adhesion is reduced 4 times more at zero humidity compared to a RH of 70%. Above a RH of 70% a decrease in the adhesion force of the smooth as well as the rough surfaces is observed. The latter is probably caused by an effective decrease of the (average) cross section of the water neck at the snap – off point with increasing RH.

## 3.5 References

1. DelRio, F. W.; de Boer, M. P.; Knapp, J. A.; Reedy Jr., E. D.; Clews, P. J.; Dunn, M. L., *Nat. Mater.***2005**, *4*, 629 – 634.
2. Ferreira, O. D. S.; Gelinck, E.; de Graaf, D.; Fischer, H., *Appl. Surf. Sci.* **2010**, *257*, 48 – 55.
3. Mastrangelo, C. J., *Photogr. Sci. Eng.* **1982**, *26*, 194 – 197.
4. Persson, B. N. J.; Tosatti, E., *J. Chem. Phys.* **2001**, *115*, 5597 – 5610.
5. Xiao, X.; Qian, L., *Langmuir* **2000**, *16*, 8153 – 8158.
6. Asay, D. B.; Kim, S. H., *J. Chem. Phys.* **2006**, *124*, 174712.
7. Feiler, A. A.; Stiernstedt, J.; Theander, K.; Jenkins, P.; Ruthland, M. W., *Langmuir* **2007**, *23*, 517 – 522.
8. Fukunishi, A.; Mori, Y., *Adv. Powder Technol.* **2006**, *17*, 567 – 580.
9. He, M.; Blum, A. S.; Aston, D. E.; Buenviaje, C.; Overney, R. M.; Luginbühl, R., *J. Chem. Phys.* **2001**, *114*, 1355 – 1360.
10. Paajanen, M.; Katainen, J.; Pakarinen, O. H.; Foster, A. S.; Lahtinen, J., *J. Colloid Interface Sci.* **2006**, *304*, 518 – 523.
11. Rabinovich, Y. I.; Adler, J. J.; Esayanur, M. S.; Ata, A.; Singh, R. K.; Moudgil, B. M., *Adv. Colloid Interface Sci.* **2002**, *96*, 213 – 230.
12. Sedin, D. L.; Rowlen, K. L., *Anal. Chem.* **2000**, *72*, 2183 – 2189.
13. Jang, J.; Schatz, G. C.; Ratner, M. A., *J. Chem. Phys.***2004**, *120*, 1157 – 1160.
14. Zhao-Xia, L.; Li-Juan, Z.; Hou-Hui, Y.; Hai-Ping, F., *Chin. Phys. Lett.* **2007**, *24*, 2289 – 2292.
15. Chen, S. C.; Wei, P. J.; Lin, J. F., *Jpn. J. Appl. Phys.* **2009**, *48*, 055001.
16. Butt, H. J.; Kappl, M., *Adv. Colloid Interface Sci.***2009**, *146*, 48 – 60.
17. Farshchi-Tabrizi, M.; Kappl, M.; Cheng, Y.; Gutmann, J.; Butt, H. J., *Langmuir* **2006**, *22*, 2171 – 2184.
18. Pakarinen, O. H.; Foster, A. S.; Paajanen, M.; Kalinainen, T.; Katainen, J.; Makkonen, I.; Lahtinen, J.; Nieminen, R. M., *Model. Simul. Mater. Sci. Eng.* **2005**, *13*, 1175 – 1186.
19. Chau, A.; Régnier, S; Delchambre, A.; Lambert, P., *Model. Simul. Mater. Sci. Eng.* **2007**, *15*, 305 – 317.
20. Chau, A.; Régnier, S; Delchambre, A.; Lambert, P., *J. Adhes. Sci. Technol.* **2010**, *24*, 2499 – 2510.
21. Chen, S. H.; Soh, A. K., *J. Solids, Struct.* **2008**, *45*, 3122 – 3137.
22. Ando, Y., *Wear* **2000**, *238*, 12 – 19.
23. Ando, Y., *Langmuir* **2008**, *24*, 1418 – 1424.
24. Farshchi-Tabrizi, M., *On the adhesion between fine particles and nanocontacts: an atomic force microscope study*. Ph.D. thesis, University of Siegen, **2007**.
25. Gosálvez, M. A.; Nieminen, R. M., *New J. Phys.* **2003**, *5*, 100.
26. Baum, T.; Schiffrin, D. J., *J. Micromech. Microeng.* **1997**, *7*, 338 – 342.
27. Baum, T.; Satherley, J.; Schiffrin, D. J., *Langmuir* **1998**, *14*, 2925 – 2928.
28. Tan, S. S.; Reed, M. L.; Han, H.; Boudreau, R., *J. Microelectromech. Syst.* **1996**, *5*, 66 – 72.

29. Nijdam, A. J.; Van Veenendaal, E.; Cuppen, H. M.; Van Suchtelen, J.; Reed, M. L.; Gardeniers, J. G. E.; Van Enckevort, W. J. P.; Vlieg, E.; Elwenspoek, M., *J. Appl. Phys.* **2001**, *89*, 4113 – 4123.
30. Landsberger, L. M.; Naseh, S.; Kahrizi, M.; Paranjape, M., *J. Microelectromech. Syst.* **1996**, *5*, 106 – 116.
31. Tan, S. S.; Reed, M. L.; Han, H.; Boudreau, R., *J. Micromech. Microeng.* **1994**, *4*, 147 – 155.
32. Zhang, X. G., *Electrochemistry of Silicon and Its Oxide*, Kluwer Academic Publishers, New York, **2004**, p. 151.
33. Ata, A.; Rabinovich, Y. I.; Singh, R. K., *J. Adhes. Sci. Technol.* **2002**, *16*, 337 – 346.
34. Biggs, S.; Cain, R. G.; Dagastine, R. R.; Page, N. W., *J. Adhes. Sci. Technol.* **2002**, *16*, 869 – 885.
35. Jones, R.; Pollock, H. M.; Cleaver, J. A. S.; Hodges, C. S., *Langmuir* **2002**, *8*, 8045 – 8055.
36. Binggeli, M.; Mate, C. M., *J. Appl. Phys. Lett.***1994**, *65*, 415 – 417.
37. Köber, M.; Sahagún, E.; García-Mochales, P.; Briones, F.; Luna, M.; Sáenz, J. J., *Small* **2010**, *6*, 2725 – 2730.
38. Derjaguin, B. V.; Muller, V. M.; Toporov, Y. P., *J. Colloid Interface Sci.* **1975**, *53*, 314 – 326.
39. Johnson, K. L.; Kendall, K.; Roberts, A. D., *Proc. Royal Soc. London* **1971**, *A324*, 301 – 313.

# Chapter 4

# The influence of instrumental parameters on the adhesion force in a flat-on-flat contact geometry

*Atomic force microscopy (AFM) has been used to measure the adhesion force between a flat Si(001) wafer and a micrometer sized flat silicon AFM tip. Force-distance curves have been recorded at different setpoints in order to elucidate their individual effect on the derived adhesion force. No dependence of the derived adhesion force on the applied load has been detected, making sure that no plastic changes in the morphology of either tip and/or sample occur. Other setpoints as the residence time of the tip at the substrate, the relative humidity, the size of the tip and the retraction velocity of the tip have been varied systematically. We have found that the adhesion force depends strongly on the velocity of the z-piezo and the tip size while, at least within the 0.5 - 41 s time window, the residence time does not have any measurable effect on the adhesion force. The increase of the adhesion force with increasing retraction speed is solely ascribed to the viscous force. Finally, the adhesion force increases with increasing relative humidity.*

## 4.1 Introduction

The notion of adhesion between two surfaces, i.e. that a force is required to separate two materials, is already quite old [cf. 1]. Simple experiments on a macroscopic scale show that area, humidity and separation velocity (hydrodynamic adhesion) are important parameters. The adhesion depends heavily on the roughness of a surface and thus one can manipulate the adhesion by structuring the surface on the micro-, or even the nanoscale. In some cases, e.g. wafer handling in semiconductor industry, the adhesion force needs to be minimized as much as possible in order to allow swifter handling times. In other cases, e.g. a gecko, one prefers to maximize the adhesion force. In order to benefit from the adhesion properties of a substrate in a controlled way, one has to study the adhesion on a length scale down to microns or even to nanometers.

The adhesion force between two surfaces physically originates from Van der Waals forces, electrostatic forces, intermolecular forces, Casimir forces or meniscus forces depending on physical and/or chemical properties of these surfaces [2]. With the use of atomic force microscopy (AFM), it has become possible to measure these interaction forces with a resolution down to nN or even pN using different types of AFM probes [3]. Many studies of adhesion forces have been reported and the influence of several experimental parameters has been examined. Typical variables include the relative humidity, the roughness of the substrate, the applied load on the tip, the size of the tip, the contact time and the retraction speed of the tip. However, many studies, performed so far, only consider a subset of these parameters while ignoring other, possibly relevant, ones. This renders a meaningful comparison between different results difficult.

In this study we systematically varied experimental variables, such as load, contact time, contact area, relative humidity and retraction speed in order to arrive at a complete picture of the parameters that affect the adhesion forces between flat surfaces. We did so for a well defined system: a smooth surface probed with a flat tip. This approach has two clear benefits: (1) it allows one to compare adhesion force studies and (2) it gives a more complete insight in the physics of adhesion. To the best of our knowledge our present report is the first to break down the problem by investigating each relevant parameter individually. We concentrate on hydrophilic flat surfaces for both tip and sample.

## 4.2 Experimental details

All the adhesion force measurements were performed with a Molecular Imaging AFM using a flat n-type silicon tip (Nanosensors, PL2-NCLR-10). The circular surface of the flat topped, cone shaped silicon tip has a diameter of ~ 1.8 $\mu m$ (see Figure 4.1.(a)). In order to measure the effect of the tip size on the adhesion force, the size was decreased to ~ 0.9 $\mu m$ (see Figure 4.1.(b)) using a Focused Ion Beam (FIB). The adhesion force experienced by the tip was extracted from the force-distance curve between the maximum deflection point of the cantilever just before it snaps-off and the zero deflection point at the freestanding position of the cantilever. The cantilever has a trapezoidal shape and its spring constant is calculated according to a method put forward in ref. [4].

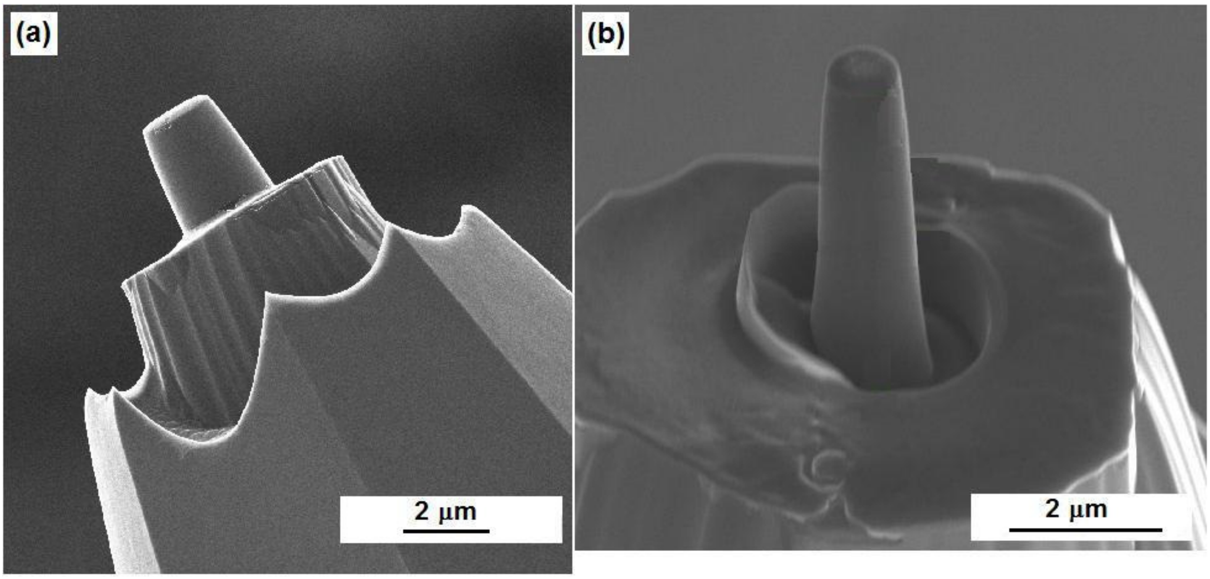

***Figure 4.1.*** *The flat AFM probe:* ***(a)*** *He Ion Microscopy (HIM) image of a tip with a diameter of ~ 1.8* $\mu m$*,* ***(b)*** *Scanning Electron Microscopy (SEM) image of a FIB modified tip with a diameter of ~ 0.9* $\mu m$.

The sample is a p-type Si(001) wafer with a 2 nm native oxide layer with a root-mean-square roughness of less than 1 nm. The sample was cleaned in an ultrasonic bath of aceton for 15 minutes, and then boiled in isopropanol for 5 min at 85 °C, and dried using a dry $N_2$ flow.

The sample was placed on a sample holder that could be adjusted at different tilt angles. The optimal angle was determined by maximizing the adhesion force [5], which corresponds to a plan parallel configuration. All data reported below have been taken with this optimum alignment, i.e. the tip and the substrate were always perfectly parallel. The humidity was controlled by adjusting the flow ratio of dry and wet nitrogen streams. The relative humidity (RH) in the chamber was measured with two humidity sensors (SHT 75 Sensirion, Switzerland) located at two different positions in the chamber with a volume of 1 liter. After changing the flow ratio, the RH was allowed to reach its equilibrium value by waiting for more than one hour. The 'dry' condition was obtained after purging with dry nitrogen for at least 12 h. The force distance curves were collected with an approach/retract cycle of the tip by modulating the cantilever at a frequency well below its resonance frequency. These curves were recorded with the Molecular Imaging (MI) software as well as via a break-out box with a HP digital oscilloscope. The much more stable time basis of the oscilloscope was used to measure the response of the cantilever deflection including snap – in, and snap – off as shown in detail in Figure 4.2. The deflection voltage and the drive voltage of the cantilever were recorded simultaneously. Several factors that were reported to have an impact on the adhesion force are elucidated with the force-time curve as depicted in Figure 4.2. The residence time is defined as the contact time between sample and tip between the snap – in and snap – off points. The total time is defined as the time to record a complete force – distance curve, including the time that the tip does not make any contact with the substrate. During the adhesion measurements, the tip is pushed to the substrate until a maximum normal load value is reached. This load is kept constant until the withdrawal of the tip. We varied the applied load between 4 $\mu N$ and 22 $\mu N$ and analyzed the impact of this variation in load force on the adhesion force. The retraction velocity of the piezo was also varied systematically. It is pointed out here that we kept the displacement distance of the tip constant and only varied the total time to record the force – distance trace in order to vary the piezo velocity. Note that only the velocity of the piezo can be measured as the actual tip velocity can not be detected. Of course, when one parameter was varied systematically, all others were kept constant. For insight into the influence of the tip size we used flat tips with diameters of about 1.8 and 0.9 $\mu m$. The influence of humidity on the adhesion force was measured at the same piezo velocity and load.

Each reported adhesion force in this work was obtained by measuring 20 consecutive force-distance curves and taking the average of these 20 measurements. This provides a highly accurate value of the adhesion force. In all cases, we did not observe any significant difference between the first measurement on a virgin surface and subsequent ones. The reported error is the standard deviation obtained from this series of measurements.

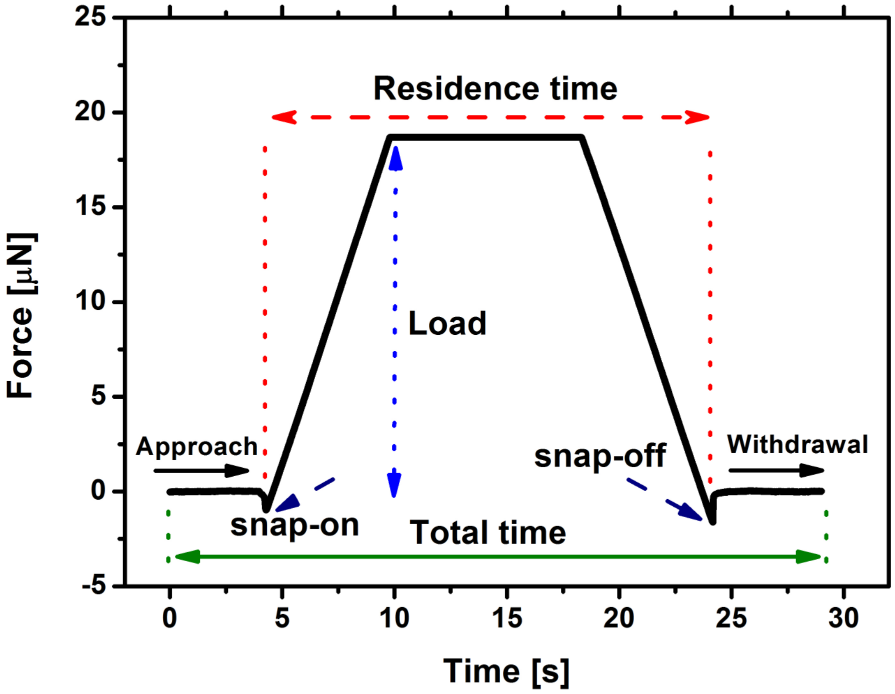

*Figure 4.2. Scheme of the force experienced by the tip as a function of time.*

## 4.3 Results and discussion

The notions adhesion force and pull – off force are used indifferently throughout literature. Their meaning is commonly considered interchangeable. Although pull – off force is certainly the most general and applicable term for the actually measured quantity, we comply with the overwhelming majority in literature and stick to adhesion force. It is noted, however, that in some highly dynamic cases the term pull – off force might be more adequate.

### 4.3.1 Impact of externally applied load on the flat AFM tip

Beforehand it is noted that not the load but rather the pressure, i.e. the load divided by contact area, is of crucial importance. Since the shape and size of the contact area is not always well known it is hard to compare the results from different experiments. However, as long as one operates in the elastic window the contact area is supposed to remain constant within one experiment. Therefore, below we stick to referring to load instead of pressure.

The adhesion force of a surface can change from measurement to measurement because the contact between tip and surface is not always elastic. This effect is illustrated nicely in Figure 4 of ref. [6], showing that the adhesion force can easily change by 20%, depending on the maximum load. Plasticity obviously leads to changes in the morphology of the contact area and thus to non-intrinsic effects. This implies that the elasticity of the contact area during adhesion force measurements should be checked for different loading forces.

Figure 4.3 shows the adhesion force between the flat AFM tip with a diameter of ~ 0.9 $\mu m$ and smooth Si(001) at various applied normal loads. The piezo velocity and the residence time were set at 0.65 $\mu m / s$ and 2 s, respectively. As is immediately obvious from the figure the adhesion force does not depend on the load within the experimental error. Obviously, the data plotted in Figure 4.3 have been recorded inside the elastic regime.

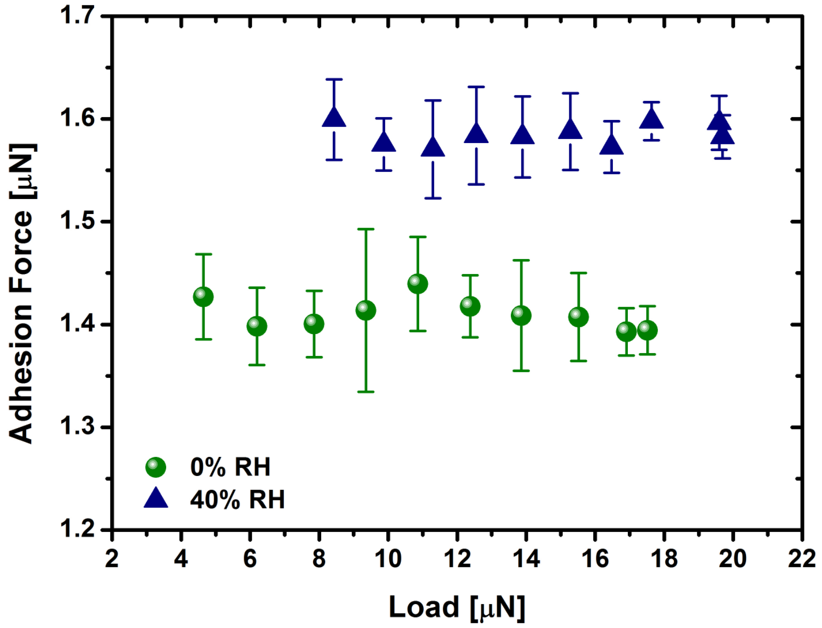

***Figure 4.3.*** *The adhesion force of a Si(001) surface measured with a flat AFM tip versus applied normal load. The flat tip diameter is 0.9 $\mu m$. The results were obtained with a piezo velocity of 0.65 $\mu m/s$.*

In Figure 4.3, the error bar for the adhesion force obtained for each individual load level is quite large. The size of the error bar is the result of variations in the adhesion force value from one measurement to another. In Figure 4.4, as an example of such variations, adhesion forces obtained in 20 consecutive measurements at the same location (neglecting some possible drift) are shown. Figure 4.4.(a) shows data for two different applied loads of 4.6 $\mu N$, and 17.5 $\mu N$, respectively, obtained at 0% RH. In Figure 4.4.(b), a similar variation of 20 consecutively adhesion force measurements are shown at 40% RH, for two applied loads of 8.4 $\mu N$, and 19.7 $\mu N$, respectively. As seen from the Figures 4.4.(a) and 4.4.(b), there is no tendency for either an increase or a decrease between the individual measurements. The variation in the data set is random, and we do not observe any indication of any dependence of the measured adhesion force on the applied load. Since the adhesion force does not depend on the applied load we have to conclude that the contact between the flat AFM tip and Si(001) sample is purely elastic, i.e. there is neither a (plastic) deformation nor any material transfer between tip and sample. In Figure 4.3, the adhesion force increases with increasing relative humidity. As pointed out before (e.g. ref. [5] and references therein), the reason that the adhesion force increases with increasing relative humidity is related to the presence of condensed water between the tip and the substrate.

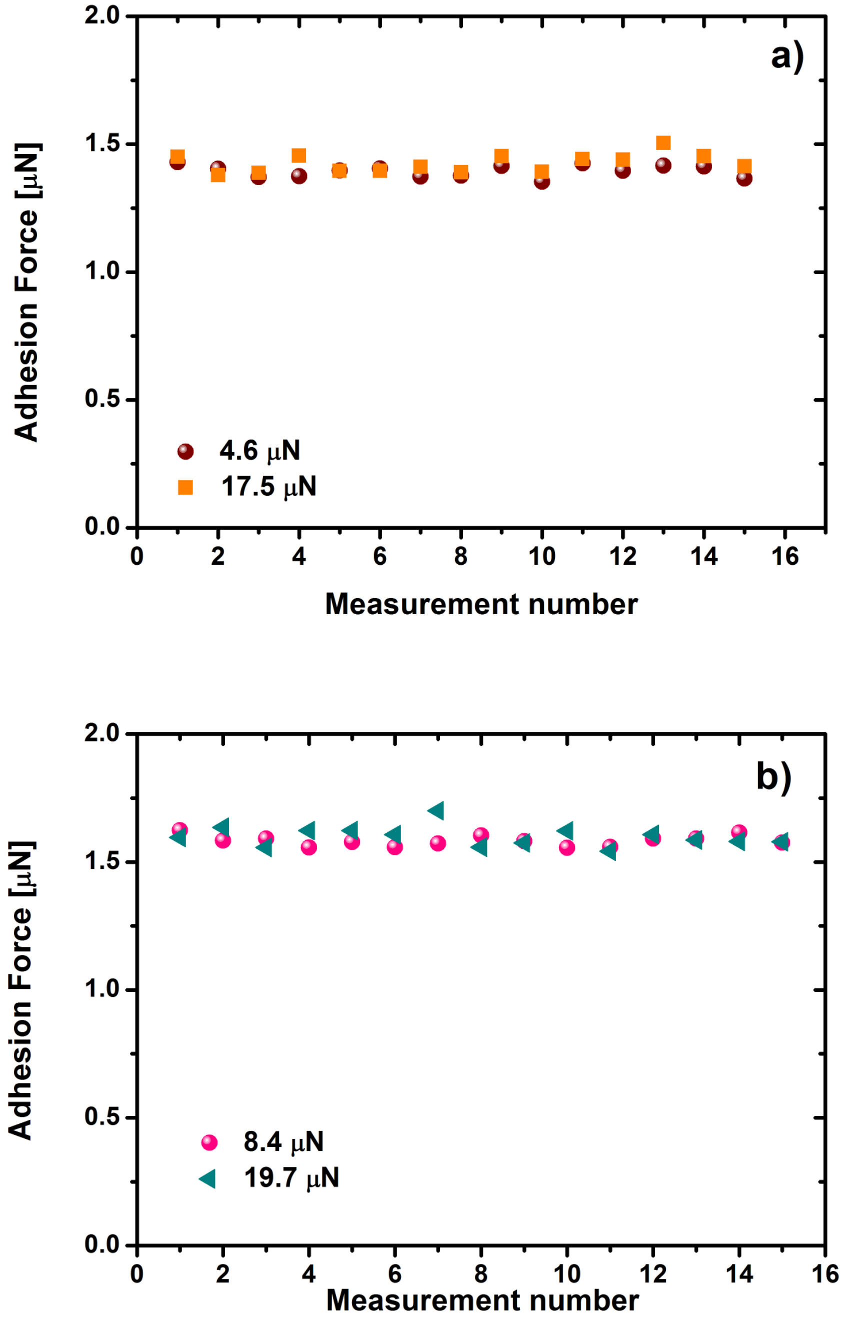

*Figure 4.4. The measured adhesion forces with 20 consecutive f-d curves at **a)** 0% RH for applied loads of 4.6 μN (brown circle), and 17.5 μN (orange square) **b)** 40% RH for applied loads of 8.4 μN (pink circle), and 19.7 μN (green triangle).*

A similar result was obtained by Yoon et al. [7] for Si(100) for applied loads of 0 to 40 nN at 30% relative humidity. The applied load of Yoon et al. was, however, significantly lower because they used a much smaller tip, hemispherical tip with a radius of only 15 nm. Therefore, the applied pressure was considerably higher, which indicates that the adhesion force may still be load independent at an order of magnitude higher loads.

An increase of the adhesion force with increasing applied normal force was observed by Ferreira et al. [6] for a SiC sample. These authors attributed this feature to an irreversible change of the apex of their 15 nm tip when applying a load higher than 50 nN.

The impact of an applied normal load on the adhesion force was also studied in ultrahigh vacuum by Stegemann et al. [8] for a Ag(100) single crystal surface using a silica sphere (radius 2.8 $\mu m$) tip. They concluded that the adhesion force does not depend strongly on the load as long as the load is less than the adhesion force, but increases as the load is larger than the adhesion force. Our present result shows that this conjecture does not apply rigorously. As can be seen from our experimental result in Figure 4.3, even though the value of the applied normal load exceeds the value of the adhesion force by an order of magnitude (1.2 $\mu N$ versus 20 $\mu N$), the adhesion force still remains constant. This shows that our tip/substrate contact remains unaltered upon applying loads as high as 20 $\mu N$. The discrepancy may be attributed to impurities, as Stegemann et al. mention that impurities tend to reduce the adhesion force. However, the present main contamination is certainly water, which tends to increase rather than decrease the adhesion force (cf. Figure 4.3). The deviation from Stegemann's rule must rather be found in the softness of the material: the shear modulus of silver is of the order of 30 GPa and that of silicon about 80 GPa. Therefore, the plasticity regime is entered for Si much later than for Ag and as a result the independence of the adhesion force on the load is maintained well beyond the value of the adhesion force.

### 4.3.2 Influence of residence time

Depending on the material's hydrophilicity and the experimental conditions (e.g. pressure, temperature and humidity) water can condense on a surface and even persist after annealing at slightly elevated temperatures. When water is present on a surface it can form a capillary bridge between the surface and the probing tip. The formation of this capillary bridge requires a characteristic time and eventually thermodynamic equilibrium will be established. Experimentally it was found that long contact times can produce huge capillary bridges [9]. When AFM is used to measure the adhesion force, the AFM tip makes contact with the surface for some time and this residence time might play a critical role in the formation of the number and size of the capillary bridges. For this reason we decided to systematically vary the residence time during the measurement of adhesion forces. We note here that for AFM related technical reasons we cannot access shorter residence times than about 0.5 s.

Figure 4.5 shows the influence of the residence time of a flat AFM tip with a 0.9 $\mu m$ diameter on the adhesion forces of Si(001). The piezo velocity was set at 0.25 $\mu m/s$ and the load was adjusted to a constant value of 14 $\mu N$. Figure 4.5 reveals that, within experimental error, the adhesion forces are independent of the actual value of the residence time in the window between 0.5 and 40 s. However, the adhesion forces strongly depends on the relative humidity. At 0% RH the adhesion force is only 1.27 $\mu N$, whilst the force is 1.7 $\mu N$ at 70% RH.

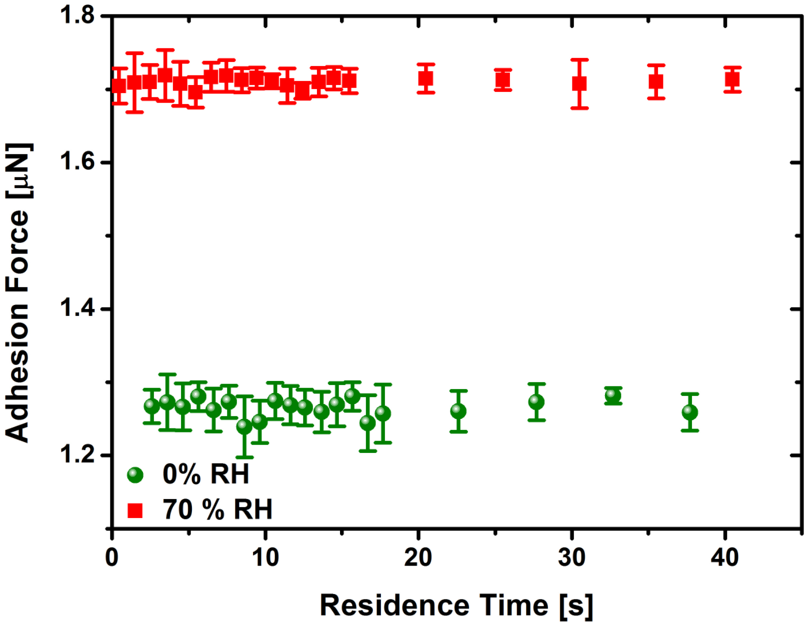

***Figure 4.5.*** *The adhesion force of a smooth Si(001) as a function of residence time. The adhesion force was measured under 0% RH (circles), and 70% RH (squares). The piezo speed was 0.25* $\mu m/s$ *and the load was set at 14* $\mu N$.

First of all, the adhesion forces at zero humidity in Figure 4.5 are about 10% lower than those exhibited in Figure 4.3. This difference is due to the different piezo speeds of, respectively, 0.65 and 0.25 $\mu m/s$ as we will see below.

Our results compare favourably with a number of results reported earlier in literature. For instance, Ando [10] reported that for a flat silicon substrate and a flat nickel AFM probe (size $1\text{x}10^5$ $nm^2$), the adhesion force decreases slightly with increasing residence time at RH of 83%. However, in the contact time window defined here (0.5 – 41 s) the decay is only 15%, while at RH = 62% and RH = 0% the variation found by Ando is virtually non-existent. The same is true for results reported by Ferreira et al. [6] for a silicon wafer: Essentially no influence of the residence time on the adhesion force was observed.

It is noted that the variation of the adhesion force with residence time seems to be substrate and tip shape dependent. Xu et al. [11] performed experiments at different RHs on mica using a pyramidal tip. They found an increase of the adhesion force at RH > 20% with increasing residence time. At lower RH values they observed a slight decrease with increasing residence time. However, the latter is marginal within our residence time window. Sedin et al. [12], using AFM tips with a radius of curvature of 20 – 40 nm, also found for mica a marginal dependence, if at all, on the residence time: at RH = 0.05 they also find a slight decrease, and at RH = 0.46 a slight increase with residence time. However, at RH = 0.24 and RH = 0.75 their results are inconclusive and thus consistent with our present data. For a completely different sample, a polymer film, using a flat – ended diamond cylindrical tip Choi et al. [13]

observed a basically constant adhesion force upon variation of the residence time over more than 600 s. For yet another sample, flat gold (rms < 1 nm), and a hemispherical tip Van Zwol et al. [14] reported a tiny increase of the adhesion force with increasing residence time. Sirghi et al. [15] reported for hydrophilic tips and substrates that for a sharp tip the formation of a stable capillary neck occurs much faster that for a blunt tip. For a sharp tip they found a typical capillary neck formation time of 5 ms, whereas for a blunt tip this time was about a 1 s. Our results (residence times > 0.5 s) are in good agreement with the blunt – tip results of Sirghi et al. [15].

In conclusion, our investigation of the influence of the residence time on the observed adhesion forces is consistent with literature data for hydrophilic (blunt/flat) tips and a wide variation of hydrophilic surfaces. For residence times between about 0.5 s and 40 s the obtained adhesion forces are grossly independent of the residence time of the tip at the sample surface.

### 4.3.3 Influence of the retraction velocity on the adhesion force

Usually, only the static component of the adhesion force is studied. However, the dynamic component of the adhesion force depends strongly on the retraction velocity of the AFM tip. In literature, the information regarding the impact of the retraction velocity on the adhesion force has not been studied in great detail. This holds in particular, for the plan – parallel tip – surface geometry. We emphasize that effects due to a possibly varying incomplete accommodation are avoided by making sure that the residence time was identical and equal to 20 s for all experiments.

In order to address this issue, the velocity of the piezo has been varied from 0.044 to 5.1 $\mu m / s$ at a constant applied load of 14 $\mu N$. For each piezo velocity value, several force – distance curves were recorded at the same location for various humidity conditions. Note again that no significant difference was observed between the initial and later measurements at the same location!

Figure 4.6.(a) shows the adhesion force on a linear scale as a function of retraction velocity of the piezo for relative humidities RH = 0, 0.40 and 0.70. As seen from this figure, the value of the adhesion force increases with increasing velocity at all humidity conditions. This data set suggests that for a vanishing piezo speed, a minimum, but finite value of the adhesion force is found. Furthermore, in order to understand the impact of humidity in more detail, the graphs are also shown in a semilogarithmic plot (see Figure 4.6.(b)). In all cases we find an increase of the adhesion force with increasing piezo speed. Within the experimental uncertainties the slope of the dependence on the piezo speed is the same in the shown range of 0.04 $\mu m / s$ – 5 $\mu m / s$. We infer that we are dealing with a combination of static, i.e. thermodynamic equilibrium, and dynamic contributions to the total adhesion force. Both contributions are of the same order of magnitude for the data in Figure 4.6. Obviously the dynamic contributions

have to fade away at very low speeds. This probably happens at even lower piezo speeds. Apparently within the parameter space probed by the data, the dynamic effects scale with a speed exponent of about 0.17 as extracted from the slopes in Figure 4.6.(b).

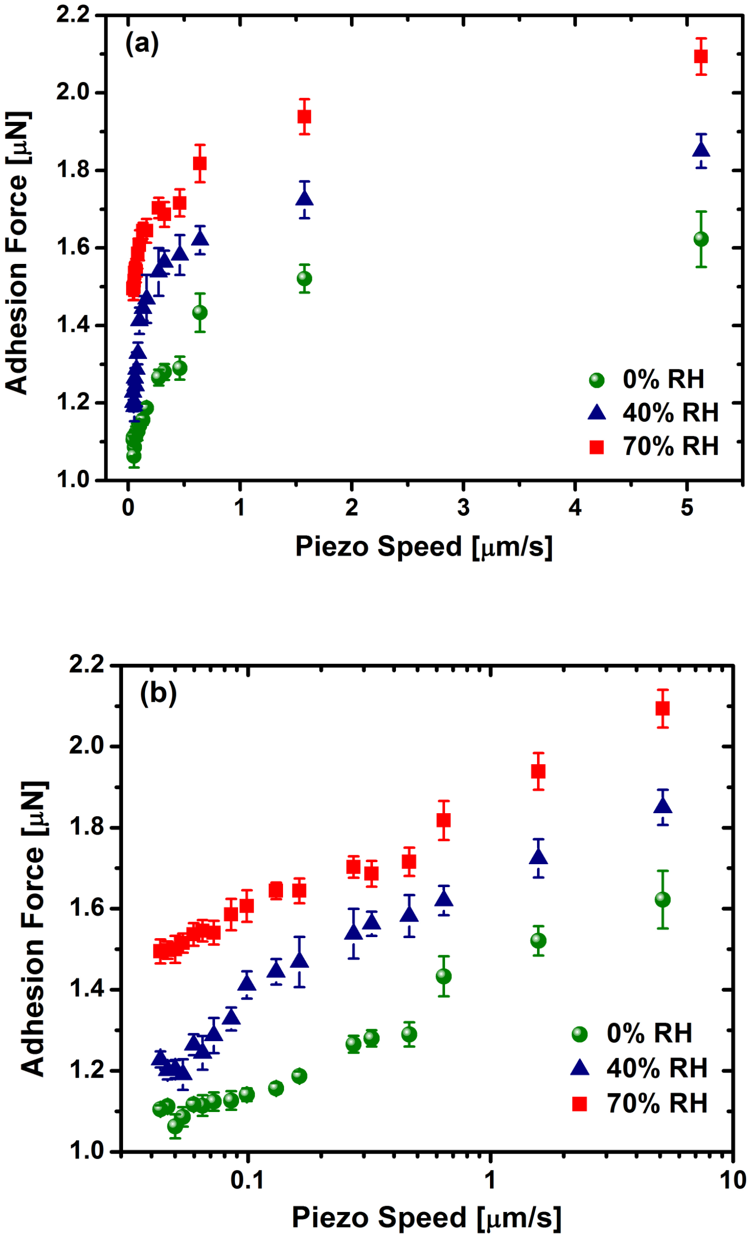

***Figure 4.6.*** *Influence of the piezo velocity of the AFM tip on the adhesion force at various humidity conditions.* ***(a)*** *linear scale,* ***(b)*** *logarithmic scale. The applied load is 14 μN and the residence time 20 s. The tip size is 900 nm.*

The influence of the piezo speed on the observed adhesion force has been studied relatively rarely. This is interesting as we observe the most eye – catching dependence on probing parameters just for this situation. For a completely different system, i.e. a polymer sample, Choi et al. [13] also measured an increase of the adhesion force with increasing pull – off velocity. However, they obtain an approximately exponentially increasing adhesion force with increasing velocity, where we find a levelling off the increase at higher velocity. Kim et al. [16] for a PDMS covered silicon surface and Zheng et al. [17] for mica and graphite samples, measured the influence of the piezo velocity on adhesion. In contrast to the present results, both papers report a decrease of the adhesion with increasing piezo speed. In the latter two references a spherical tip was used instead of a flat one in the present paper.

Cai and Bhushan [18] pointed out that the adhesion force is the sum of a meniscus (or capillary) force and a viscous force. If we assume that we have $N$ menisci between tip and the substrate, the meniscus force can be written as,

$$F_m = \frac{\pi x_n^2 \gamma (\cos\theta_1 + \cos\theta_2)}{h} + 2\sqrt{N}\pi\gamma x_n \sin\theta_{1,2} \tag{4.1}$$

where $x_n$ is the meniscus radius, $\gamma$ the surface tension of the liquid, $h$ the meniscus height, $\theta$ is the contact angle between the liquid and the solid surface, and subscripts 1 and 2 refer to the lower and upper surfaces, respectively. The first term is related to the Laplace pressure acting on the meniscus area, i.e. $\pi x_n^2$, and the second term corresponds to the contact angle of the liquid on the surface being pulled. We realize that during pull-off the contact angles might change, see Eq. (4.1), however, at this stage we do not have a clue on how they vary exactly during retraction. Cai and Bhushan [18] numerically studied the effect of contact angles during separation. Their main conclusion is that contact angles significantly affect the meniscus force, but they have hardly any effect on the viscous force. In general, large contact angles result in a smaller meniscus force.

The viscous force is a dynamic force and occurs due to the viscosity of the liquid when separating the tip and substrate. For extremely long separation times the viscous force can be safely ignored. For the flat-on-flat geometry the viscous force is given by,

$$F_v = \frac{3\pi\eta x_n^4}{4Nt_s}\left(\frac{1}{h_s^2} - \frac{1}{h_0^2}\right) \tag{4.2}$$

where $t_s$ is the time to separate tip and the surface, $\eta$ is the kinematic viscosity, $h_s$ is the break point of the meniscus, and $h_0$ is the initial meniscus height. For a smooth surface the number of menisci, $N$, is probably small and therefore the viscous force can play a more prominent role during pull off. During pull-off the meniscus force will decrease, while the viscous force will increase. The higher the retraction speed, the shorter $t_s$ and thus the larger the viscous force will become. However, the meniscus force is independent of the retraction speed and therefore the increase of the adhesion force with increasing retraction speed should be fully ascribed to the viscous force. Probably even so feasible is a situation in which the speed is too high to allow the neck(s) to follow equilibrium conditions. In that case, $x_n$ at the breaking point will decrease with increasing speed and the dynamic contribution to the adhesion force will increase with speed. Obviously, this effect becomes more important when probing flat samples with flat tips since the diameter of the water necks at the breaking point is larger compared to the case of a rough surface. The latter effect may be responsible for the flattening out of the increase of the adhesion at high tip speeds.

### 4.3.4 Influence of the size of the flat tip

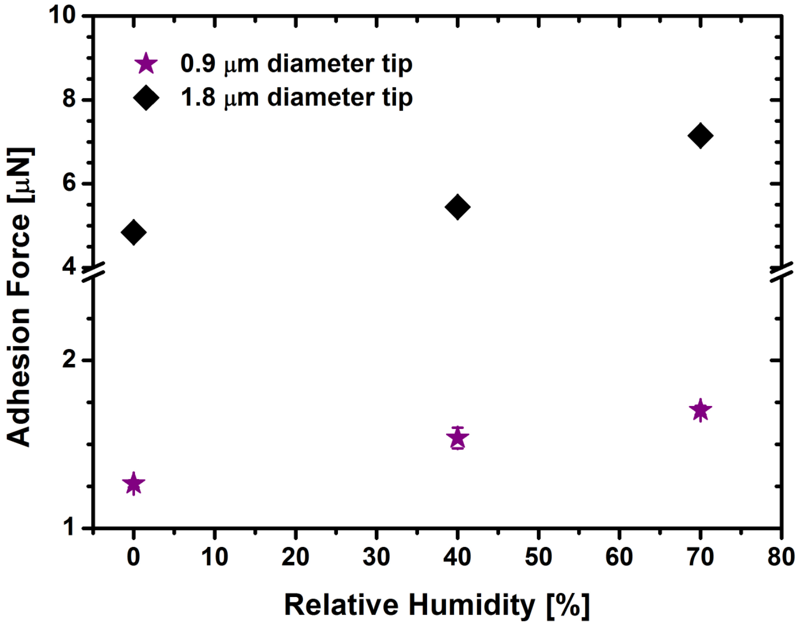

**Figure 4.7.** Comparison of adhesion forces of flat AFM tips with ~ 0.9 $\mu m$ (purple stars) and ~ 1.8 $\mu m$ (black diamonds) diameters, at various humidity conditions. The retraction speed is 0.25 $\mu m/s$ and the applied load is 14 $\mu N$.

Figure 4.7 shows the adhesion force of Si(001) measured with two different flat AFM tips (Figure 4.1) having a diameter of 0.9 $\mu m$ (purple stars) and 1.8 $\mu m$ (black diamonds), respectively. The measurements were performed at a fixed tip speed of 0.25 $\mu m/s$ and at a constant applied normal load of 14 $\mu N$. As seen from the graph, the value of adhesion force increases with increasing RH for both tips. The increase of the adhesion force is a direct consequence of the increase of the water layer thickness with increasing relative humidity. The impact of humidity on the adhesion force was discussed before in ref. [5] for the flat – flat contact geometry and will not be discussed here again. Within the experimental limits the adhesion force of the large tip (1.8 $\mu m$ diameter) is 4 times larger than the adhesion force of the small tip (0.9 $\mu m$ diameter) at all RH conditions. For the flat-on-flat geometry the Van der Waals and meniscus forces increase quadratically with the tip diameter. This means that the first term in Eq. (4.1) dominates the second (edge) term in that expression, even for the smaller tip size. So for a quantitative interpretation of adhesion measurements not only the relative humidity, but also the size of the AFM tip is a key factor. As mentioned further above the plan parallel alignment of flat tip and sample is crucial and any experimental result obtained without a clear reference to this issue should be considered uncertain.

## 4.4 Conclusions

In an extensive set of different experiments we have measured the adhesion force as a function of various experimental parameters, including applied load, residence time, piezo speed and tip size. We have done so for a flat-flat tip-sample geometry, with hydrophilic tip and hydrophilic sample. In the experimental parameter space, especially the residence time varying between 0.4 and 40 s, we find no dependence on load, and residence time, while a significant increase of the adhesion force with increasing piezo speed is observed. The adhesion forces depend significantly on the size of the flat AFM tip, and are proportional to the area for the used 900 and 1800 nm tip radii. Thus, for flat AFM probes, the velocity of the tip and its size are the main experimental factors that affect the value of measured adhesion forces, and therefore they need to be kept constant during the measurements.

We find a remarkably high reproducibility of the obtained adhesion forces. On a day to day basis or even a month to month basis we found no evidence for any significant variation of the obtained forces. Crucial to this observation is the ability to align tip and sample in an exactly plan parallel configuration. Before the realization of the tip alignment device our measured data showed substantial scatter.

## 4.5 References

1. Bradley, R. S., *Philos. Mag.* **1932**, *13*, 853 – 862.
2. Chau, A.; Régnier, S.; Delchambre, A.; Lambert, P., *J. Adh. Sci. Technol.* **2010**, *24*, 2499 – 2510.
3. Israelachvili, J.N., *Intermolecular and Surface Forces*; Academic Press: London, **1992**.
4. Poggi, M. A.; McFarland, A. W.; Colton, J. S.; Bottomley, L. A., *Anal. Chem.* **2005**, *77*, 1192 – 1195.
5. Çolak, A.; Wormeester, H.; Zandvliet, H. J. W.; Poelsema, B., *Appl. Surf. Sci.* **2012**, *18*, 6938 – 6942.
6. Ferreira, O. D. S.; Gelinck, E.; de Graaf, D.; Fischer, H., *Appl. Surf. Sci.* **2010**, *257*, 48 – 55.
7. Yoon, E. –S.; Yang, S. H.; Han, H. –G.; Kong, H., *Wear* **2003**, *254*, 974 – 980.
8. Stegemann, B.; Backhaus, H.; Kloss, H.; Santner, E., *Modern Research and Educational Topics in Microscopy*; Formatex: Spain, **2007**; *Vol.1*, pp. 820 – 827.
9. Szoszkiewicz, R.; Riedo, E., *Phys. Rev. Lett.* **2005**, *95*, 135502.
10. Ando, Y., *Langmuir,* **2008**, *24*, 1418 – 1424.

11. Xu, L.; Lio, A.; Hu, J.; Ogletree, D. F.; Salmeron, M., *J. Phys. Chem. B* **1998**, *102*, 540 – 548.
12. Sedin, D. L.; Rowlen, K. L., *Anal. Chem.* **2000**, *72*, 2183 – 2189.
13. Choi, S. T.; Lee, S. R.; Earmme, Y. Y., *J. Phys. D: Appl. Phys.* **2008**, *41*, 074023.
14. Van Zwol, P. J. ; Palasantzas, G.; de Hosson, J. T. M., *Phys. Rev. E* **2008**, *78*, 031606.
15. Sirghi, L.; Szoszkiewicz, R.; Riedo, E., *Langmuir* **2006**, *22*, 1093 – 1098.
16. Kim, M. S.; Lee, M. K.; Park, J. Y.; Kwon, Y. S.; Choi, B. K., *NSTI Nanotech.* **2010**, *2*, 405 – 408.
17. Zheng, W.; Chin, Y. -P., *Chin. Phys. Lett.* **2004**, *21*, 616 – 619.
18. Cai, S.; Bhushan, B., *Mater. Sci. and Eng.* **2008**, *R61*, 78 – 106.

# Chapter 5

# The influence of instrumental parameters on the adhesion force in a flat-on-rough contact geometry

*We have studied the pull-off forces, often considered as synonymous for adhesion forces, between a rough Si(001) surface and a micron sized flat silicon atomic force microscope (AFM) tip. Special attention is paid to the dependence on several experimental parameters. Care was taken to make sure that the measured adhesion forces do not depend on the load applied on the tip, warranting an elastic contact between the tip and the substrate. We found no dependence on the residence time, the sequence of the measurements, and hardly on the tip size. The tip alignment is important but less critical than in the flat-on-flat geometry. For all instrumental parameters the adhesion force increases with increasing relative humidity. We found a clear decrease of the pull-off force with increasing tip retraction speed, in obvious contrast with the flat-on-flat geometry, where the opposite behaviour applies. The current observation is attributed to a predominance of capillary forces over dynamic forces as opposed to the pull-off forces measured with a flat tip on a smooth surface.*

## 5.1 Introduction

Atomic Force Microscopy (AFM) is an important measurement technique in widespread branches of science and technology [e.g., 1-3]. It can be used to study every kinds of insulating and conducting structures with a minimal sample preparation in a variety of environmental conditions, for instance at different humidity and temperature. It is mostly used for a topographic scan of surfaces, but it can measure physical properties of surfaces including elasticity, hardness [4], friction [5-6], and adhesion [7-8].

The adhesion force, that is needed to separate two bodies from one another, plays an important role in many engineering applications as well as in everyday life. In the past decades, a great deal of attention has been paid to understand the mechanisms that determine the adhesion force between materials and devices at micro and nanometer length scales. Even today, the knowledge about the physical mechanisms dominating the adhesion forces, as probed by AFM, is still limited.

In general, the adhesion force between an AFM tip and a sample surface should include the capillary force as well as the solid-solid interactions, consisting of Van der Waals forces, electrostatic forces, and the chemical bonding forces [9]. When the tip and the sample stay in air for a relatively long time (of the order of a few hours), no net charges are expected to remain. The electrostatic forces can thus be ignored [10]. The chemical bonding force can also be neglected, if ionic or covalent bonds are not expected to form during contact depending on the chemistry of surfaces [10]. When the surfaces are hydrophilic, then theoretically, the Van der Waals and capillary forces dominate the adhesion force.

Experiments show that the adhesion force can be modified by varying the roughness of the interacting surfaces, and/or changing the relative humidity of the environment [11]. Furthermore, the adhesion force has been reported as being subject to changes by applying a different load on the tip, and/or by varying the residence time of the tip on substrate. The retraction velocity of the AFM tip can also be an important parameter for measuring the adhesion force, due to the viscosity of condensed water between the tip and the substrate. Unfortunately, the experiments, performed so far, only consider a subset of aforementioned parameters while ignoring other possibly relevant ones. Moreover, the results from the performed experiments show differences between one to another that hinder the acquisition of a consistent picture of the adhesion force between surfaces.

In the present work, the effects of the applied load on tip, the residence time of the tip on substrate, the tip's retraction speed and the tip size on the adhesion force of a rough Si(001) (rms of 13.6 nm) are investigated using a flat and micron sized Atomic Force Microscopy (AFM) probe. The experiments have been performed in a controlled environment at different relative humidity.

## 5.2 Experimental details

The sample used in experiments is a rough Si(001) wafer that was roughened with an anisotropic wet chemical etchant. Before etching, the sample was cleaned in an ultrasonic bath of methanol for 15 min. Subsequently, the Si wafer was placed in a piranha solution with a 3:1 volume ratio mixture of $H_2SO_4$ and $H_2O_2$ for 30 min. After these two cleaning steps, the Si wafer was rinsed in deionized (DI) water, and dried using a dry $N_2$ flow. Finally, the sample was chemically roughened in a solution of $NH_4OH / H_2O$ (1/5) at 80 °C [12-13] for 5 min, again rinsed in DI water and dried using a flow of $N_2$. Subsequent to the etching process, the sample roughness was recorded, with a silicon tip (Nanosensors, PPP-NCL-20) in tapping mode AFM. The resulting rms value was determined at 13.7 nm.

Unless otherwise mentioned, we used for the present adhesion force measurements a cone shaped silicon tip (Nanosensors, PL2-NCLR-10) with a flat circular top with a diameter of ~ 0.9 $\mu m$. While working with this flat AFM tip care has been paid to align the tip and the substrate parallel to each other. We varied the alignment between the tip and the sample by placing the sample on a sample holder that could be adjusted at different tilt angle. The optimal angle was determined by maximizing the adhesion force, [11] which corresponds to a plan parallel configuration between the flat tip and the average surface. The alignment was done with the flat sample. All data reported below have been taken with this optimum alignment, i.e. the tip and the macroscopic substrate were perfectly parallel.

The adhesion force measurements were performed in a humidity controlled environment, where the humidity can be adjusted by varying the flow ratio of dry and wet nitrogen streams. The relative humidity (RH) in the chamber was measured with two humidity sensors (SHT 75 Sensirion, Switzerland) located at two different positions in the chamber with a volume of 1 liter. After changing the flow ratio, the RH was allowed to reach its equilibrium value by waiting for more than one hour. The ‘dry’ condition was obtained after purging with dry nitrogen for at least 12 hours.

In order to measure the adhesion force, the cantilever is moved in the vertical direction towards the sample, and then withdrawn. During the approach/retraction cycle of the cantilever, the cantilever deflects due to the forces acting between the tip and the substrate. We recorded the deflections of the cantilever with the Molecular Imaging (MI) software. In the study of the temporal behavior it is important that the response is not limited by the AFM electronics. Therefore, we used a break – out box to monitor the normal displacement signal and piezo voltage with a HP digital oscilloscope. The high resolution time basis of the oscilloscope was used to measure the response of the cantilever deflection including snap – in, and snap – off. At the end, deflections of the cantilever are recorded as a function of time as shown in detail in Figure 5.1. From such curves the adhesion force experienced by the tip is extracted from the positions between the maximum deflection point of the cantilever just before it snaps – off and the zero deflection point at the freestanding position of the cantilever. The value of the adhesion force is obtained by multiplying this distance with the spring constant of the cantilever which is calculated according to the method of Poggi et al. [14]. In Figure 5.1, the residence time defines the contact time between sample and the tip between the snap – in and snap – off points. The total time is defined as the time to record a complete force – distance (f – d ) curve, including the time that the tip does not make any contact with the substrate. When measuring the adhesion force, the tip is pushed to the substrate until a maximum normal load value is reached. This load is kept constant until the withdrawal of the tip. We varied the applied load between 3 $\mu N$ to 18 $\mu N$ and analyzed the impact of this variation in load force on the adhesion force. For measuring the impact of retraction speed of piezo on the adhesion force, we varied the piezo speed systematically, by keeping the distance that the tip moves constant and only varying the total time to record an approach/retraction cycle of the tip. Of course, when one parameter was varied systematically, all others were kept constant.

Twenty consecutive f – d curves were recorded with the AFM for each reported adhesion force. We did not observe any significant difference between the first measurement and subsequent ones. From these f – d curves an average value of adhesion force is obtained. The reported error is the standard deviation obtained from this series of measurements. The measurements are repeated at various humidity to analyze the influence of humidity on adhesion.

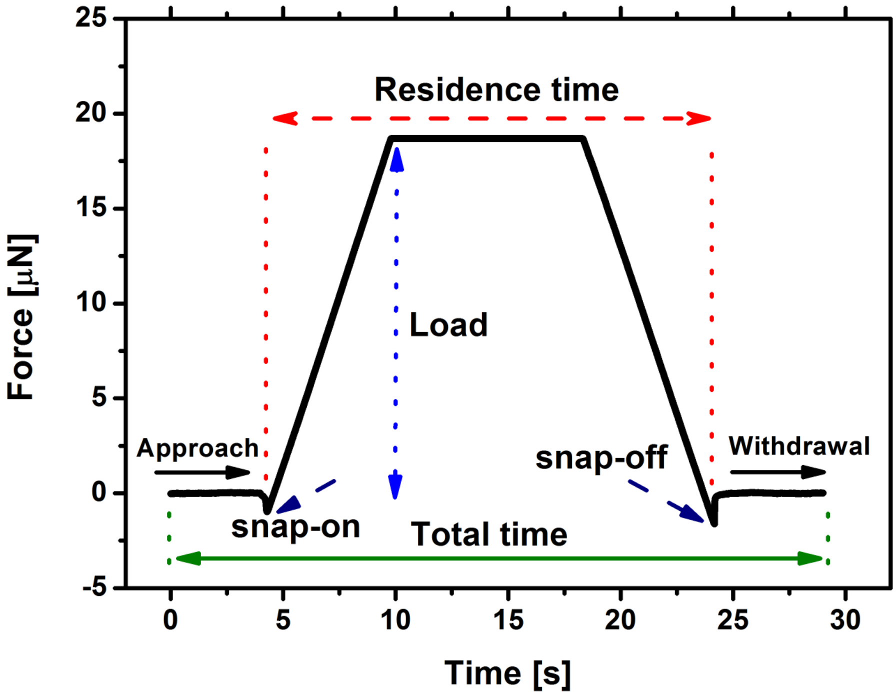

*Figure 5.1. Scheme of the force experienced by the tip as a function of time.*

## 5.3 Results and discussion

### 5.3.1 Impact of externally applied load on the flat AFM tip

The asperities on surfaces can be elastically, viscoelastically or plastically deformed during contact by surface forces. [15]. If a solid is deformed inelastically, this leads to increase of the adhesion force [16-17]. In order to obtain accurate values of the adhesion force with an AFM, it is necessary to ensure a purely elastic contact between the substrate and the tip. Thus, there is always a distinct need to study the behaviour of the adhesion force as a function of the externally applied load for flat AFM tip and rough Si(001) surface.

Figure 5.2 shows the adhesion force between the flat AFM tip with a diameter of ~ 0.9 $\mu m$ and the rough Si(001) (with 13.2 nm rms) at various applied normal loads. The measurement was done for the applied loads varied from 3 $\mu N$ to 18 $\mu N$, with the piezo velocity, and the residence time were set at 2 $\mu m / s$, and 5 s, respectively. As is immediately obvious from the figure there is no discernible influence of the applied load on the adhesion force. The error bar for the adhesion force obtained for each individual load level is quite large. The size of the error bar, in Figure 5.2, is the result of variations in the adhesion force value from one measurement to another. In Figure 5.3.(a), as an example of such a variation, 20 measured adhesion forces are shown, at two applied loads of 4.5 $\mu N$, and 17.5 $\mu N$, respectively, obtained at 0% RH. In Figure 5.3.(b), a similar variation of 20 measured adhesion forces are shown at 40% RH, for two applied loads of 3.4 $\mu N$, and 16 $\mu N$, respectively. As seen from the Figures 5.3.(a) and 5.3.(b), there is no tendency for either an increase or a decrease between the individual measurements. This implies that the measurements have been performed well within the elastic regime. Note that the first data point applies for the virgin surface. The variation in the data set is random, even though the position of the tip at the surface remains the same if one neglects drift. The relative variation of the measured adhesion force is considerably higher than that obtained for probing a flat Si(001) surface with a flat tip as shown in Chapter 4 of this Thesis. This fact might be partly attributed to a less homogeneous distribution of roughness compared to the flat silicon. In a largely oversimplified view, one may think of a tip – wide contact for the flat surface and a contact with the three highest protrusions in the area below the flat tip which make contact. A different location would then imply three different asperities with (slightly) different effective contact areas. However, even in the total absence of drift there is a most probably more important reason for the decreased relative accuracy of the measured adhesion force. Compared to the flat-on-flat geometry, the absolute value of the adhesion force is 15-20 times lower for the presently studied rough surface. This not only supports the view of a much smaller effective contact area in the latter case, but also stresses that uncertainties in the tip position far out of contact, which is used as a reference point for zero force, are much more important in a relative sense: A ripple (as a result of interference between the laser reflected from the cantilever and random parts in the scan tube) in the reference level would cause relative uncertainties in the adhesion force which are multiplied 15-20 times when compared to the flat surface case. We believe that this latter factor is by far the most important contributor to the current relatively large error bars. This appears further corroborated by the fact that the error bars for the 1.5 times stronger adhesion forces at RH = 0.40, as compared to those at RH = 0, are about 1/3 smaller. Summarizing, we do not observe any indication of any dependence of the measured adhesion force on the applied load. This important observation indicates that under the given conditions no plastic deformation of neither the tip nor the contacting asperities at the sample takes place. Therefore, the measured adhesion force is believed to represent the real adhesion force between the rough surface and the used flat tip. Assuming that the adhesion forces scales with the contact area as shown in Chapter 4 of the Thesis, the integrated contact area in the present situation amount to about 0.04 $\mu m^2$. In Figure 5.2, the adhesion force increases with the increase of humidity as pointed out before (ref. [11]). This is attributed to the larger diameter of the meniscus bridges formed between apex of the rough substrate and the tip at higher humidities.

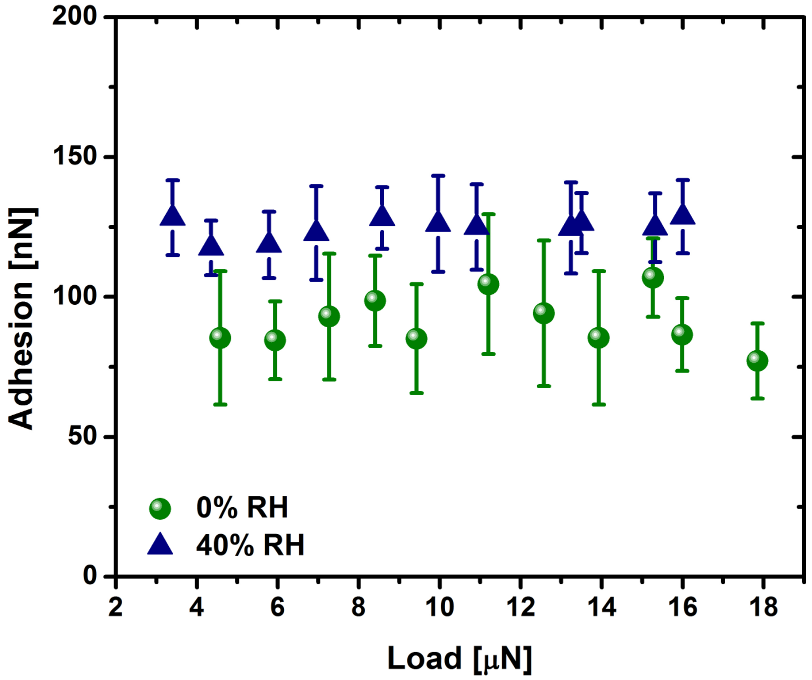

***Figure 5.2.*** *The adhesion force as a function of an externally applied normal load for a rough Si(001) surface measured with a flat AFM tip with a diameter of 0.9* $\mu m$. *The piezo speed was 2.0* $\mu m/s$ *and the residence time was set at 5 s for the two given values of the relative humidity.*

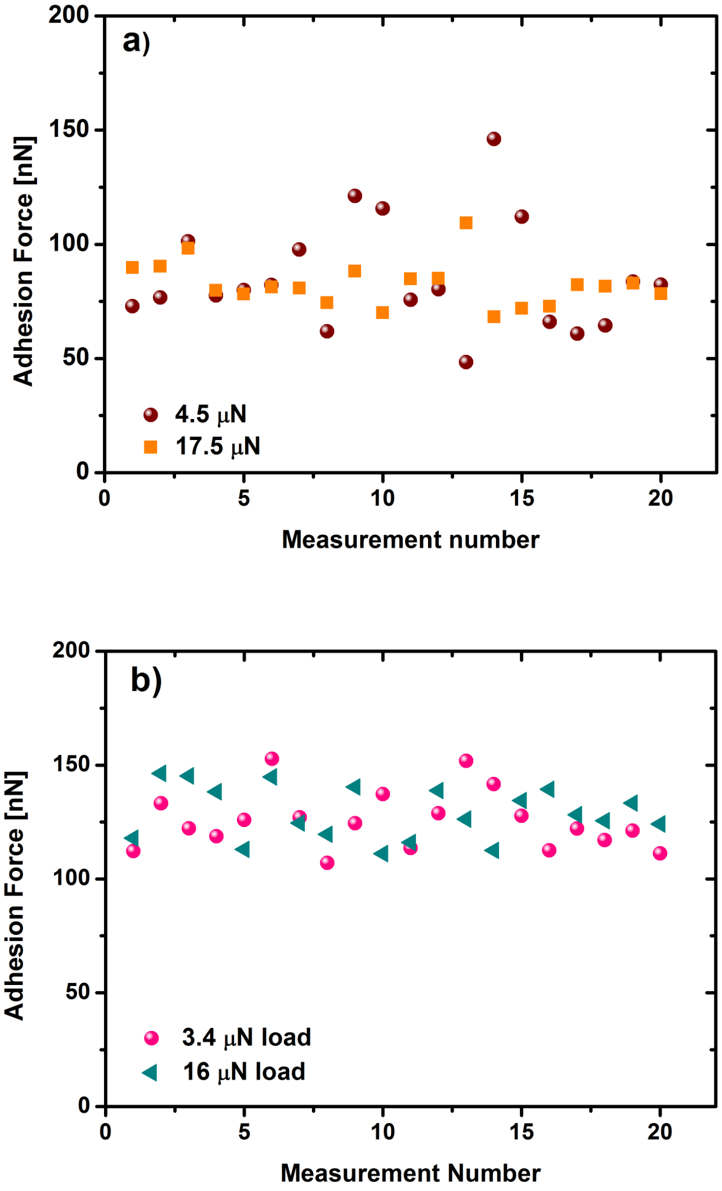

***Figure 5.3.*** *The measured adhesion forces with 20 consecutive f-d curves at* ***a)*** *0%RH for applied loads of 4.5 μN (brown circles), and 17.5 μN (orange squares)* ***b)*** *40%RH for applied loads of 3.4 μN (pink circles), and 16 μN (green triangles).*

### 5.3.2 Influence of residence time

Under ambient conditions, when two hydrophilic bodies are brought in sufficiently close contact to each other, menisci as pendular rings are formed around the contacting and near-contacting asperities, due to the presence of a thin liquid film on surfaces or condensation of water from the ambient. The formation of the menisci causes a capillary force that leads to an increase in the adhesion force between solids. When an AFM is used for measuring the adhesion force, the tip and the substrate remain in contact for some time. Depending on the length of this time period, the value of the adhesion force may change due to the variations on the number and size of the capillary bridges. Actually, several authors have reported that the adhesion force of surfaces is (in some cases slightly) residence time dependent [18-22].

The influence of the residence time (see Figure 5.1 for a definition) of a flat AFM tip (diameter of 0.9 $\mu m$) on the adhesion force of a rough Si(001) is shown in Figure 5.4. The measurements were done for the residence times varying from 0.5 s to 35 s, while the applied load, and the piezo velocity were kept constant at 6 $\mu N$, and 2.0 $\mu m / s$, respectively. Figure 5. 4 shows that, within the experimental errors, the adhesion force is independent of the actual value of the residence time. No significant difference was observed between the initial and later measurements for the same residence time. In other words, the values obtained for the virgin substrate are identical to those obtained subsequently at the same position. However, the relative humidity was found as the parameter to have a distinct influence on the value of the adhesion force. For 0% RH, the adhesion force is around 80 nN, whereas a distinctly higher adhesion force around 130 nN is measured at 40% RH. The latter is a result of the increase of the contact area due to the condensation of more water between asperities of rough substrate, and the AFM tip with increasing relative humidity.

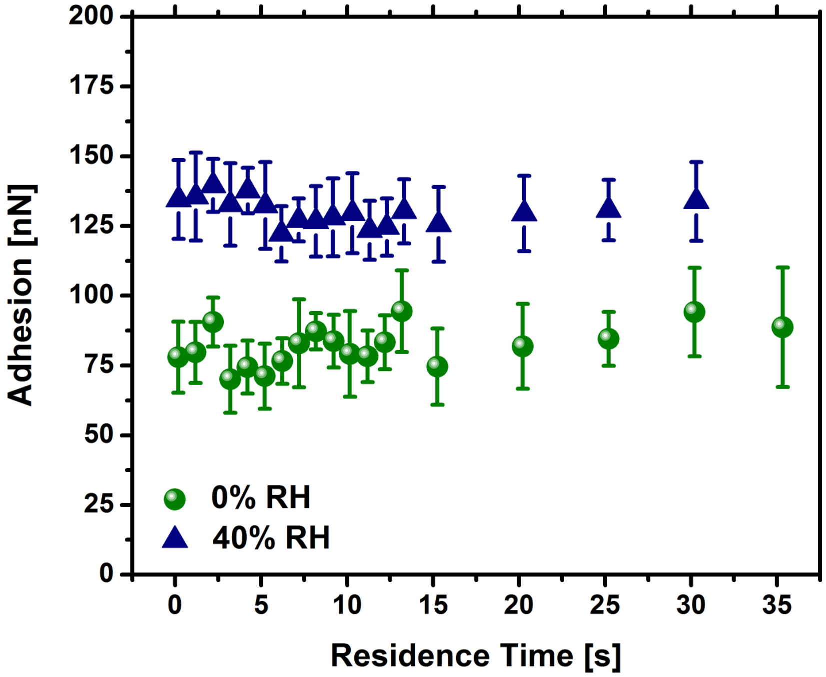

*Figure 5.4.* *The residence time dependent adhesion force of a rough Si(001). Piezo speed, and applied normal load were set at 2.0 $\mu m / s$ and 6 $\mu N$, respectively. The tip diameter was 0.9 $\mu m$.*

Due to instrumental (AFM-related) limitations we could only start measuring the residence time in a reliable way from about 0.5 s onwards. In the range up to 35 s we measure an essentially constant adhesion force. This is in agreement with the findings reported by Van

Zwol et al. [22], who observed a slight increase of the adhesion with increasing residence time for surfaces with a low or even vanishing roughness. For rough surfaces they find adhesion forces, which are basically independent on residence time. Our sample with an rms roughness of 13.7 nm would certainly qualify as rough. Sedin and Rowlen [20] measured the influence of pull – off forces from mica and found only marginal, if at all, influences on contact time in agreement with our current observations. Xu et al. [19] found an increase and a decrease of the adhesion force with increasing residence time at respectively high and low relative humidity. However, within the residence time interval overlapping with ours, the variations are constant well within their error bars.

We note that the main variations in the pull – off force are reported for short contact/residence times. We attribute this fact to features related to the accommodation (or equilibration) of the tip at the surface after its arrival. If the accommodation is not complete the pull – off force may not at all be a relevant measure of the adhesion force but rather (partly) probe.

### 5.3.3 Influence of the retraction velocity on the adhesion force

First of all we emphasize that we made sure that the possible consequences of a varying incomplete accommodation are excluded. We did so by ensuring that the residence time of the tip was the same (20 s) for all measurements, irrespective of the applied piezo speed.

When two contacting surfaces are continuously pulled apart, the capillary bridge between them deforms gradually. While the height of menisci increases, their radius decreases during pull – off. After the initial motion, both the capillary force, and viscous forces operate inside the meniscus. During separation, the capillary forces decrease due to the decrease in the meniscus radius, whereas the viscous force, that is the dynamic contribution on the total adhesion force, increases with the separation distance and increasing retraction speed [23]. Either the capillary or the viscous force can be dominant, and this can be accessed by varying the retraction speed of the piezo. In order to address this issue, the adhesion forces of a rough Si(001) substrate were measured at different retraction speeds of the piezo.

The retraction velocity of the flat AFM probe has been varied between 80 and 4030 nm/s. For this measurement the load, and the residence time were set fixed at 5 $\mu N$ and 20 s, respectively. Figure 5.5 shows the adhesion force as a function of retraction velocity of the piezo for three values of the relative humidity: RH = 0, 0.40 and 0.60. We observe hardly any dependence of the adhesion force for zero humidity, RH = 0. However, for finite humidity, RH = 0.40 and RH = 0.60, we observe a strong decay of the adhesion forces with increasing retraction speed. This is true especially for the tip speeds at the lower end of applied speed window appears to slow down for the higher speeds. Komkov [24] has observed a similar behaviour for the dependence of surface forces on the distance between a steel disc and a steel sphere (radius of 2.5 mm) at different separation velocities. He found the capillary forces to decrease with increasing velocity. In his studied velocity window (20 nm/s - 80 nm/s) also the most eyecatching changes occur at the lowest velocities. Komkov rationalized the velocity dependence as follows: With increasing distance between the separating bodies (asperity and flat tip in our case) the liquid is constricted to the axial line. Because of inertia and viscosity of the liquid this process takes some time and with increasing velocity the diameter of the meniscus neck can decrease resulting in a lower capillary force. As mentioned in the beginning, only the static capillary force decreases during the pull – off due to the decrease of the meniscus radius and increase of the meniscus height. Therefore, the observed decrease in Figure 5.5 for 40% and 70% RH would be the result of the static capillary force between the AFM tip and the rough Si(001). Different from 40% and 70% RH, for RH = 0 the piezo speed does not have a clear impact on the adhesion force of rough Si(001). Even though before measurements the sample was kept in 0% RH over night, this will not eliminate the water that was already condensed on the surface. As a result, even at dry conditions, the capillary force dominates the adhesion force. However, at 0% RH the size of the menisci is likely insufficient to show variations from one velocity of the piezo to another. This essentially independence on tip speed would then be maintained until a certain minimal humidity level is reached at which the dimension of the menisci is large enough to respond the piezo velocity variations.

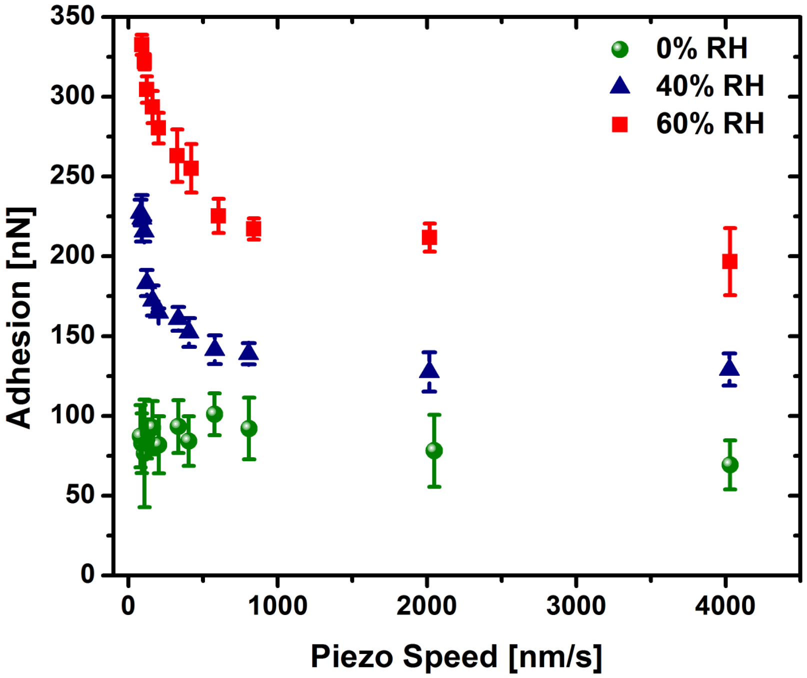

***Figure 5.5.*** *Influence of the flat AFM tip's retraction speed on the adhesion force at different relative humidity while the tip diameter is 0.9 $\mu m$. The load was 5 $\mu N$ and the residence time was set at 20 s.*

The current results obtained with the flat tip on the rough surface differ completely from those obtained with the same tip and a flat surface. In Figure 5.6 we have reproduced our measured data for the adhesion force for flat Si(001) as a function of the retraction speed of the piezo at 0%, 40% and 70% relative humidity. For this measurement, the velocity of the piezo has been varied from 44 to 5100 nm/s at a constant applied load of 14 $\mu N$ and a residence time of 20 s.

Opposite to the behaviour for the rough surface the adhesion forces increase with increasing tip speed for the smooth surface at all humidity conditions. We attribute the latter behaviour to a dominant contribution of viscous forces which increase with increasing tip speed [23]. Obviously the viscous force contributions have to fade away at very low speeds. The essential difference between the observed response of the flat and rough surface has to be attributed to the very different response of the water minisci which are of very different size for the flat and rough surfaces.

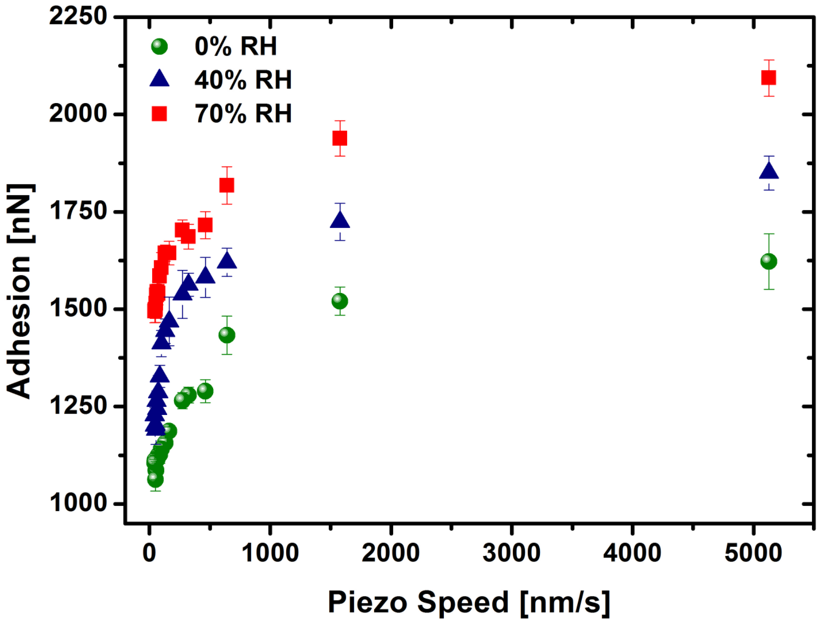

***Figure 5.6.*** *Influence of the flat AFM tip's retraction speed on the adhesion force at different relative humidity for the flat tip – flat surface configuration. The load was 14 $\mu N$ and the residence time was fixed at 20 s, while the tip diameter is 0.9 $\mu m$.*

Cai and Bhushan [23] reported that the adhesion force is the sum of a capillary force and a viscous force. For $N$ menisci between tip and the substrate, they have derived for the adhesion force:

$$F_a = \frac{\pi x_n^2 \gamma (\cos\theta_1 + \cos\theta_2)}{h} + 2\sqrt{N}\pi\gamma x_n \sin\theta_{1,2} + \frac{3\pi\eta x_n^4}{4Nt_s}\left(\frac{1}{h_s^2} - \frac{1}{h_0^2}\right) \tag{5.1}$$

where $x_n$ is the meniscus radius, $\gamma$ the surface tension of the liquid, $h$ the meniscus height, $\theta$ is the contact angle between the liquid and the solid surface, $t_s$ is the time to separate tip and the surface, $\eta$ is the kinematic viscosity, $h_s$ is the break point of the meniscus, $h_0$ is the initial meniscus height and subscripts 1 and 2 refer to the lower and upper surfaces, respectively. This equation is normalised to one of the $N$ presumed identical contacts with a characteristic meniscus with contact area $\pi x_n^2$. The first term is related to the Laplace pressure acting on the meniscus area, i.e. $\pi x_n^2$, and the second term corresponds to the contact angle of the liquid on the surface being pulled. The third term represents the dynamic force and occurs due to the viscosity of the liquid when separating the tip and substrate. Cai and Bhushan [23] numerically studied the effect of contact angles during separation. Their main conclusion is that contact angles significantly affect the meniscus force, but they have hardly and effect on the viscous force. In general, large contact angles result in a smaller meniscus force.

For a smooth surface the number of menisci, $N$, is relatively small and therefore the viscous force play a more prominent role during pull – off. During pull – off the meniscus force will decrease, while the viscous force will increase. The higher the retraction speed, the shorter $t_s$ and thus the larger the viscous force will become. Assuming that the meniscus force is independent of the retraction speed, the increase of the adhesion force with increasing retraction speed is ascribed to the viscous force. The flattening out of the increase of the adhesion force is ascibed to a decrease of the diameter of the contact $x_n$ if the contact fluid is not able to follow the equilibrium situation. In other words the expanding "cylindrical" part in the centre of the contact will rapidly get a smaller diameter and a larger length. The resulting change of force counteracts the effect of the third term in Eq. (5.1).

The latter effect is then consistently responsible for the observed decrease of the adhesion force with increasing speed for the flat tip – rough surface system. Due to the larger number of contacts in this case and also due to the smaller characteristic $x_n$ values, the third term in Eq. (5.1) becomes negligible with respect to the first term, while at the same time the second term gains relative influence. This would imply that the decay of the adhesion force with increasing speed is attributed to a decrease in the size of the contact at breaking with increasing tip speed.

### 5.3.4 Influence of the size of the flat tip

Figure 5.7 shows the adhesion force of Si(001) measured with two different flat AFM tips with a diameter of 0.9 $\mu m$ (purple stars) and 1.8 $\mu m$ (black diamonds), respectively. For small size tip (0.9 $\mu m$), the measurements were performed at a fixed tip speed of 0.3 $\mu m/s$, at a constant applied normal load of 5 $\mu N$. For the large size tip (1.8 $\mu m$), the measurements were performed at a fixed tip speed of 0.3 $\mu m/s$, at a constant applied normal load of 14 $\mu N$. As seen from the graph, the value of the adhesion force increases again with increasing RH for both tips. This increase of the adhesion force is a direct consequence of the increase of the water layer thickness with increasing relative humidity. As a result the diameter of the meniscus upon breaking will be higher and both the capillary forces as well as the viscous forces will increase [23]. The data show no significant dependence on the tip size. For this rough surface this can be rationalized if the number of contact is independent of the tip size and the latest asperities in contact with the tip are similar. An increase of size of the tip will lead to three, perhaps different asperities on the surface in contact with the tip. In contrast, the results obtained for the flat-on-(extremely) flat geometry the adhesion forces increase quadratically with the tip diameter. Therefore, we have probed two extreme cases: the flat-on-flat geometry with the quadratic dependence and the flat-on-extremely rough situation with no dependence on tip size at all. It is therefore no surprise that the reported results in literature show intermediate dependences, especially when taking into account that the probing AFM-tip has typically a spherical shape [7-8,18].

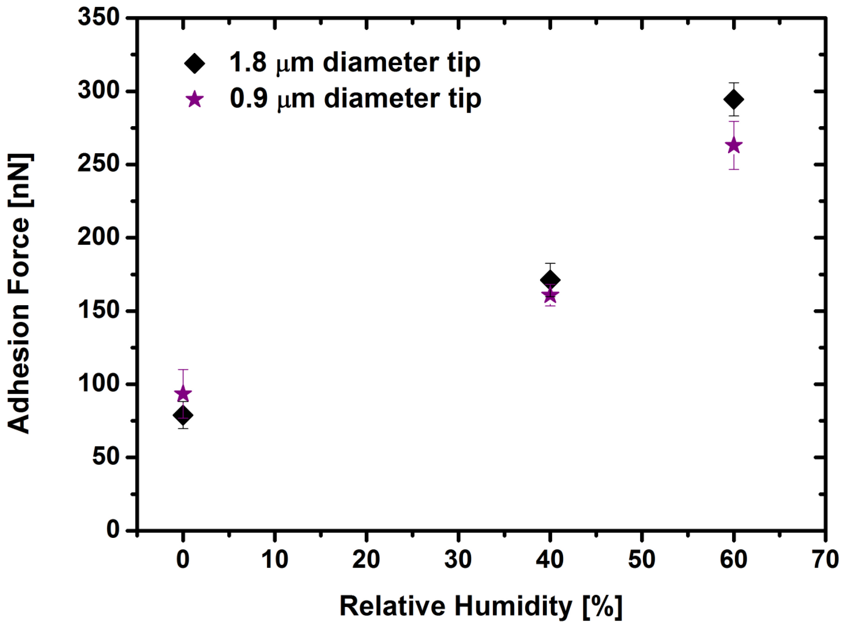

***Figure 5.7.*** *Comparison of the adhesion forces of flat AFM tips with ~ 0.9 $\mu m$ (purple stars) and ~ 1.8 $\mu m$ (black diamonds) diameters, at various humidity conditions. The retraction speed is 0.3 $\mu m/s$ for both tips and the applied loads are 5 $\mu N$ and 14 $\mu N$, for small size tip (0.9 $\mu m$) and large size tip (1.8 $\mu m$), respectively.*

## 5.4 Conclusions

We have measured the adhesion force as a function of several experimental parameters, including applied load, residence time, piezo velocity and tip size. We have done the measurements for a flat – rough tip – sample geometry, with hydrophilic tip and hydrophilic samples. We have found that the adhesion force of rough Si(001) (rms roughness is 13.7 nm) is independent of the applied load on the tip, certifying that our measurements are performing in the elastic regime. Under these circumstances, the obtained adhesion forces do not depend on the residence time of the tip on the substrate and neither on the flat tip size. In the experimental parameter space, for an applied load of 5 $\mu N$, and residence time of 20 s, a decrease of the adhesion force was measured for rough Si(001) with an increase of the piezo velocity. This is in clear contrast to the flat surface, where we observed the opposite behavior, i.e., an increase of the adhesion force with increasing piezo velocity. The difference is attributed to a predominant dependence on viscous force for the flat surface and a predominant influence of capillary forces for the rough surface in combination with a decreasing of the contact area during breaking for increasing tip speed.

## 5.5 References

1. Alessandrini, A.; Facci, P., *Meas. Sci. Technol.* **2005**, *16*, R65 – R92.
2. Carpick, R. W.; Salmeron, M., *Chem. Rev.* **1997**, *97*, 1163 – 1194.
3. Sugimoto, Y.; Pou, P.; Abe, M.; Jelinek, P.; Perez, R.; Morita, S.; Custance, O., *Nature* **2007**, *446*, 64 – 67.
4. Garcia-Manyes, S.; Güell, A. G.; Gorostiza, P.; Sanz, F., *J. Chem. Phys.* **2005**, *123*, 114711.
5. Tambe, N. S.; Bhushan, B., *J. Phys. D: Appl. Phys.* **2005**, *38*, 764 – 773.
6. Hu, J.; Xiao, X.-d.; Ogletree, F.; Salmeron, M., *Surf. Sci.* **1995**, *327*, 358 – 370.
7. Jones, R.; Pollock, H. M.; Cleaver, J. A. S.; Hodges, C. S., *Langmuir* **2002**, *18*, 8045 – 8055.
8. Segeren, L. H. G. J.; Siebum, B.; Karssenberg, F. G.; Van den Berg, J. W. A.; Vansco, G. J., *J. Adh. Sci. Technol.* **2002**; *16*, 793 – 828.
9. Bingelli, M.; Mate, C. M., *Appl. Phys. Lett.* **1994**, *65*, 415 – 417.
10. Xiao, X. D.; Qian, L. M., *Langmuir,* **2000**, *16*, 8153 – 8158.
11. Çolak, A.; Wormeester, H.; Zandvliet, H. J. W.; Poelsema, B., *Appl. Surf. Sci.* **2012**, *18*, 6938 – 6942.
12. Gould, G.; Irene, E. A., *J. Electrochem. Soc.* **1989**, *136*, 1108 – 1112.
13. Utani, K.; Suzuki, T.; Adachi, S., *J. Appl. Phys.* **1993**, *73*, 3467 – 3471.
14. Poggi, M. A.; McFarland, A. W.; Colton, J. S.; Bottomley, L. A., *Anal. Chem.* **2005**, *77*, 1192 – 1195.
15. Maugis, D.; Pollock, H. M., *Acta Mettal.* **1984**, *32*, 1323 – 1334.
16. Johnson, K. L., *Tribology International* **1998**, *31*, 413 – 418.
17. Cleaver, J. A. S.; Looi, L., *Powder Technology* **2007**, *174*, 34 – 37.
18. Ando, Y., *Langmuir* **2008**, *24*, 1418 – 1424.
19. Xu, L.; Lio, A.; Hu, J.; Ogletree, D. F.; Salmeron, M., *J. Phys. Chem. B* **1998**, *102*, 540 – 548.
20. Sedin, D. L.; Rowlen, K. L., *Anal. Chem.* **2000**, *72*, 2183 – 2189.
21. Choi, S. T.; Lee, S. R.; Earmme, Y. Y., *J. Phys. D: Appl. Phys.* **2008**, *41*, 074023.
22. Van Zwol, P. J.; Palasantzas, G.; de Hosson, J. T. M., *Phys. Rev. E* **2008**, *78*, 031606.
23. Cai, S.; Bhushan, B., *Mater. Sci. and Eng.* **2008**, *R61*, 78 – 106.
24. Komkov, O. Y., *Journal of Friction and Wear* **2007**, *28*, 19 – 31.

# Summary

A semiconductor wafer is exposed to several processing steps when it is converted from a bare silicon wafer to one populated with millions of transistor circuits. Lithography is one of the most important and critical steps in semiconductor wafer manufacturing. It is directly responsible for shrinking feature sizes to increase transistor densities. However, with further down scaling of the feature size on wafers, the magnitude of adhesive forces becomes a prohibitive factor in further increasing handling speeds and throughput of wafers. This has inspired us to investigate the adhesion forces of hydrophilic surfaces with an atomic force microscope (AFM) by recording force – distance curves. All adhesion force measurements were performed with flat topped, cone shaped, micron sized hydrophilic silicon tips, in order to mimic the adhesion between two parallel surfaces as in the wafer stepper machines between the wafer and the wafer table. Great care has been paid to align the tip and the substrate parallel to each other for all measurements. We varied the alignment between the tip and the sample by placing the sample on a sample holder that could be adjusted at different tilt angles. The optimal angle was determined by maximizing the adhesion force, which corresponds to a plan parallel configuration between the flat tip and the average surface.

In our experiments two different samples were used to study the adhesion forces. Chapter 2 provides information about the fabrication of these samples. The first sample is a flat Si(001) wafer with a 2 nm native oxide layer. The second sample is a less smooth Si(001) wafer that was roughened in a solution of ammonium hydroxide ($NH_4OH$). Anisotropic wet chemical etching was prefered as the method for surface roughening due to its ease of use and low cost. It also provides rather rough surfaces without physical damage to the bulk structure of the material. As a result of chemical etching, the formation of near – pyramidal hillocks, and shallow round pits with different sizes were observed on Si(001).

The influence of surface roughness on the adhesion force is discussed in Chapter 3 by using as received (rms roughness smaller than 1 nm) and etched Si(001) surfaces (rms roughness of ~14 nm). The adhesion force of flat Si(001) substrate is measured more than an order of magnitude larger than that of rough Si(001) substrate with the use of a 1.8 $\mu m$ tip radius. The influence of the relative humidity on the adhesion force is also described in Chapter 3 for both surfaces in the range of 0% to 80%. It was shown that the adhesion force increases with increasing humidity until a relative humidity of about 70%. Beyond a relative humidity of 70% a slight decrease of the adhesion force is observed for both the flat and the rough Si(001).

In Chapter 4, for the flat-on-flat contact geometry, we have measured the adhesion force as a function of various experimental parameters, including applied load, residence time, retraction velocity of the piezo and tip size in different relative humidity in order to elucidate their individual effect on the derived adhesion force. In all cases, it was certified that the externally applied load on the tip does not affect the measured value of the adhesion forces. Possible distortions due to plastic deformations are thus excluded. Within the applied 0.5 – 41 s time window, we have found that the adhesion force increases with increasing retraction velocity of the piezo, while the residence time of the tip on substrate does not have any measurable effect on the adhesion force. The increase of the adhesion force with increasing retraction speed is attributed to the viscous force. It was also found that the adhesion forces scale with the size of the flat tip with radii of 0.9 and 1.8 $\mu m$. Consistent with the result of Chapter 2, for all instrumental parameters the adhesion force increases with increasing relative humidity, which is related to the presence of condensed water between the tip and the substrate.

It is also a necessity to know the influence of the singular instrumental parameters, introduced in Chapter 4, on the adhesion force of flat-on-rough contact geometry for correct and reproducible analysis of the adhesion force. This was presented in Chapter 5. Again we verified that the adhesion force of rough Si(001) (rms roughness is 13.7 nm) does not dependent on the applied load on the tip, ruling out significant artifacts due to plastic deformation. We also found no dependence on the residence time of the tip on the substrate, and the size of the flat tip. We measured a clear decrease of the adhesion force with increasing tip retraction speed, in obvious contrast to the flat-on-flat geometry, where an increase of the adhesion force with increasing piezo speed was observed. The difference is attributed to the dominance of the capillary force over the dynamic force for the rough surface. For all covered instrumental parameters the adhesion force increases with increasing relative humidity.

# Samenvatting

Een groot aantal proces stappen zijn noodzakelijk om op een silicium wafer miljoenen transistor schakelingen te maken. Met lithografie worden steeds kleinere afmetingen mogelijk, noodzakelijk voor het realiseren van een grotere dichtheid van transistoren en is daarmee één van de belangrijkste en tegelijk ook een kritische stap in de halfgeleider fabricage. Het verkleinen van de karakteristieke afmeting op wafers heeft ook als effect dat adhesiekrachten een beperkende factor zijn in de noodzakelijke verhoging van de processnelheid in dit fabricage proces. Dit heeft ons er toe geïnspireerd om onderzoek te doen naar de adhesiekrachten van een hydrofiel oppervlak door middel van kracht – verplaatsings metingen met een atomaire kracht microscoop (AFM). Om de adhesie tussen twee parallelle oppervlakken te kunnen na bootsen zijn alle adhesiekracht metingen gedaan met kegelvormige silicium naalden met een vlakke, hydrofiele bovenkant en een diameter in het micrometer bereik. Voor iedere meting zijn de vlakken gevormd door het te bestuderen oppervlak en de testnaald zo goed mogelijk parallel uitgelijnd. Dit is bereikt door het te meten substraat te plaatsen op een roteerbare houder. De optimale uitlijning is bepaald als die hoek waarbij de hoogste adhesiekracht kan worden gemeten. Bij deze hoek is sprake van een plan parallelle configuratie van de vlakke tip en het gemiddelde oppervlak van het substraat.

In onze experimenten om de adhesiekrachten te bepalen is gebruik gemaakt van twee verschillende substraten. In hoofdstuk 2 is beschreven hoe deze substraten verkregen zijn. Het eerste substraat is een vlakke Si(001) wafer met een 2 nm natuurlijk gegroeide oxide laag. Het tweede substraat is een minder vlakke Si(001) wafer, waarbij de ruwheid is verkregen met behulp van een ammonium hydroxide ( $NH_4OH$ ) oplossing. Gekozen is voor een anisotrope nat chemische ets vanwege de eenvoud en de lage kosten om een oppervlak te verruwen. Deze methode geeft ook een redelijk ruw oppervlak zonder dat er fysische schade ontstaat aan het onderliggende bulk materiaal. Het resultaat van deze chemische ets is de vorming van haast piramidale heuvels en ondiepe ronde gaten van verschillende afmetingen op het Si(001) oppervlak.

De invloed van oppervlakte ruwheid op de adhesiekracht, het onderwerp van hoofdstuk 3, is onderzocht met een ongeprepareerd (rms ruwheid kleiner dan 1 nm) en een geëtst (rms ruwheid van ongeveer 14 nm) Si(001) oppervlak. Een tip met een diameter van 1.8 $\mu m$ is gebruikt om de adhesiekracht op het vlakke Si(001) oppervlak te meten, welke meer dan een orde van grote hoger is dan op het verruwde oppervlak. De invloed van de relatieve luchtvochtigheid in het bereik van 0 – 80% op de adhesie van beide oppervlakken is bestudeerd. Er is gevonden dat de adhesiekracht toeneemt met de relatieve luchtvochtigheid tot een relatieve luchtvochtigheid van ongeveer 70%. Boven deze 70% wordt een kleine daling van de adhesiekracht gezien voor zowel het vlakke als het verruwde Si(001) oppervlak.

In hoofdstuk 4 is voor de vlak-op-vlak contact geometrie de adhesiekracht bepaald als functie van verschillende experimentele parameters, inclusief de aangebrachte druk, contact tijd, de terugtrek snelheid van de piëzo en de tip afmeting bij verschillende relatieve lucht vochtigheid om zo het afzonderlijke effect van deze parameters op de adhesiekracht te bepalen. In alle gevallen werd gevonden dat de aangelegde druk de gemeten adhesiekracht niet beïnvloed. Een eventuele afwijking door plastische vervorming kan daarmee uitgesloten worden. Binnen het gekozen contacttijd bereik van 0.5 tot 41 sec. is gevonden dat de adhesiekracht toeneemt met de snelheid waarmee de piëzo wordt teruggetrokken, terwijl de contacttijd zelf geen meetbare invloed heeft op de adhesiekracht. Deze toename van de adhesiekracht met terugtreksnelheid wordt toegeschreven aan de viskeuze kracht. Er is ook gemeten dat de adhesiekracht schaalt met de afmeting van de vlakke tip voor diameters van 0.9 en 1.8 $\mu m$. Consistent met de resultaten zoals beschreven in hoofdstuk 3, neemt voor alle instellingen van de experimentele parameters de adhesie toe voor toenemende relatieve luchtvochtigheid, dit is direct gerelateerd aan de aanwezigheid van gecondenseerd water tussen tip en substraat.

Het is noodzakelijk om ook de invloed van de afzonderlijke experimentele parameters op de adhesiekracht, zoals beschreven in hoofdstuk 4, te bepalen voor een vlak-op-ruw geometrie om zo een correcte en reproduceerbare analyse te verkrijgen van de adhesiekracht. Dit wordt gepresenteerd in hoofdstuk 5. Opnieuw is geverifieerd dat de adhesiekracht met een verruwd Si(001) (rms ruwheid 13.7 nm) niet afhangt van de aangelegde druk op de tip, waarmee significante afwijkingen ten gevolge van plastische deformatie uitgesloten kunnen worden. We hebben ook gezien dat zowel de contacttijd als de afmeting van de tip geen invloed heeft. Een duidelijke afname van de adhesiekracht met een vergroting van de terugtreksnelheid is in dit geval gemeten. Dit verschilt duidelijk met de vlak-op-vlak metingen, waar een toename van de adhesiekracht met een vergroting van de terugtreksnelheid van de piëzo is gezien. Dit verschil wordt toegeschreven aan de dominantie van de capillaire kracht boven de dynamische kracht voor een ruw oppervlak. Voor alle onderzochte experimentele parameters neemt de adhesiekracht toe met een toename van de relatieve luchtvochtigheid.

# Acknowledgements

Last 4 years of my life were great experience with full of uncertainties, challenges, and explorations which helped me to develop myself enormously, both scientifically and personally. I want to express my pleasure to all people who have made a contribution to this Thesis and to my life during my PhD years.

First of all, I would like to thank my *Allah* Who bestowed of His Mercy on me, and Who granted me to finish this Thesis.

I would like to thank my promotor, *Prof. Dr. Ir. Bene Poelsema* for giving me the opportunity to work his research group and to live through such a great life experience. All the information his provided, and his critical views and questions during the discussions pushed me to dig more deeply into the fundamental phenomena behind my results and analysis which are important to the completion of this Project. I am grateful for his guidance, and scientific support.

I would like to express my heartfelt gratitude to my promotor, *Prof. Dr. Ir. Harold. J. W. Zandvliet* for his continuous guidance, support, all kinds of ideas and all the patience to advise me on this Project. His support and corrections took this Thesis to a better level. His encouragement and guidance were always moral boosting and motivating. I have learnt to view the problems from different perspective with the help of him. I feel myself very lucky to meet and work such a great scientist, and a very kind, thoughtful person like him.

My sincerest appreciation goes to my daily supervisor *Dr. Ir. Herbert Wormeester*. I would not finish this Thesis without the help of his critical thinking, and very constructive conversation we have had. I improved my abilities in the laboratory with the help of him. He pushed me to become an independent researcher.

I would like to express my utmost gratitude to European Community's Seventh Framework Programme (FP7) for providing financial contributions to the Project called "A supra-disciplinary approach to training in surface physics for advance manufacturing", acronym SPAM, with a Marie Curie Early Stage Researcher (ESR) fellowship.

I would like to thank all of the members of my graduation committee, *Prof. Dr. Sylvia Speller, Dr. George Palasantzas, Prof. Dr. Jan C. T. Eijkel, and Dr. Michel H. G. Duits* for reading my manuscript.

It is my pleasure to express my gratitude to *Dr. Stefan Kooij*, and *Dr. Raoul van Gastel* for their useful advices during work discussions, and nice chats during coffee breaks, and group outings. I owe a special thank to *Dr. James R. T. Seddon* for his fruitful comments, and suggestions to solve the problems that we encountered in the Project. I am also extremely grateful to *Dr. Gregor Hlawacek* for valuable comments on the Project and for performing HIM measurements.

I would like to say specials thanks to *Herman Oerbekke* and *Hans Bevers*. My words are not enough to express my gratitude to them. God knows how important, and valuable they are for me. I am thankful to them for taking an interest on me, wondering my health, asking my mood, and listening to me whenever I needed to talk someone. They were always there for me to give me courage, and strength to face difficulties. My parents and I will always be grateful to them. I also thank them for providing technical support whenever I needed for AFM and IBS systems. Dear *Herman* and *Hans*, I will be very happy to welcome you in Istanbul one day.

I would like to express my gratitude to *Rianne Nales*, and *Simone ter Hedde* for their helps with all the administrative issues, and nice chats during coffee breaks, and group outings.

I am grateful to all former and present members of *PIN group* for all nice moments we had together.

I also would like to thank *Mark A. Smithers* for SEM measurement, *Gerard A. M. Kip* for XPS measurement, and *Henk. A. G. M. van Wolferen* for providing me the AFM probes with decreased radii with FIB.

Furthermore, I would like to thank *Edwin Gelinck*, and *Hartmut Fischer* from TNO for extended discussions, fruitful exchange of ideas on the topic, and providing opportunity in performing some AFM experiments at TNO. I would also like to express my gratitude to *Rene Compen*, *Fred Huizinga*, *Bensely Albert* (currently in GE Power & Water, USA), and *Twan van Schijndel* from ASML B.V. for their continued fruitful collaboration in order to give additional support to ensure that I received relevant background information to be able to put my research activities in the right context.

Many thanks to *Dr. Mehmet Refii Kileci* for honoring me by giving the permission to use one of his great Ebru (marbling), that you see on the cover of this Thesis.

I owe a special thank to *Mustafa İncel*, and *Özlem Durmaz İncel* for making my life easier when I first came to Enschede. I will always be grateful to them for their kindness, support and friendship.

I would also like to express my deep appreciation to *Ioannis Kostakos* for helping me out in the laboratory, as well as being so patient, and supportive. I owe him a big thank, since with our friendship we showed how peaceful and loving people we are in reality, despite the belief

that Greek and Turkish people do not like each other. Efharisto poli Ioannis, for beautiful presents of your grand mother and your parents. I will always keep them.

My deepest thanks to *Adil Acun*, *Hasan Ateşçi*, and *Hüseyin Ateşçi*. I am grateful to Allah for giving me chance to meet such humble, generous, and kind people like you. There are very few people with whom I feel comfortable to share my ideas, and problems, and *Adil*, *Hasan*, and *Hüseyin* are definitely some of them. Thanks for accepting me as your elder sister, and being a part of my small family in Enschede.

Personally, I want to thank a special person, *Hande Cıngıl,* one of the strongest woman I have ever met. Dear *Hande*, the difficulties, that you had encountered during your short stay in Enschede, were incredible life experiences for both of us. We both learned that life could be worse suddenly. However, by finding a lifelong friend like you, I understood one more time that every cloud has a silver lining. You are a special gift that I got in the Netherlands. Thanks for being my sister.

I must express my deepest gratitude to my beautiful friends *Fulya Kunter*, *Özlem Pehlivan*, *Özlem Yılmaz*, and *Damla Şendoğdu* for their continued friendship, and love. The distance between Turkey and the Netherlands did not separate us, and you were always there for me to give me courage, and support whenever I needed. Ladies, thanks a lot for being a part of my life.

Throughout my education life, I have been fortunate to be educated by valuable teachers, and professors who all have made indelible imprints in my journey with their guidance. I will always be thankful to all of them for each word that they have taught me. It is to my chagrin that I will not be able to acknowledge each one of them here, so this acknowledgement is not, and can not be, complete. But, I would like to highlight and thank two of them who have left the deepest impressions and consequently, molded me intellectually. It was a honor for me to be a student of *Aytem İmre*, who was my first teacher. During my childhood, she shaped my personality with my family, and I owe my willingness to work hard with passion to her. I also owe a special thank to my dearest instructor *Süheyla Kiraz* for being my role model, and inspiration. She is the reason of my eagerness to be an academician. I feel myself very lucky to have a lifelong friend like her. *Süheyla hocam*, thanks for your great support at any time and any field of my life.

Last but not least, I would like to extend my sincere thanks to my aunts, *Belgin Arslan Özyiğit*, and *Nuray Özyiğit*, my uncles *Murat Özyiğit*, and *Nuh Arslan*, my cousins, *Arif Arslan*, *Ebru Arslan,* and *Nurgül Özyiğit* without whose love and support throughout my years in the Netherlands, all this would never have been possible. *Belgin teyzecim ve Nuh eniştecim, Murat dayıcım ve Nuray yengecim, Hollanda'daki yaşantım boyunca evinizin kapısını açtığınız, aşınıza ortak ettiğiniz, yeğeniniz değil de kızınızmışım gibi muamele yaptığınız, her derdimde yanımda olduğunuz ve anne-babamın eksikliğini hissettirmediğiniz için çok teşekkür ederim. İyi ki varsınız.* My lovely cousin *Ebru,* and dear *Nurselin* thanks a lot for being my paranymphs, and sharing such special moments on stage with me.

Finally, this thesis is dedicated to my parents, *Kâmuran* and *Ömer Çolak* and my brother, *Ercan Çolak*. Without the unconditional love, prayers, support and encouragement of them, I would not have been able to accomplish this research. *Canım annecim ve babacım, bugüne kadar bana verdiğiniz sonsuz sevginiz, emeğiniz, destekleriniz ve dualarınız için çok ama çok teşekkür ederim. Hayallerimi gerçekleştirebilmem için yıllardır evlat hasreti çekiyor ve her türlü sıkıntıya katlanıyorsunuz. Bugünlere gelebilmem önce Allah'ın sonra sizlerin sayesindedir. Hakkınızı asla ödeyemem. Allah sizleri başımdan eksik etmesin.* My brother *Ercan*, thanks for being my best friend, my greatest support, and taking care of mom and dad when I was away from home. I love all of you.

*Arzu Çolak*
*June 2013*
*Enschede, the Netherlands*

# *List of publications*

1. **Çolak, A.**; Wormeester, H.; Zandvliet, H. J. W.; Poelsema, B.
   "Surface adhesion and its dependence on surface roughness and humidity measured with a flat tip"
   ***Appl. Surf. Sci.*** 2012, *258*, 6938 – 6942. (Chapter 3)

2. **Çolak, A.**; Wormeester, H.; Zandvliet, H. J. W.; Poelsema, B.
   "The influence of instrumental parameters on the adhesion force in a flat-on-flat contact geometry"
   Submitted (Chapter 4)

3. **Çolak, A.**; Wormeester, H.; Zandvliet, H. J. W.; Poelsema, B.
   "The influence of instrumental parameters on the adhesion force in a flat-on-rough contact geometry"
   In preparation (Chapter 5)

# Curriculum Vitae

Arzu Çolak was born on September 27, 1979 in Kocaeli, Turkey. After graduation from the Izmit High School (Kocaeli, Turkey) in 1997, she joined the Department of Physics of the Istanbul University (Istanbul, Turkey) for her bachelor's studies. In 2002 she graduated from BSc program with a first degree and continued her Master of Science studies at the Department of Physics of the Boğaziçi University (Istanbul, Turkey). During her master study, she also worked as a physicist at the Acoustics Groups Laboratories of the National Metrology Institute (UME) of the Scientific and Technological Research Council of Turkey (TUBITAK) for 3 years. In 2006, she obtained her MSc degree with the thesis "Photoacoustic Spectroscopy" by obtaining third position in her master's class. In February 2009, she joined the Solid State Physics group (now known as Physics of Interfaces and Nanomaterials) at the University of Twente (Enschede, The Netherlands) to pursue her PhD degree under the supervision of Prof. Dr. Ir. Bene Poelsema, Prof. Dr. Ir Harold J.W. Zandvliet, and Dr. Ir. Herbert Wormeester. The aim and the results of her Project, "Measuring adhesion forces between hydrophilic surfaces with Atomic Force Microscopy using flat tips" are described in this PhD dissertation.